THE ANALYSIS AND INTERPRETATION OF VHE ($E_\gamma > 1$ TeV) GAMMA RAY MEASUREMENTS

Ocker Cornelis de Jager,
M.Sc

Thesis submitted to the Faculty of Natural Sciences at the Potchefstroom University for Christian Higher Education for the degree Doctor Scientiae.

POTCHEFSTROOM
SOUTH AFRICA
February 1987

To Estie,
for her love, help, patience and understanding.

ABSTRACT

It is well known that Very High Energy Gamma Ray Astronomy (VHEGRA) is facing a dilemma in the sense that all reported sources are very weak emitters of VHE γ-rays. The status of most sources are also questionable on statistical grounds, while very few sources have been confirmed.

This dilemma can be solved by improving the sensitivities of telescopes. In this study it is however reasoned that some light can be shed on this dilemma by treating the data in a more consistent way. Since one is dealing with a strong stochastic component of background cosmic radiation, the data should be analysed by means of sound statistical techniques. The analysis of low counting statistics are treated, with the accent on periodic analysis. Existing statistical tests for uniformity on a circle are reviewed and it is concluded that they are only usable if one has some a priori information about the form of the light curve. A 'new' test (the H_m-test) is developed to identify sources for which the form of the light curve is unknown. It is also shown how one can overestimate the significance of a signal if a search is conducted within one independent Fourier spacing: With the Rayleigh test one can report a 'probability for uniformity' which is a factor of three too small, while this factor can be up to twenty for tests like Z^2_{10} or Pearson's χ^2-test with twenty bins. It is also shown how a γ-ray light curve can be estimated from the data (phases) alone without making any ad hoc assumptions. It is a fact that such a light curve estimator will converge to the true unknown light curve if the sample size increases to infinity and if the phases are independently and identically distributed. The MeV light curve of the Vela pulsar (using the COS-B data) is estimated as an example. It is also shown how the signal strength of a periodic source can be estimated in some cases.

The isolated pulsar PSR 1509-58 is identified by means of the H_m-test at a confidence level of 99.9%. The light curve is a triple sinusoid and it is shown that the observed radiation from night to night is steady and coherent. The data on PSR 1802-23 are reanalysed, taking the effect

of oversampling within one independent Fourier spacing into account. Indications of steady emission is found at a confidence level of 98.6%.

Existing models for γ-ray emission from isolated pulsars are investigated with the aim of predicting the VHE γ-ray luminosity. It is found that only millisecond pulsars can produce observable VHE polar cap γ-rays while an outer gap near the light cylinder can provide observable VHE γ-rays from pulsars like Crab, Vela and PSR 1509-58. The outer gap model provides consistent results in the sense that the predicted MeV and TeV luminosities agree with COS-B and VHE observations respectively.

From the existing theory of outer gaps it is found that transients above 1 TeV should occur more often than transients below 3 GeV. It is also shown from this theory that a pulsar with the tentatively identified parameters of PSR 1802-23 is an ideal VHE emitter. Furthermore, certain pulsars can be MeV quiet but TeV loud. Finally, there may be one or more pulsars in the Southern Sky which could cause the observed count rate to double - thus solving the VHEGRA dilemma.

TABLE OF CONTENTS

GLOSSARY OF TERMS

The identification of γ-ray sources rely heavily on statistical methods. Analysis techniques improved little during the course of γ-ray astronomy which can partly be ascribed to the poor communication between γ-ray Astronomers and Statisticians. This glossary list some terms used by Astronomers and the corresponding terminology in Statistics.

H_o: The null hypothesis, i.e. there is no source of γ-rays.

H_A: The alternative hypothesis, i.e. there is a source of γ-rays.

Test statistic: A function of the experimental data which is used to test H_o against H_A. Well known examples are the χ^2- and Rayleigh test statistics.

Type I error: to falsely reject H_o.

Type II error: to falsely reject H_A.

significance level: a chosen number between zero and one which represents the probability to make a Type I error. This number can also be called the 'detection threshold'. VHE γ-ray Astronomers sometimes choose this level as $\approx 10^{-4}$.

p-level: The smallest significance level which can be chosen such that H_o can still be rejected. VHE γ-ray Astronomers usually refer to this number as the 'probability for uniformity'. If this p-level is less than the significance level, H_A will be accepted. Otherwise H_o will be accepted.

confidence level: equals one minus the p-level and represents the confidence at which H_A can be accepted. However, a confidence level should only be quoted after all the trials made to obtain an apparent positive effect, have been taken into account.

significance: This term serves the same purpose as a 'p-level'. Thus, one can also say: 'the significance of the result is 10^{-4}' which means that H_o can be rejected at a significance level of at least 10^{-4}. Furthermore, one will say that the 'significance' of a 10^{-6} result is larger than the corresponding 'significance' of a 10^{-4} result. If the test statistic is normally distributed, one can also refer to the number of standard deviations as the 'significance of the result'. However, one should not confuse the terms 'significance' and 'significance level'.

The power $(1-\beta)$ of a test: the probability of accepting H_A (if H_A is true) after a significance level had been fixed beforehand.

UMP test: Uniformly most powerful test, which means that the test under consideration has the largest power of all possible tests, for all values of parameters on which the density function (e.g. a light curve) under H_A depends.

Independent trials: The number of independent trials made before obtaining a positive result is usually wrongly referred to as the 'degrees of freedom'. Astronomers should avoid using the latter terminology since it may confuse those not familiar with the field of VHEGRA.

The following abbreviations and notations will be used in this thesis:

ACT: The Atmospheric Cerenkov Technique applicable to primary energies above 100 GeV.

MSH: A synonym for the isolated pulsar PSR 1509-58.

NSB: Night sky brightness

UHEGRA: Ultra high energy γ-ray astronomy ($E_\gamma > 100$ TeV).

VHEGRA: Very high energy γ-ray astronomy ($E_\gamma > 0.1$ TeV).

$N(\mu,\sigma)$: The normal density function with mean μ and standard deviation σ.

χ^2_K: The χ^2 variable with K degrees of freedom.

$S = {}^{d}(f(S))$: The random variable S is distributed according to the probability density function f(S). Sometimes the notation $S = {}^{d}(X)$ will be used which means that S has the same distribution as X.

E(X): the mean or expected value of the random variable X.

Pr: the p-level. Sometimes the form -log(Pr) will be used for graphical purposes. The larger -log(Pr), the more 'significant' a result will be.

CHAPTER 1

VHEGRA - A DILEMMA?

It was realised in the late fifties (see Jelley, 1982 for a review) that γ-rays may 'penetrate' the atmosphere by means of secondary visible light production. This opened a new branch of Astronomy which could be conducted at ground level with relative ease and at low cost. These experiments are based on the ACT which will be discussed in Section 1.1. Due to the small capital investments, the technique was not rapidly developed as e.g. the astronomies conducted from satellites.

Only during the last few years new developments came into being, trying to establish more sophisticated experiments in VHEGRA. It is therefore not very surprising that during the first fifteen years of its existence only a few sources (Cyg X-3, Crab, Vela and CEN-A) were reported as VHE γ-ray emitters. A further reason for the lack of sources was the rudimentary statistical techniques used by experimenters to search for sources (see Section 1.4). Since the introduction of more sophisticated data analysis techniques in the early 1980's, the number of sources increased dramatically - the catalogue of reported point sources stands at thirteen. There is however some scepticism concerning the status of this catalogue, mainly due to the fact that VHEGRA have not found a strong source (like Sco X-1 in X-ray Astronomy) and also due to the many negative reports indicating that the sources are not only weak but also of a transient nature.

The 'VHEGRA dilemma' can then be described as an apparent upper limit of $\approx 5\sigma$ for the significances of observed sources, despite the total time ON-source (see Section 1.5). This dilemma can be solved in three ways: (a) By implementing more sophisticated experimental and (b) statistical techniques - the latter being the main thrust of the work done for this thesis (see Chapter 2). (c) A better understanding of the nature of ideal

VHE γ-ray sources should be obtained. This aspect will be studied in Chapters 4 and 5 with respect to the selection of ideal VHE γ-ray pulsars.

At the beginning of the decade it was realised at Potchefstroom that most objects considered to be candidates for VHE γ-ray radiation are situated in the Southern Sky (see Section 1.3). Apart from the galactic centre region which is visible in the Southern Sky, most X-ray binaries and young pulsars are also Southern Sky objects. This prompted the Potchefstroom group to start with an experiment in the Southern Hemisphere (see Section 1.2). This effort was crowned with success: Using some of the techniques suggested in this thesis, the group was able to identify three sources within the first year of operation. Some of the results will be discussed in this thesis to illustrate the proposed techniques.

1.1. GENERAL ASPECTS OF THE ACT.

At energies less than 10 GeV the γ-ray fluxes from some sources are still high enough to permit observations by satellites. However, at $E_\gamma > 100$ GeV the flux of γ-rays with respect to the general cosmic ray flux is low and large collection areas are needed to collect these photons. Fortunately the VHE γ-rays undergo reactions in the atmosphere of Earth such that a thin Cerenkov light pool is formed high above sea level with the γ-ray arrival direction remaining conserved. The whole atmosphere with its complexity serves as the light producer, while directional ground based telescopes serve as collectors of this light. Due to the weakness of the Cerenkov light, observations are usually done during dark moonless nights. It is also best to have a site which is isolated from city lights. The humidity should also be relatively low to prevent absorption of blue light. Coincidence techniques are normally used to discriminate against the high flux of unwanted background illumination. The atmosphere may also introduce a lot of unknown fluctuations in the data, suggesting a very careful treatment thereof (see Section 2.2).

The effective collection areas obtained (due to the large Cerenkov light pools) are between 10^8 and 10^9 cm^2 (compared to the collection area of a 50 MeV γ-ray satellite of $\approx$ 20 cm^2) and lead to count rates of $\approx$ 60 min^{-1}. However, despite the large collection areas the signal strengths obtained at $E_\gamma > 100$ GeV are $\approx$ 2% (see Table 1.1), while the signal strengths obtained for high energy satellite experiments ($E_\gamma > 50$ MeV) may be up to 60%. The biggest problem of VHEGRA is the large cosmic ray background produced by protons and nucleons, which dilutes the already weak γ-ray signal. This background is however isotropic and time independent which enables the search for local and timelike enhancements which are then ascribed to γ-rays.

In order to enhance the signal to noise ratio, one can increase the mirror area, or, imaging techniques can be used to discriminate against proton and nucleon induced events (see e.g. Weekes, Lamb and Hillas, 1987).

Unfortunately the response function, threshold energy and collection area of VHEGRA telescopes cannot be determined exactly since there are no VHE γ-ray calibrators available. Consequently, one has to rely on simulations of the Cerenkov light production in the atmosphere and assumptions as to the behaviour of the telescope to estimate such parameters. Uncertainties of up to a factor of five may be applicable.

1.2. THE VHEGRA TELESCOPE OF POTCHEFSTROOM.

The VHEGRA telescope of the Potchefstroom University is situated on a farm called Nooitgedacht. The mean geodetic position of the telescope is: height = 1439.87 m, longitude = 332.818 351 degrees west and latitude = -26,904 257 degrees. The atmosphere is relatively dry with rain occurring only during the summer months (Oct - March).

This experiment was proposed in Bangalore by Raubenheimer et al. (1983) and described by De Jager (1985) and De Jager et al. (1986a). The telescope consists of four independent units, each consisting of three

Table 1.1. A selected list of reported periodic sources with periods less than 300 s.

Name of source	threshold energy (TeV)	sample size (n)	signal strength (p)%	duty cycle (δ)	DC excess x (sigma)	reference number
Crab	2	1 906	{1,6 1,1	{0,024 0,024	{0,70 0,48	78
Crab	0,8	8 675	1,1	0,024	1,03	62
Crab	1,8	18 475	0,7	0,024	0,96	62
Crab	0,8	8 650	1,7	0,024	1,58	62
Crab	20	603	3,2	0,02	0,77	42
Crab	0,9	242 220	0,15	0,018	0,74	64
Crab	0,9	59 689	0,27	0,018	0,66	64
Crab	3	161	34	0,15	4,31	50
Crab	1	154 600	0,23	0,01	0,92	39
Crab	0,2	12 466	1,70	0.06	1,90	123
Crab	1,2	3 868	1,90	0,03	1,18	5
Vela	0,5	48 159	{0,58 0,25	{0,044 0,022	{1,27 0,55	4
HER X-1	1	98	33	0,3	3,27	38
HER X-1	200	41	29	0,06	1,86	2
HER X-1	0,25	2 868	{3,6 2,8	{0,2 0,2	{1,94 1,50	53
HER X-1	0,6	14 434	2,3	0,2	2,76	54
PSR 1953 + 29	2	14 286	3,5	0,4	4,18	14
4U 0115 + 63	1	37 000	3,8	0,5	7,31	15
CYG X-3 (12 ms)	1	450	38	0,5	8,06	16
PSR 1802-23?	1	447	28	0,5	5,92	111
VELA X-1	1,5	54 100	3,1	0,5	7,21	100
PSR 1509-58	2	37 334	1,3 x 3	0,17 x 3	2,5 x 3	Chapt. 3

1.5 m rhodium coated, paraxially mounted mirrors. Three units are spaced equidistantly on the perimeter of a circle with radius of 55 m while the fourth unit is situated at the centre of the circle. All mirrors are mounted on an equatorial mount which is computer-controlled by means of optical shaft encoders and stepper motors. All zenith angles less than 45 degrees are accessible and the positioning is accurate to within 0.1 degree. The expected field of view for TeV γ-rays is $\approx$ 2.2 degrees.

The effective area of the telescope is $\approx 9 \times 10^8$ cm^2 at a threshold energy of $\approx$ 1 TeV at the zenith, assuming the cosmic ray spectrum to be applicable. The count rate obtained at the zenith is $\approx$ 65 min^{-1}. Assuming an average count rate of $\approx$ 48 min^{-1}, the sensitivity or minimum observable flux (at a level of significance of 4σ) after a total time of T seconds ON-source for a periodic source with a beam width of $\beta \in [0,1]$ is

$$F_{min}(>1 \text{ TeV}) = 3.6 \times 10^{-9} \sqrt{\beta/T} \text{ (cm}^{-2}.\text{s}^{-1}\text{)}$$

A very important aspect of the Potchefstroom telescope is its ability to record the arrival times of the Cerenkov events with a resolution of 0.1 μs. By using the available 1 kHz radio frequency standard of ZUO and a Time Transfer Control Unit (TTCU) (Lake, 1981) which uses the standard TV transmission system, one can transform the arrival times to UTC with an accuracy of at least 10 μs. One can also use this TTCU to measure the drift in the local clock with respect to UTC. In Chapter 3 it will be shown how the TTCU readings are used to correct for the clock's drift when doing timing analyses.

1.3. SOURCE DISTRIBUTION.

The Northern Sky had been covered quite extensively during the past few decades by many experiments, while the Southern Sky had been covered only during 1972-1974 by Grindlay et al. (1973) and Grindlay et al. (1975a and b), leading to the discovery of CEN-A while some indications of radiation was found from the Vela pulsar. Other observations

of a part of the Southern Sky was done by the Ooty group. Their main contribution was the identification of a double peaked light curve from the Vela pulsar (Bhat et al., 1980). Since May 1985, Potchefstroom University had a Southern Hemisphere facility at Nooitgedacht (South Africa) while the Durham University started in Narrabri (Australia) in November 1986. The University of Adelaide also started with a pilot detector at White Cliffs (Australia). These experiments may lead to exciting new results.

Apart from the extragalactic source CEN-A, the large majority of X-ray binaries (e.g. in the Centaurus region, the Small- and Large Magelannic clouds) are in the Southern Sky due to the favourable positioning of the galactic disc with respect to the Southern Sky. It is somewhat difficult to compile a model independent priority list of these binaries, due to the uncertainties involved in the production mechanisms of VHE γ-rays. However, it is possible to derive a model independent priority list of isolated pulsars. This list was compiled (using relation (4.7)) by identifying those pulsars which are close enough to Earth and which have a large enough kinetic energy loss rate $\dot{E}$ (relation (4.1)) to be observable to existing VHEGRA telescopes (see Table 1.2).

It is clear from this table that the majority of these pulsars are in the Southern Sky. The distribution in declination of these candidates in Figure 1.1 shows that $\approx$ 75% of them are visible from the Potchefstroom facility, although some only during the rainy season.

1.4. SOURCE STATUS

The analysis of DC sources is not difficult from a statistical viewpoint. The only requirement is that the stabilisers of the telescope should be in working order (see Section 2.2 on the analysis of DC sources). The DC sources which have been identified are CEN A (Grindlay et al., 1975a) and M31 (Dowthwaite et al., 1984a). However, confirmative observations of these sources are necessary to establish them as VHE emitters. The

Table 1.2. A model independent list of candidate pulsars.

Pulsar	P(s)	$\dot{P}(s.s^{-1}) \times 10^{-15}$	d(kpc)	$F_{min}(>1\ TeV)$ $\times 10^{-12} cm^{-2}.s^{-1}$
0136+57 O	0.27	10.69	2.50	5.9
* 0203-40	0.63	1.20	0.47	1.5
0355+54 O	0.16	4.39	1.60	31.0
0403-76	0.55	1.54	0.79	1.1
0450+55	0.34	2.36	0.45	20.4
0458+46	0.64	5.59	1.20	1.0
0531+21 O	0.03	422.44	2.00	201487.4
* 0540-69 O	0.05	479.00	55.00	86.6
0540+23 O	0.25	15.43	2.60	10.6
0611+22 O	0.33	59.63	3.30	10.1
* 0656+14 O	0.38	54.30	0.40	411.8
* 0727-18	0.51	18.95	1.50	4.4
* 0740-28 O	0.17	16.83	1.50	111.5
* 0743-53	0.21	2.73	2.40	3.3
0823+26	0.53	1.72	0.71	1.6
* 0833-45 O	0.09	124.69	0.50	48619.9
* 0834+06	1.27	6.80	0.43	1.2
* 0905-51	0.25	1.83	0.86	10.5
* 0906-17	0.40	0.67	0.51	2.8
* 0919+06	0.43	13.73	1.00	11.9
* 0950+08	0.25	0.23	0.09	120.6
x * 1001-47 O	0.31	22.07	1.60	20.6
x * 1055-52 O	0.20	5.83	0.92	62.3
* 1133+16	1.19	3.73	0.15	6.8
* 1133-55	0.36	8.23	2.90	1.4
* 1221-63 O	0.22	4.96	2.70	4.6
* 1317-53 O	0.28	9.26	3.50	2.4
* 1336-64	0.38	5.05	2.30	1.2
* 1356-60 O	0.13	6.34	8.80	2.7
* 1449-64 O	0.18	2.75	2.20	6.8
* 1451-68	0.26	0.10	0.23	7.1
* 1504-43	0.29	1.60	1.70	1.6

Pulsar	P(s)	$\dot{P}(s.s^{-1}) \times 10^{-15}$	d(kpc)	$F_{min}(>1\ TeV)$ $\times 10^{-12} cm^{-2}.s^{-1}$
1508+55	0.74	5.03	0.73	1.6
x * 1509-58 O	0.15	1540.00	4.20	1779.0
* 1556-44	0.26	1.02	1.90	1.2
* 1558-50 O	0.86	69.57	2.50	1.2
* 1604+00	0.42	0.31	0.36	2.2
* 1642-03	0.39	1.78	1.30	1.3
* 1702-18	0.30	4.14	0.74	19.6
* 1706-16	0.65	6.38	0.81	2.4
* 1719-37 O	0.24	10.82	2.50	9.1
* 1727-47	0.83	163.67	4.10	1.2
* 1740-03	0.44	3.17	1.20	1.7
* 1742-30	0.37	10.70	2.20	3.1
* 1749-28	0.56	8.15	1.00	3.2
* 1754-24 O	0.23	13.00	4.20	4.0
x * 1800-21 O	0.13	125.00	5.30	129.1
* 1802-23?O	0.11	110.00	3.00	593.9
* 1820-31	0.28	2.92	1.60	3.4
* 1821-19 O	0.19	5.24	6.80	1.2
* 1822-09	0.77	52.32	0.56	25.4
* 1823-13 O	0.10	76.00	5.50	166.7
* 1830-08 O	0.09	9.00	10.00 ?	10.0
* 1842+14	0.38	1.87	1.30	1.4
* 1844-04	0.60	51.90	3.70	1.2
* 1914+09	0.27	2.52	1.60	3.4
* 1915+13 O	0.19	7.20	2.40	11.7
* 1916+14	1.18	211.40	0.76	15.4
* 1929+10	0.23	1.16	0.08	1076.4
1930+22 O	0.14	57.78	7.00	27.1
1937+21 O	0.0015	0.00001	2.00	635.5
2020+28	0.34	1.90	1.30	1.9
2021+51	0.53	3.05	0.68	3.1
2224+65	0.68	9.67	1.20	1.5

x A pulsar is considered to be a candidate if 10% of the rate of kinetic energy loss (relation (4.1)) can provide a minimum flux above 1 TeV of 10^{-12} $cm^{-2}.s^{-1}$.

* These pulsars are visible to the Potchefstroom telescope.

? The pulsar is a suspect.

O Outer gap candidates.

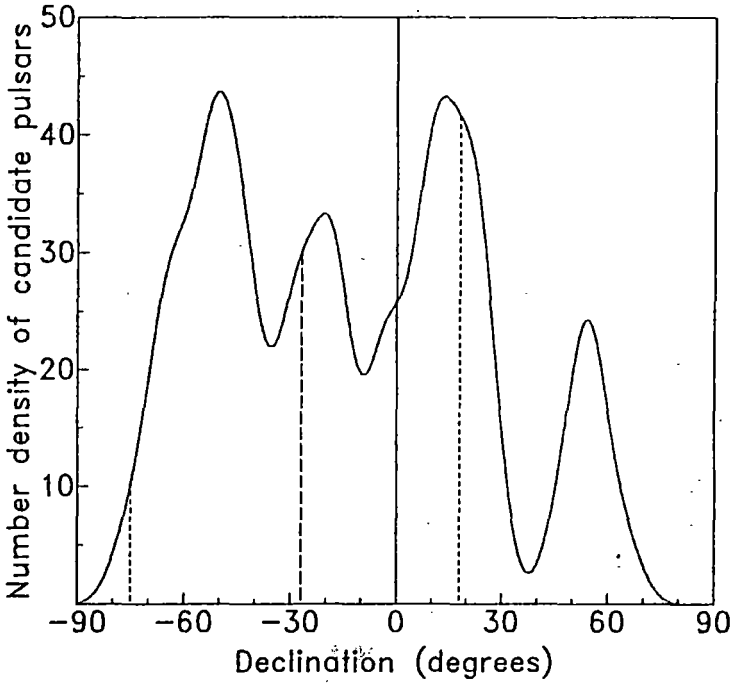

Figure 1.1. The distribution of the pulsars in Table 1.2 as a function of declination. Pulsars with declinations between -71 and 18 degrees (indicated by two vertical lines) are visible to the Potchefstroom telescope. The central vertical line defines the latitude of the telescope. A kernel density estimate (see Section 2.4) with a smoothing parameter of = 10 degrees was used to estimate the density.

galactic plane in the Northern Sky is a confirmed source of VHE γ-rays (Weekes, Helmken and L'Heureux, 1979 and Dowthwaite et al., 1984b).

The source which received the most attention so far is Cyg X-3. This unusual source with its 4.8 hour periodicity had been observed since 1972 (see Weekes, 1986 for a review). Despite all the observations during the past 14 years, no single identification ever exceeded a significance of $\simeq 5\sigma$, although this source can be considered as being confirmed. The most impressive result is that of the Crimean and Tien Shan observatories in the USSR during 1972-1980 (Nesphor et al., 1981). By combining all their observations, those observers managed to exceed the 5σ level with experimental conditions remaining the same during the eight years of observations. Statistically speaking, one can say that all their independent observations were done in an identical fashion (see Section 2.1 on 'Random Sampling') which improves the quality of their data.

There are even allegations that the Cyg X-3 results (and by implication all VHE and UHE results) are nothing but fluctuations of the background noise (Chardin, 1986). To deny such allegations, one can evaluate all observations of Cyg X-3, done by different observers around the world, by combining all their data - even those data sets which yielded negative results. Even the detector sensitivities of different experiments need not be similar for this combination since the hypothesis of a uniform background from the source direction is tested (see Chapter 2 for hypothesis testing procedures applied to VHEGRA).

Pulsar observations are experimentally easier to conduct since the implementation of stabilising systems (i.e. padding lights) is not crucial. One searches for a periodic signal with a duty cycle which may be small with respect to the period so that pulsar observations can be considered to be more sensitive than DC observations. One also has a greater scope with periodic analyses since any known timing structure can be confirmed. It is always good to have contemporary measurements of such a pulsar at longer wavelengths (i.e. radio or X-ray) where the pulsar can be easily observed. Due to the low signal to noise ratios observed in VHEGRA, one can easily miss a periodic signal due to the wrong use of a statistical technique.

Before 1982 observations of other pulsars yielded mostly upper limits (Porter and Weekes, 1978). However, Pearson's χ^2-test (Section 2.3.3.1) with 20 or 30 bins was usually used to identify periodic emission. Consequently their searches were most sensitive to peaks with a duty cycle of $\approx 4\%$ so that either sinusoids or peaks with a width less than 1% were missed in these analyses. Thus, their searches can be considered as 'light curve limited'. Furthermore, their confidence levels were calculated from the work of Hearn (1969) and O'Mongain (1973) which are wrong as pointed out by Li and Ma (1983).

A new era in VHEGRA was introduced by Gibson et al. (1982a): They started to gain more information from their data by not limiting themselves to χ^2-tests. Their main thrust came with the use of the Rayleigh test (Section 2.3.2.1) which searches for power at the fundamental frequency of the source's rotation. In Section 2.3 it will be shown that the Rayleigh test is most powerful for sinusoids when considering the presence of the large isotropic cosmic ray background. Their list of identified sources showing such light curves became quite impressive: Her X-1 (Dowthwaite et al., 1984c), PSR 1953+29 (Chadwick et al., 1985a), 4U 0115+63 (Chadwick et al., 1985b) and the 12.59 ms pulsar in Cyg X-3 (Chadwick et al., 1985c). Their flexibility in the analysis techniques also allowed them to identify a microstructure with a duty cycle of less than 1% in the light curve of the Crab pulsar (Dowthwaite et al., 1984d). The Potchefstroom group followed in their steps with the use of the Rayleigh test when they reported emission from the pulsar suspect PSR 1802-23 (Raubenheimer et al., 1986) and Vela X-1 (North et al., 1987). The Mount Hopkins group also started with more sophisticated statistical tools (e.g. the FFT techniques) and confirmed Dowthwaite et al.'s report of radiation from Her X-1. Furthermore, they even found evidence of radiation in the higher harmonics of Her X-1's frequency of rotation. Confirmation of radiation from 4U 0115+63 was also reported by the Mount Hopkins group (Lamb et al., 1987). Lamb et al. confirmed 4U 0115+63 as a transient and not as a source with steady radiation as reported by Chadwick et al. (1985b). The reason being that Lamb et al. used the 'transient method' of analysis (see Sections 3.3.1 and 3.3.2) and not the 'coherent method' of Chadwick et al. (see also Section 3.2.5). Consequently one is apt to report any radiation as being 'transient' instead of 'steady' if

the latter is true, when using the 'transient method'. Gamma ray astronomers should be aware of such pitfalls which may contribute to the VHEGRA dilemma. It is expected that the Hawaian and Adelaide groups will also follow with improved statistical methods.

The Indian group never started using the Rayleigh test or FFT's. They still use Pearson's χ^2-test with $\approx$ 20 bins which explains why they always identified pulsars with duty cycles of $\approx$ 5% (Gupta et al., 1982 and Bhat et al., 1980). On the other hand, they mostly observed the Crab and Vela pulsars which may indeed have duty cycles of 5% or less. They also concentrate on bursts and transient emission from pulsars, but the correct way to identify such effects will be to use change point procedures (Vardeman and Ray, 1985 and Lombard and Schultz, 1986).

It is therefor clear that although the number of sources has increased, the existing techniques are not sufficient. Buccheri (1985) made an important contribution to γ-ray Astronomy in general by bringing some order to the statistical techniques applicable to γ-ray data. Protheroe (1987) and De Jager et al. (1985) also reviewed some techniques and introduced a few new ones. They stressed the need to keep acquainted with existing theory and new developments in Statistics. The main purpose of this thesis is to bring further order to the techniques related to VHEGRA. In this way one may be able to shed some light on the VHEGRA dilemma:

1.5. THE VHEGRA DILEMMA

VHEGRA has a dilemma as pointed out by Ramana Murthy in Durham, U.K. (1986). This dilemma is called the '5σ syndrome': Experimenters do not seem able to identify sources with a significance exceeding $\approx$ 5σ. This may be best demonstrated in the case of periodic sources if existing results are discussed in the following two ways: A correlation study of the DC-excess versus pulsar duty cycle and the signal strength versus sample size.

An observed effect from a periodic source can be characterised by the total sample size n, the signal strength p and duty cycle δ. The parameters p and n are related to an effective DC-excess of x sigma (Gaussian standard deviations) by means of the relation

$$x = p/\sqrt{n} \tag{1.1}$$

Furthermore, any light curve can be written in the form of a density function (see Section 2.3) on the interval $[0,2\pi]$:

$$f(\theta) = pf_s(\theta;\delta) + (1-p)/2\pi \tag{1.2}$$

such that $f(\theta) = f(\theta + 2\pi)$. The source function $f_s(\theta;\delta)$ contains all information about the geometry of radiation. Most observations indicate that $f_s(\theta;\delta)$ is either unimodal or bimodal. It is important to know that all sources are not equiluminous, equidistant and VHE telescopes do not all operate at the same threshold energy. Consequently one would expect x (calculated from (1.1)) and δ to be uncorrelated for a set of randomly selected sources. A linear regression of x versus δ was done using the data in Table 1.1. A good fit was obtained with a correlation coefficient of 0.95. This good correlation and the small scatter of points are disturbing and raise the question why x and δ should be correlated.

The fitted line in Figure 1.2 represents the average detection threshold for all experiments if one assumes a nearly constant level of significance of $\approx 10^{-4}$ for a source. Since all reported p-levels are of the same order, it can be understood why the scatter of points on Figure 1.2 is not too large. The positive slope in Figure 1.2 can be explained if one considers the power curves in Figure 2.3, i.e. for most tests the power decreases with increasing duty cycle. The question remains then whether this is an artefact of the statistical tests used which only identified statistical fluctuations from the cosmic ray background or a true effect indicating that all the sources are radiating at the detection threshold. A final conclusion can only be drawn when a larger sample is available and if all negative reports are also taken into account when interpreting the apparent dilemma.

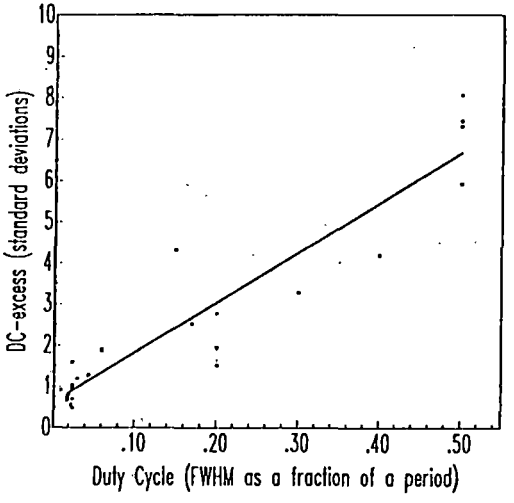

Figure 1.2. A plot of the DC excess x as a function of the pulsar duty cycle for all observations given in Table 1.1. Points connected with a dotted line represent double peaked light curves. The solid line represents a linear fit through the points.

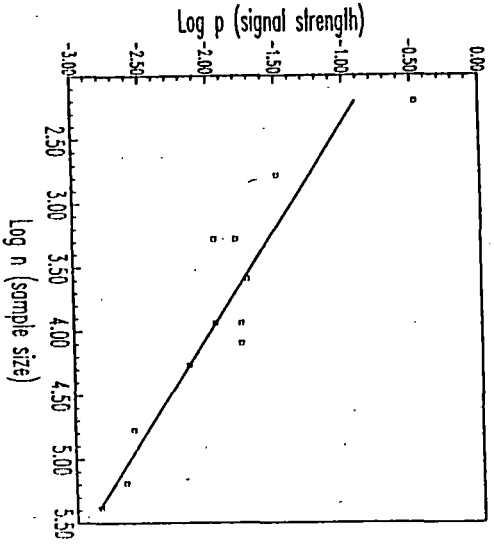

Figure 1.3. A plot of signal strength versus sample size of observations of the Crab pulsar. The two connected points represent the double peak observed by Jennings et al. (1974). The solid line is a linear fit through all points.

The next problem is the relationship between p and n for a given source. When dealing with a source which radiates steady, one should expect that p remains constant with n, with some fluctuations around that constant value of the signal strength which are due to differences in the threshold energy of the different telescopes. The Crab pulsar provides the largest sample (12 values) for this study. A linear fit through the 12 values, yields a signal strength of

$$p = (3.4 \pm 2.1)n^{(-0.61 \pm 0.08)} \qquad (1.3)$$

with a correlation coefficient of -0.93. This fit is shown in Figure 1.3. For a steady source the exponent of n should be zero. A comparison of (1.1) with (1.3) yields

$$x = (3.4 \pm 2.1)\, n^{(-0.11 \pm 0.08)} \qquad (1.4)$$

Relation (1.4) shows that it becomes increasingly difficult to uphold a fixed level of significance of say 10^{-4} as $n \to \infty$. The decrease of p with n cannot be explained by means of an intrinsic decrease in the VHE luminosity with time, since there is no time order in the results of Figure 1.3. This figure can have three explanations: (1) Nearly all results are statistical fluctuations from the cosmic ray background, whereby a result is reported if one observation's p-level exceeded the 10^{-3} or 10^{-4} level of significance. It is then questionable whether all the trials which have been made to obtain the apparent positive result, have been taken into account in the correct way. (2) One expects a low but constant value of the signal strength (less than 1%) to be present for Crab. This signal strength can have large fluctuations. Due to the apparent sensitivities of existing VHE telescopes, only the largest positive deviations of the signal strength are detectable and the longer one observes, the smaller the average positive deviation will be. (see Section 4.6.7 for a theoretical treatment of this problem). (3) Crab's VHE radiation is mainly in the form of bursts and transients with no steady level of emission so that the behaviour in Figure 1.3 is expected. However, more observations and theoretical input on TeV γ-ray production mechanisms of the Crab pulsar and others are necessary to solve this problem (see Chapter 4).

In view of the aforementioned problems, one should be very careful with the analysis of γ-ray data. It would be unwise to decrease the detection threshold to say 10^{-6}, but it would be much better to get a complete understanding of the data and the behaviour of test statistics on the data. If this can be done, it would be worthwhile to accept 10^{-2} as a detection threshold. If not, even a 10^{-4} level of significance may sometimes be questionable.

1.6. MOTIVATION FOR THIS STUDY.

It is clear from the discussion so far that VHEGRA has a number of problems - many of them cannot be solved by more sophisticated measuring techniques. In Chapter 2 the analysis of DC-sources will be discussed and the bin-free Gini-test will be proposed to test for exponentiality. The analysis of DC-sources is straightforward and less attention will be given to this field. However, periodic analyses are more difficult and will be covered in detail:

In Section 2.3 it will be shown that all the information of a light curve is contained in the trigonometric moments which can be estimated from the data. It can be shown that most test statistics are biased towards certain forms of light curves, so that pulsars will be identified which radiate according to the light curves for which the tests were designed. However, statistical fluctuations which follow the same form of light curves will also be identified (Buccheri, 1986). After a review of a representative sample of tests, the H_m-test will be developed which is powerful over the whole range of duty cycles. It is suggested that this test should be used if nothing is known a priori about the form of the light curve.

The effect of searching in period will also be discussed: It will be shown how the light curve and some test statistics change if the data are analysed at a period which differs slightly from the true period. It will also

be illustrated how one can underestimate a p-level due to oversampling within one or more independent Fourier spacings.

Another problem area identified is the estimation of γ-ray light curves. Researchers always used the 20- or 30-bin histogram to estimate a light curve. Due to the weak signals usually encountered in VHEGRA, one looses precious information with this procedure. It will therefor be shown how to estimate the true unknown light curve in a consistent way such that the estimator converges to the true unknown light curve with a probability of one as the sample size increases to infinity. These techniques will be illustrated by means of the COS-B data on the Vela pulsar. It will be shown how one can derive properties of the Vela light curve which is impossible to do so with the histogram.

Finally the estimation of a signal strength will also be covered. It will be shown how this parameter can be estimated by equating the theoretical trigonometric functions with the trigonometric functions obtained from the data alone.

To illustrate the techniques developed in Chapter 2, the data on three sources (CEN-A, PSR 1509-58 (MSH) and the pulsar suspect PSR 1802-23), which were obtained at the Potchefstroom facility (as described in Section 1.2), will be analysed in Chapter 3. The most important result obtained in Chapter 3 is the coherent and steady signal observed from PSR 1509-58. It is questionable whether this pulsar could have been identified without the techniques developed in Chapter 2.

In Chapter 4 the attention is shifted towards the physics of isolated pulsars with the purpose of evaluating the results in Chapter 3. The polar cap model of Usov (1983) and the outer gap model of Cheng, Ho and Ruderman (1986) will be applied to VHE γ-ray sources. Estimates of the VHE γ-ray luminosity and -spectrum will be given. The expected and observed high energy and VHE luminosities of Crab, Vela, MSH, PSR 1937+214 and PSR 1802-23 will be compared. The 'ideal' VHE γ-ray pulsar will be discussed and it will be shown that a pulsar with the tentatively identified parameters of PSR 1802-23 is such a pulsar. The reason is that most of the power of the outer gap is converted to VHE γ-rays via the

inverse Compton process. Such ideal VHE γ-ray pulsars are usually MeV quiet so that they need not be COS-B sources. The possibility of VHE transient phenomena will also be discussed and it will be shown on the basis of theoretical considerations that transients are more likely to occur at very high energies than at $E_\gamma < 3$ GeV.

CHAPTER 2

THE STATISTICAL ANALYSIS OF GAMMA RAY DATA

Charged TeV cosmic rays arrive isotropically from the sky so that they cannot be traced back to particular sources. There is also no coherency in their arrival, which may be due to their production mechanisms and interstellar scattering. Consequently their arrival times are stochastic. Gamma rays produced by point sources cause spatial anisotropies. In the case of pulsars, the γ-rays are emitted periodically. However, as said before, the ratio of these γ-ray fluxes to the charged cosmic ray flux is low and one is forced to approach the problem with the proper statistical tools if these γ-rays are to be identified. Consequently one has to rely on hypothesis testing to provide a 'yes' or 'no' answer to the possible presence of these γ-rays. The most general formulation for the hypotheses in VHE γ-ray Astronomy (VHEGRA) is the following:

H_o: The population under consideration consists only of the isotropic cosmic ray flux (null hypothesis).

H_A: There exists a signal of γ-rays amongst the isotropic flux of cosmic rays (alternative hypothesis).

Using a suitable test statistic one can calculate a p-level or 'probability' (as astronomers call it) of rejecting H_o.

In this study extensive attention will be given to procedures of hypothesis testing which is only a first step towards the identification of possible sources of γ-rays. The next step is on a higher level: This is called 'estimation' and is applicable after a 'yes' answer (i.e. H_A had been accepted) had been provided by the hypothesis test. Usually one estimates the signal strength and in the case of periodic sources, also the duty cycle of radiation, the form of the light curve and the phase(s) of the peak(s). This information can then be compared to the corresponding information from lower energy measurements. The information about the

light curve is obtained from a kernel density estimate (KDE) of the true unknown light curve. These KDE's will be discussed in a later section of this chapter.

2.1. RANDOM SAMPLING

Before searching for a γ-ray signal, one should make sure whether there are any systematic and instrumental errors present in the data. Even if this is not the case, one may still be hampered by unpredictable time structures in the data, which may be due to meteorological changes or a possible time variability of the γ-ray flux. In general terms, these effects refer to the violation of a certain condition in the statistical terminology - the sample drawn is not random - and cannot be treated in the usual way.

Non-randomness can result in false identifications and may also explain why the significance of reports has never exceeded the 5σ level - despite the large data samples obtained, i.e. the 'VHEGRA dilemma' as discussed in Section 1.5. Intrinsic changes in the signal strength cause the data sample not to be identically distributed. Such time structures can be reliably identified by using a modern class of statistical techniques called 'change point procedures' (see Shaban (1980) for a review). Lombard and Schultz (1986) developed a sequential technique to search for changes in the shape of the light curve in the case of low counting statistics. Their technique can be used to identify VHE transients while taking the effective 'number of trials' into account.

Random sampling can be considered as the most fundamental point of departure in Statistics and can be defined as follows:

> Let $x_1, x_2, \ldots, x_n$ be a sample drawn from a common probability density function $f(x)$. The sample is 'random' if and only if:
>
> 1. x_i is independent from x_j for all $i \neq j$ and $i, j = 1, \ldots, n$.

2. and if the probability density function of each x is the same. This means that each x is identically distributed.

■

Thus, with random samples it is not meant that observations are 'uniformly' distributed. An example where condition 1 is violated, is when data samples overlap so that they cannot be treated as independent. However, a violation of condition 2 causes most of the problems: In the case of ON-OFF-region comparisons, the ON- and OFF-source count rates may not differ in the absence of a γ-ray source. In the case of periodic data, condition 2 may be violated when searching for long period pulsars if the time scale for meteorological changes is less than the test period or when non-uniform drifts and glitches in the local clock occur.

2.2. THE ANALYSIS OF DC DATA

In the case of DC sources (where no periodic signature is present) it is compulsory to have the OFF-source data available. In VHEGRA there are many different ways by which a telescope can be operated to register both ON- and OFF-source data (Porter and Weekes, 1978). In this study only drift scans in Right Ascension will be considered, i.e. the telescope is aimed at a fixed region in the sky (before the source) and the source is allowed to drift through the aperture of the telescope so that the data are zenith independent. The total duration of a scan was taken to be 36 minutes. According to De Jager (1985) and De Jager et al. (1986a) the aperture (FWHM) of the mirrors for γ-rays is expected to be 2.2 degrees. If one assumes that the opening function is Gaussian, the standard deviation is 0.9 degrees. A defined ON-source time of 10 minutes corresponds to 82% of the signal. If one rejects the last 3 minutes of the first OFF-region and the first 3 minutes of the second OFF-region, there remains an approximate 1% contribution of the γ-ray signal to each OFF-source region which is negligible. Consequently one is sure that any γ-ray signals are excluded from the OFF-regions. A graphical illustration of a DC drift scan is given in Figure 2.1.

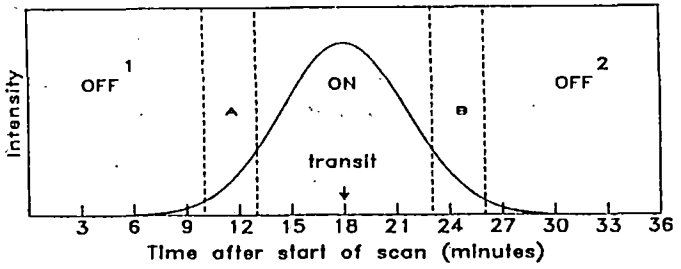

Figure 2.1. A graphical illustration of the assumed Gaussian response function of the telescope for γ-rays. Regions A and B represent the rejected regions.

At this stage it would be informative to summarise some previous approaches towards the analysis of DC-data: Danaher et al. (1981) discussed a method which was followed to identify usable drift scans: (a) The OFF-parts of a scan divided into 120 ten second intervals should obey a Poisson homogeneity test at a confidence level of 99%. (b) The number of counts in the two OFF-regions should not differ by more than 2 Poisson standard deviations. (c) In any 10s interval the count rate should differ from the mean level by less than 4σ. It was found that more scans were rejected than was expected. Dowthwaite et al. (1983) used a three-fold coincidence system and found that the distribution of counts in the OFF region were essentially Poissonian. Consequently they did not have to reject any scans. They also developed a likelihood ratio test to compare the count rates from two regions in the sky. Their method (reviewed by Li and Ma (1983)) has a wide scope of application in γ-ray Astronomy.

The Gini-test (Gail and Gastwirth, 1978) can be used to test whether the time differences in each OFF-region are exponentially distributed. The advantage of this test is that it is bin- and scale-free and is normally distributed for sample sizes as small as 10. It is believed that this test will be able to identify small trends in the count rate which cannot be identified with a test which bins the OFF-source data into 10 second bins. Thus, the Gini-statistic should be used to test whether the OFF-source data are Poissonian distributed. Secondly, it is suggested that the test statistic of Dowthwaite et al. (1983) should be used to compare the count

rates of two OFF-source data sets. Thus, if the count rates in each pair of OFF-source data sets can be confirmed to be identically distributed by means of the Gini- and Dowthwaite et al.'s tests, all the scans can be used to test for a γ-ray signal by means of the same method of Dowthwaite et al.. These two tests will be discussed:

2.2.1. THE GINI-TEST

Gail and Gastwirth (1978) showed that the Gini-test is a powerful scale-free test for exponentiality against a variety of alternatives. The procedure is the following:

Let $v_i = t_{i+1} - t_i$ be the time differences and $v_{(i)}$ be the corresponding ordered sample such that $v_{(1)} \leq v_{(2)} \leq \ldots \leq v_{(n)}$. The statistic

$$G = (g_n - \tfrac{1}{2})[12(n-1)]^{\frac{1}{2}} = {}^{d}(N(0,1)) \qquad (2.1)$$

if v_i is exponentially distributed. The expression for g_n is given by

$$g_n = [\sum_{i=1}^{n-1} i(n-i)(v_{(i+1)} - v_{(i)})]/[(n-1)\sum_{i=1}^{n} v_i]$$

The quoted distribution of G is valid for sample sizes as small as 10. The value of G gives the number of standard deviations, so that one can reject exponentiality for large values of $|G|$. Rejection when $|G| \geq 1.96$ would imply a level of significance of 5%. The reason for the preference of the bin-free Gini-test above a test which bins the data into intervals, is that one does not know on which time scales deviations from exponentiality may occur and because it is also applicable to cases where the sample size is extremely small ($n > 10$). It is proposed that this test should be used for each OFF-source data set. A large number of OFF-source data sets will yield a distribution of G which can be compared with the N(0,1) distribution.

2.2.2. THE UMP TEST FOR EXCESS COUNTS

Consider again a typical drift scan shown in Figure 2.1 where a set of arrival times $t_1, \ldots, t_n$ had been measured ON-source. In the case of true random sampling one can assume that

$$v_i = t_{i+1} - t_i = {}^{d}(\lambda e^{-\lambda v}) \qquad (2.2)$$

which means that the time differences are exponentially distributed. The parameter λ is the count rate so that $1/\lambda = E(v)$ which should be time independent to ensure random sampling. The hypothesis to be tested for the presence of an excess count rate if the background level λ_o is known is

$$H_o: \quad \lambda = \lambda_o$$

$$H_A: \quad \lambda > \lambda_o$$

Since (2.2) belongs to the class of exponential functions, it can be shown through the Neyman Pearson lemma (Hoel, 1971) that the UMP test statistic for H_o against H_A is the estimated ON-source count rate $\hat{\lambda}$ which satisfies

$$\hat{\lambda} = n/t_{on} > C \qquad (2.3)$$

where n is the number of observations within the ON-source time interval t_{on}. One should determine the constant C such that the probability of making a Type 1 error is α. Thus $Pr(\hat{\lambda} > C|H_o) = \alpha$ where α is the level of significance which is usually chosen to be small ($\simeq$ 1% or 5%). If H_A is true, the power $(1-\beta)$ (i.e. the probability of identifying a source if it is indeed present) of the statistic λ is:

$$1-\beta = Pr(\hat{\lambda} > C|H_A) \qquad (2.4)$$

However, since (2.3) is UMP it means that there exists no other test with a power function larger than (2.4) for any excess $\lambda-\lambda_o > 0$. After de-

ciding upon a value for α, one can determine C as follows: Since v is exponentially distributed with parameter λ_o under H_o, it means that $n = \hat{\lambda} t_{on}$ is Poisson distributed with parameter $n_o = \lambda_o t_{on}$ under H_o. The probability to obtain n counts during the time t_{on} is

$$Pr(n;n_o) = n_o{}^n \exp(-n_o)/n!$$

so that the probability of rejecting H_o falsely is

$$Pr(\hat{\lambda} > C|H_o) = Pr(n>n_c|H_o) = \sum_{n=n_c+1}^{\infty} n_o{}^n \exp(-n_o)/n! = \alpha$$

The critical values n_c and $C = n_c/t_{on}$ can then be determined from the above equation. If $n_o > 100$, it follows that n is approximately normally distributed:

$$n = {}^d(N(n_o,\sqrt{n_o}))$$

and the number of standard deviations of n above the background level n_o is

$$S_o = (n-n_o)/\sqrt{n_o} \approx {}^d(N(0,1)) \qquad (2.5)$$

The latter statistic is still used by some γ-ray astronomers. However, (2.5) cannot be used since n_o (or λ_o) is always unknown. The best one can do then is to estimate λ_o by $\hat{\lambda}_o$. Unless the standard error of $\hat{\lambda}_o$ is very small and $n_o > 100$, it is wrong to compute S_o from (2.5). The reason is that the N(0,1) distribution does not apply anymore as Li and Ma (1983) have shown (the latter authors gave a review of many wrong approaches by gamma ray astronomers concerning the evaluation of the significance of a result). Dowthwaite et al. (1983) developed a statistic to evaluate the significance of a signal if λ_o should be estimated. Li and Ma (1983) gave an extensive theoretical treatment of Dowthwaite et al.'s method and showed it to be correct by means of simulations. This procedure works as follows:

Let $a = t_{on}/t_{off}$ be the fraction of the time ON-source with respect to the time OFF-source. Let n_{on} and n_{off} be the number of events

ON-source and OFF-source respectively, so that the total number of events is $n = n_{on} + n_{off}$.

Let n_γ be the excess counts in the ON-region. In this case the hypothesis to be tested is one sided:

$$H_o: \quad n_\gamma = 0 \quad \text{against}$$

$$H_A: \quad n_\gamma > 0$$

The maximum likelihood estimates of n_γ and the expected number of counts ON-source n_b, under H_o and H_A are:

$$H_o: \quad n_\gamma = 0 \; ; \qquad n_b = an/(1+a)$$

$$H_A: \quad n_\gamma = n_{on} - an_{off} > 0 \; ; \quad n_b = an_{off}$$

The authors formed the likelihood ratio statistic

$$S_1^2 = -2 \left(n_{on} \ln\left[\frac{an}{n_{on}(1+a)}\right] + n_{off} \ln\left[\frac{n}{n_{off}(1+a)}\right]\right)$$

which is χ^2 distributed with one degree of freedom under H_o. For $n_\gamma \geq 0$ one has that S_1 is distributed according to the positive side of an N(0,1) distribution. In general one can test for any deviations in the data: By letting $\text{sign}(n_\gamma) = 1$ if $n_\gamma > 0$ and -1 if $n_\gamma < 0$, it follows that

$$S_1 = \text{sign}(n_\gamma)\sqrt{S_1^2} \overset{d}{=} (N(0,1)) \qquad (2.6)$$

In the case of holes, n_b should be > 0 to avoid the cases where $n_{on} = 0$. In this section the case was discussed where the ON-source region is to be compared with a corresponding OFF-source region. However, this method can also be used to compare two OFF-regions with each other, thus establishing randomness for the OFF-regions.

2.2.3. STEPS TO FOLLOW IN THE ANALYSIS OF DC DATA

Only those scans should be used during which there were no clouds seen overhead and when night sky conditions were stable. The individual phototube count rates (scalers) which monitor the NSB are an excellent reference for the status of meteorological conditions during observation times. Let there be k usable scans. The next step will be to reject the mentioned first and last three minutes of the two OFF-regions, leaving two OFF-source and one ON-source region, each with a duration of 10 minutes. Perform the Gini test on the two OFF-source parts of each scan, yielding the numbers G_1 and G_2 for the OFF^1- and OFF^2-regions respectively. Search for significant bursts of data in those OFF-source data sets for which $|G_{1(2)}| > 4$ and take only those spurious events out. Compare the sets of G_1 and G_2 numbers with the expected N(0,1) distribution: This can be done by observing the frequency for which $|G_{1(2)}| > 1.96$ occurs. Only ≈ 5% scans from each OFF-source side should yield Gini-values larger than 1.96. If the latter is found to be true, one can expect the time differences for each OFF-source region to be exponentially distributed. If not, one can either reject those scans which yielded $|G_{1(2)}| > 1.96$, or, if they are kept, it may be necessary to set a stricter level of significance when identifying the source.

The next step will be to compare the count rates of the OFF^1- and OFF^2 regions using (2.6) yielding $S_1(1,2)$. The '(1,2)' implies OFF^1 against OFF^2. One can combine the k scans by computing $\sqrt{k}\,\bar{S}_1(1,2)$. The latter statistic is also N(0,1) distributed: The sum of k, N(0,1) variables yields a $N(0,\sqrt{k})$ distribution. Division by k (to give $\bar{S}_1$) and multiplication by $\sqrt{k}$ yields again the N(0,1) distribution. It is suggested that two further criteria should be met before attempting to test for the presence of a γ-ray signal:

a) The whole data base would be acceptable if $|\sqrt{k}\bar{S}_1(1,2)| < 1.96$.

b) Record the proportion of scans f_1 for which $S_1(1,2) < -1.96$ and f_2 for which $S_1(1,2) > 1.96$. Usually $f_1 = f_2 = 0.025$.

If condition (a) is not met, it may be due to a few scans for which meteorological conditions were not favourable. In such cases condition (b) will also be violated since $f_{1(2)} > 0.025$. One can rightfully reject those scans which yielded abnormally large values of $|S_1(1,2)|$ and re-evaluate $|\sqrt{k}\bar{S}_1(1,2)|$ again. However, if the latter is still unacceptably high, the one OFF-region would be consistently higher than the other OFF-region and one can think of rejecting the whole data base.

Finally, if stability can be verified with a total of say k scans, one can combine the data in two ways to obtain the significance of the γ-ray signal: (a) If the duration of all the scans are identical, one can sum all the OFF-source events and all the ON-source events and calculate the significance $S_1(on,12)$ of the ON-source count rate above the mean OFF-source count rate. (b) If the duration of all scans are not identical, one can calculate $S_1(on,12)$ for each scan and combine all k values through the statistic $\sqrt{k}\bar{S}_1(on,12)$.

If all the mentioned criteria indicate that the data were indeed stable, it may be justified to accept a level of significance of 2 to 3σ as reliable indication of a DC γ-ray signal. If the number of bursts or rejections of one OFF-region is more than expected, or if the excess from the source direction is not consistent with steady emission from the source, a somewhat stricter criterion for source identification must be adopted, e.g. 4σ (Porter and Weekes, 1978).

2.2.4. ESTIMATION OF A DC GAMMA RAY FLUX

If H_o is rejected at a satisfactory confidence level in favour of evidence for γ-ray emission, one can estimate the number of γ-rays $n_\gamma(i)$ for each scan i independently (where $n_{on}(i)$ is the number of ON-source counts, $n_{off}(i)$ is the sum of the number of counts in the two OFF-source regions and $a = t_{on}/t_{off}$):

$$n_\gamma(i) = n_{on}(i) - a n_{off}(i), \quad i = 1, \ldots, k$$

If there were k scans, the mean number of γ-rays per scan at a confidence level of s Guassian standard deviations is

$$n_\gamma = \sum_{i=1}^{k} n_\gamma(i)/k \pm s[(\sum_{i=1}^{k} n_\gamma(i)/k - (\sum_{i=1}^{k} n_\gamma(i)/k)^2)/k]^{\frac{1}{2}} \qquad (2.7)$$

The estimated γ-ray flux for a total observation time of t_{on} per scan ON-source, above a threshold energy of E_o, for a collection area of A, is then

$$F_\gamma(> E_o) = n_\gamma/(t_{on} A) \ (cm^{-2}.s^{-1}) \qquad (2.8)$$

If the significance level is not satisfactory, one can quote a 3σ upper limit for n_γ by using

$$n_{on} = \sum_{i=1}^{k} n_{on}(i), \qquad n_{off} = \sum_{i=1}^{k} n_{off}(i)$$

and estimating that n_γ from (2.6) which results in the rejection of H_o at a 99% confidence level. Using this value of n_γ, one can estimate an upper limit to the γ-ray flux using (2.8).

2.3. THE ANALYSIS OF PERIODIC DATA

The first observation of pulsars in the TeV range came just after their discovery in 1968. Charman et al. (1968) and Fazio et al. (1968) made observations of a few pulsars and they were the first to analyse TeV data for periodicity, using the radio periods known at that time. From the start it became evident that those pulsars which may radiate TeV γ-rays, do so at a flux level which is usually below the sensitivity level of existing Cerenkov experiments. At the time even high energy γ-ray Astronomy had difficulties in detecting a luminous pulsar like the Crab (Vasseur et al., 1971). The latter authors reported 1 to 2σ effects from the Crab using balloon detectors. However, high energy γ-ray Astronomy improved over the years when SAS-2 and COS-B confirmed the Crab and Vela pulsars as strong radiators above $\simeq$ 30 MeV. Unfortunately,

VHEGRA still operates at approximately the same sensitivity levels as 20 years ago.

The basic requirement for a periodic analysis is an accurate timing system such that the timing errors are much smaller than the periods searched for. If a source is to be observed at high energies, it is best to have contemporary measurements of the same source in lower energy regions where the source is luminous enough to permit a reliable estimation of its period parameters. Using these parameters, one can construct a light curve from the TeV data and test it for uniformity.

Unfortunately, there is no rigorous set of rules for analysing TeV data for periodicity due to the uncertainty of the form of VHE γ-ray light curves and the low associated signal to noise ratios. Porter and Weekes (1978) gave a short review in this regard: The phases obtained after the folding of the arrival times with the period parameters, are binned in a histogram. If the light curve and the period parameters are known, the bins at the expected position of the γ-ray pulse corresponds to the ON-region, while the rest of the bins corresponds to the OFF-region. The significance of such an ON-region can be estimated from (2.6). When period or phase variability is considered, the extra independent trials must be taken into account when determining the confidence level of the observed effect.

In this chapter most aspects concerning the analysis of periodic γ-ray data will be covered. In the first case the definition and properties of a γ-ray light curve will be discussed. Thereafter different tests for periodicity will be discussed. The purpose of this is to get a better understanding of the philosophy behind the tests and to select the best test for a given situation. The effect of searching in period will also be covered since it is usually neglected in many cases and has a marked effect on claimed results. In this regard there are two possibilities: Either the period parameters are known due to contemporary measurements, so that one can show that the expected periodicity is indeed present, or, little information about the true period is available, so that one has to search for this periodicity while taking the number of independent trials into account. Finally, attention will be given to estimation

procedures: It will be shown how to estimate a γ-ray light curve in an objective way from the data alone as well as the signal strength and other light curve parameters.

2.3.1. THE NATURE OF GAMMA RAY LIGHT CURVES.

It is Poincarè's theorem (Mardia, 1972) which allows one to test for a periodic signal with period P. For the arrival times of cosmic rays, this theorem can be rewritten as follows:

Let t_i, i = 1, ..., n be a set of arrival times. Since the time difference $t_{i+1}-t_i$ is exponentially distributed, it can be shown that the distribution of the i'th arrival time is a gamma function of the form

$$f_i(t) = \lambda(\lambda t)^{i-1}e^{-\lambda t}/(i-1)! \qquad (2.9)$$

If the spread of t_i (i.e. the standard deviation $(i/\lambda)^{\frac{1}{2}}$) is large relative to the period P, the wrapping of t_i/P around a circle results in the random variable (Mardia, 1972)

$$\theta_i = t_i/P(\mathrm{mod}2\pi) = 2\pi(t_i/P-[t_i/P]) \qquad (2.10)$$

where $[t_i/P]$ is the truncated integer of t_i/P. The random variable θ is then uniformly distributed with probability density function

$$f(\theta) = 1/2\pi, \quad \theta \in [0,2\pi] \qquad (2.11)$$

In the case where $P = 1/\nu$ itself is a function of time, (2.10) can be generalised by the following Taylor expansion:

$$\theta_i = 2\pi(\phi_o+\nu(t_i-t_o)+\tfrac{1}{2}\dot{\nu}_o(t_i-t_o)^2 + (1/6)\ddot{\nu}_o(t_i-t_o)^3) \qquad (2.12)$$

$$= 2\pi[\phi_o + (1/P)(t_i - t_o) - (\tfrac{1}{2}\dot{P}/P^2)(t_i - t_o)^2 + (1/6)(2\dot{P}^2/P^3 - \ddot{P}/P^2)(t_i - t_o)^3]$$

where $\nu_o = 1/P_o$ is the frequency at an epoch t_o, $\dot{\nu}_o$ and $\ddot{\nu}_o$ are the first and second time derivatives of the frequency. The phase offset is given by ϕ_o.

If a periodic γ-ray signal is present with a period P and duty cycle δP (with $0 < \delta < 1$), one has for every pulsed γ-ray

$$t_i = NP + \varepsilon P \tag{2.13}$$

where N is some integer and ε is a random variable with probability density function $f_s(\varepsilon)$ which is determined by the radiation pattern of the source and interstellar scattering. The density function f_s may be quite complicated, i.e. it may be a bimodal density with an interregion component as observed for the Crab and Vela pulsars at γ-ray energies $E_\gamma > 30$ MeV.

Consequently, the density function $f(\theta)$ will be some mixture of (2.11) (due to the isotropic cosmic ray flux) and the density function $f_s(\theta)$ (due to pulsed γ-rays):

$$f(\theta) = pf_s(\theta) + (1-p)/(2\pi) \ , \ \theta \in [0, 2\pi] \tag{2.14}$$

The signal strength p = number of γ-rays/total number of events. Note that $f_s(\theta)$ actually gives the density of the scaled variable $\theta = 2\pi\varepsilon$ to enable the direct application of trigonometric functions to θ.

This brings one to the statistical definition of a light curve in γ-ray Astronomy:

> Let n be the total number of events registered ON source. Let θ be the phase of the light curve and $n^* = \ln(n)$. The differential fraction is then $dn^* = dn/n$ and the function
>
> $$f(\theta) = dn^*/d\theta$$

is called the Radon-Nikodym derivative of n^* with respect to the measure θ. This can be taken as the statistical definition of a light curve. A useful property of $f(\theta)$ is that it is normalised, i.e., ${}_0\int^{2\pi} f(\theta)d\theta = 1$. One can work with $nf(\theta)$ which is then normalised with respect to n and shows the intensity of radiation per unit phase interval directly. ∎

In Section 2.4 it will be shown how one can estimate $f(\theta)$ from the data.

A very important property of any density function on a circle is that it can be rewritten as a Fourier series, due to the inversion formula (Mardia, 1972):

$$f(\theta) = (2\pi)^{-1}[1 + 2\sum_{\ell=1}^{\infty}(\alpha_\ell \cos\ell\theta + \beta_\ell \sin\ell\theta)] \qquad (2.15)$$

provided that $\Sigma||R_\ell||^2$ is convergent where $R_\ell = \alpha_\ell + i\beta_\ell$ is the characteristic function of the ℓ^{th} harmonic with corresponding trigonometric moments:

$$\alpha_\ell = {}_0\int^{2\pi}(\cos\ell\theta)f(\theta)d\theta \quad , \quad \beta_\ell = {}_0\int^{2\pi}(\sin\ell\theta)f(\theta)d\theta \qquad (2.16)$$

The integer values of ℓ refer to all the harmonics. The value $\ell = 1$ refers to the fundamental or first, depending on the terminology used. The statement 'all the power is in the fundamental' implies that $R_\ell = 0$ for all $\ell \neq 1$ while $R_1 \neq 0$. If $R_\ell = 0$ for all values of $\ell \geq 1$, then $f(\theta) = 1/2\pi$, which implies uniformity. One can thus see that all the information of a signal is contained in the characteristic functions $R_\ell = \alpha_\ell + i\beta_\ell$. Fortunately, one can obtain unbiased estimators of (2.16) from the data $(\theta_1, \ldots, \theta_n)$ using (2.10) or (2.12)

$$\hat{\alpha}_\ell = (1/n)\sum_{i=1}^{n}\cos\ell\theta_i \quad \text{and} \quad \hat{\beta}_\ell = (1/n)\sum_{i=1}^{n}\sin\ell\theta_i \qquad (2.17)$$

Then $\hat{R}_\ell = \hat{\alpha}_\ell + i\hat{\beta}_\ell$ and the resultant length of the ℓ^{th} harmonic is given by

$$\bar{R}_\ell = (\hat{\alpha}_\ell^2 + \hat{\beta}_\ell^2)^{\frac{1}{2}} \qquad (2.18)$$

An unbiased estimator of the true resultant length of $||R_\ell||$ is not simply $\bar{R}_\ell$, but rather (Mardia, 1972)

$$(n\bar{R}^2_\ell - 1)/(n-1) = ||R_\ell||^2 \qquad (2.19)$$

The quantity $n\bar{R}^2_\ell$ is also called the Rayleigh power of the ℓ^{th} harmonic.

This knowledge of $f(\theta)$ (from (2.14) to (2.19)) will be used for most tests of uniformity, the estimation of light curves and signal strength estimation. In Section 2.3.2 parametric tests (where $f(\theta)$'s analytic form is used) for uniformity will be discussed, while non-parametric tests (nothing about $f(\theta)$ is assumed) will be discussed in Section 2.3.3.

2.3.2. LIKELIHOOD RATIO TESTS FOR PULSED GAMMA RAY DATA.

The likelihood ratio test (Lehman, 1959) is based on the likelihood principle and has proved to be very successful throughout the statistical literature. Its first application followed in Section 2.2.2. It will be shown how important this test is for periodic VHE γ-ray sources.

Consider the most general parametric representation of (2.14): $f(\theta;p,\underline{\xi}) = pf_s(\theta;\underline{\xi}) + (1-p)/2\pi$ where p is the signal strength and the vector $\underline{\xi}$ contains all necessary parameters which characterises the form and position of $f_s(\theta)$ on the phasogram. In other words, $f(\theta;p,\underline{\xi})$ represents all possible light curves for a certain periodic source. The hypothesis to be tested is

$$H_o: p = 0 \qquad \text{against} \qquad H_A: p > 0$$

which implies a one sided alternative hypothesis since only the 'larger than' sign is involved in H_A. Let $(\theta_1, \ldots, \theta_n)$ again be a random sample. The likelihood function is then

$$L = \prod_{i=1}^{n} f(\theta_i;p,\underline{\xi})$$

The objective is to find those parameters p and $\underline{\xi}$ which maximise L. Let them be $\hat{p}$ and $\hat{\underline{\xi}}$ and let this maximum of L be L_A. If $L_o = (1/2\pi)^n$ is the likelihood value for uniformity, one can form the likelihood ratio L_A/L_o and the null hypothesis will be rejected at a significance level of α if

$$L_A/L_o \geq K_\alpha \tag{2.20}$$

where K_α is a constant depending on α. If the sample size n is large, it follows that $-2\ln(L_A/L_o)$ is χ^2 distributed where the number of degrees of freedom is determined by the number of parameters in $\underline{\xi}$. Usually this test (for large n) will be UMP, but if $f(\theta)$ can be rewritten as a member of the class of exponential functions, this test will always be UMP (Lehman, 1959).

One can obtain all the necessary information from the likelihood ratio test if $f(\theta)$ is specified correctly: One obtains the best estimate of the confidence level, the best estimates of $\underline{\xi}$ and p and their corresponding confidence intervals.

However, VHEGRA is in an unfortunate position: There is no theoretical predictions which give a general form for $f(\theta;p,\underline{\xi})$. Even if this could be done, the numerical problem of finding the optimal solutions $\hat{p}$ and $\hat{\underline{\xi}}$ (even for small sample sizes) would require an unacceptably large amount of computer time.

Due to the difficulties of this test, one is left in the darkness, which may be one reason why one has difficulties with the credibility of TeV γ-ray sources. However, there is one likelihood ratio test which slipped through and is used extensively by some γ-ray astronomers. This test is the well known Rayleigh test (Mardia, 1972) and is easy to apply since $f(\theta)$ contains only two parameters.

2.3.2.1. The Rayleigh Test

Gibson et al. (1982a) introduced this test to VHEGRA and made the point that it tests for power in the fundamental harmonic of the frequency. Statisticians consider this test as one of the most basic tests for uniformity on a circle. The density function which is applicable here is the von Mises density function

$$f(\theta) = (2\pi I_0(\kappa))^{-1}\exp(\kappa\cos(\theta-\mu)) \qquad (2.21)$$

The normalising parameter $I_0(\kappa)$ is the modified Bessel function of the first kind.

This density is closely related to the Gaussian density wrapped around a circle. The von Mises density has the following characteristics:

1. This density is symmetric around the phase μ, so that μ characterises the position of the peak on the circle,

2. the concentration parameter κ is related to the width of the peak, with $\kappa \to \infty$ resulting in a normalised periodic Dirac delta function while $\kappa = 0$ yields a uniform density.

3. The most important contribution of (2.21) to γ-ray Astronomy is the case where κ is small. Then (2.21) is approximately equal to the cardioid density function (Mardia, 1972) which is obtained by writing out the series expansion for (2.21) and neglecting the higher order terms.

$$f(\theta) = (1 + \kappa\cos(\theta-\mu))/2\pi \qquad (2.22)$$

It is easy to prove that (2.15) equals (2.22) if $R_\ell = 0$ for all values of $\ell \neq 1$, so that the statement 'all the power is in the fundamental' is equivalent to the statement 'the light curve is cardioid'. It can also be shown that the cardioid can be rewritten in the form (2.14) if one takes $\kappa = p$. In the language of the astrophysicist, (2.22) is

a sinusoidal wave with a signal strength of ρ (or κ), added to the uniform cosmic ray background. Note the printing error in Mardia (1972) on page 60: Mardia printed $\frac{1}{2}\kappa$ instead of κ in the cardioid density. Consequently one underestimates the signal strength (see Section 2.6) with a factor of 2 if Mardia's expression is used.

The Rayleigh test statistic follows from (2.20) when Neyman Pearson's lemma is applied to the hypothesis

$$H_o: \kappa = 0 \quad \text{against} \quad H_A: \kappa > 0,$$

where no assumption is made about μ. The resulting test statistic is

$$2n\bar{R}^2 = 2n(\hat{\alpha}^2 + \hat{\beta}^2) \tag{2.23}$$

where $\hat{\alpha} = \hat{\alpha}_1$, $\hat{\beta} = \hat{\beta}_1$ and $\bar{R} = \bar{R}_1$ were taken in (2.17) and (2.18). The distribution of $2n\bar{R}^2$ is χ^2_2 if n is large. The p-level for $n > 100$ is then calculated from the Rayleigh formula

$$Pr = Pr(> n\bar{R}^2 | H_o) = e^{-n\bar{R}^2} \tag{2.24}$$

For the sake of graphical illustration it is useful to work with the significance $-\log_{10}(Pr)$, so that

$$-\log_{10}(Pr) = 0.43n\bar{R}^2 \tag{2.25}$$

A value of $-\log_{10}(Pr) = x$ refers to a p-level of 10^{-x}. If $n < 100$, one should compute the p-level using the result of Greenwood and Durand (1955): Let $K = n\bar{R}^2$ be the Fourier power. Then

$$Pr(\geq K | H_o) = e^{-K}(1+(2K-K^2)/4n - (24K-132K^2+76K^3-9K^4)/288n^2$$

$$- (1440K+1440K^2-8280K^3+4890K^4-870K^5+45K^6)/17280n^3) \tag{2.26}$$

This formula can be trusted down to the 10^{-5} level for n as small as 14, but for $n = 7$ it is only accurate down to the 10^{-3} level. It is especially those working with small sample sizes in the PeV region who will find this

formula very useful. Figure 2.2 compares the true significance level (2.26) for some values of $n < 100$ with the Rayleigh formula (2.24) at different values of the Rayleigh power. Thus, for small n and large K one is apt to underestimate the significance (2.25) of a signal if (2.24) is used instead of (2.26) so that the probability of making a Type 1 error is decreased.

There are two cases where the Rayleigh test fails. These are the cases where the data are not distributed according to the von Mises density:

1. If one thinks carefully about (2.21), then $f(\theta)$ yields a very narrow peak for very large values of κ, but no care is taken of a background. As a matter of fact, (2.21) implies a signal strength of 100% in that case, which is never applicable to γ-ray Astronomy. The Rayleigh test is therefor not UMP for a narrow peak plus background and there are better tests in this case (see e.g. Gerardi et al. (1982), Leahy et al. (1983), De Jager et al. (1985) (Paper 1) and Protheroe, 1985)

2. Expression (2.21) is strictly unimodal and no reservation is made for bimodality. On can thus see that the Rayleigh test fails for sources where two pulses are expected. The reason is that the two nearly opposing vectors will cancel each other, so that the resulting distribution of $\bar{R}$ will be nearly consistent with $\bar{R}$'s distribution under H_0. Hence, bimodal light curves will pass by unnoticed if the Rayleigh test is used.

Thus, one can see that κ can act as the duty cycle ($\kappa > 1$) or as the signal strength ($\kappa < 1$). The first result is useless since the background is not taken into account. However, the latter case is useful because many X-ray pulsars seem to emit TeV γ-rays according to the cardioid density (2.22). Although the Rayleigh test was developed as a parametric test, it is also used for non-parametric purposes, e.g. in Power Spectrum Analysis. In the latter case the Rayleigh test gives the amount of power of the fundamental frequency tested.

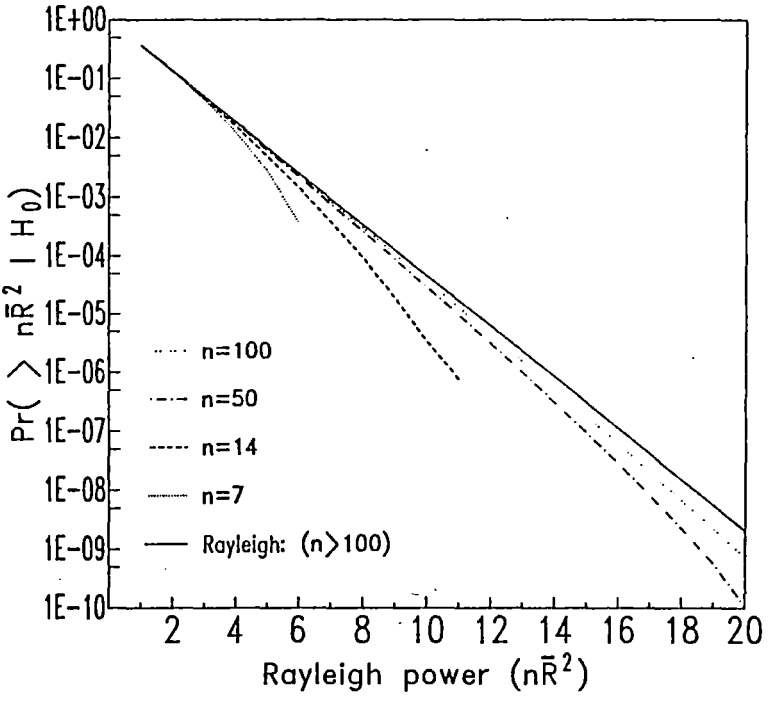

Figure 2.2. A graphical illustration of the correct p-level distribution calculated from (2.26) as a function of the Rayleigh power for various values of n (dotted lines). Also shown (solid line) is the distribution of the Rayleigh power calculated from the χ^2_2 distribution, which is valid for n>100.

In general it is found that not all the power is concentrated in the fundamental and one has to use those tests which take the relevant power in the higher harmonics into account and since it is not always known how to do the latter, it is best to rely on non-parametric procedures.

2.3.3. NON-PARAMETRIC TESTS FOR UNIFORMITY

Tests for which no assumptions about f(θ) are made are called 'non-parametric' and they will be divided into two groups: smoothed and non-smoothed tests. Examples of smoothed tests are Pearson's test and the Z^2_m-test of Gerardi et al. (1982): Pearson's test bins the data into say M bins while the Z^2_m-test considers the first m harmonics in (2.15) as representative of the true light curve. These two tests are similar if one takes M = 2m and narrow structures with widths much less than the resolution of 1/M or 1/2m are smoothed out. Also, broad structures with widths much larger than the resolution are unlikely to be identified with these tests. However, the number of steps necessary to calculate a smoothed test statistic is of the order of the sample size n. Tests which do not smooth are Watson's U^2-test, Kuiper's V_n-test and Protheroe's T_n-test, but the number of steps necessary to calculate one of these statistics is of the order of n^2 since the data have to be ordered. Thus, in terms of computer time, it is preferable to work with smoothed tests. The philosophy behind these tests and their practical applicability to γ-ray data will be discussed.

In the case of non-parametric tests the hypothesis to be tested is similar to the hypothesis of Section 2.3.2:

$$H_o: f(\theta) = 1/2\pi \quad \text{against} \quad H_A: f(\theta) \neq 1/2\pi$$

The Neyman Pearson approach fails to yield a UMP test. One has to examine a few non-parametric tests and determine which test fares best for all possible forms of light curves.

2.3.3.1. The Pearson test

Since the null hypothesis is that of uniformity, it is practice to divide the sample space $[0, 2\pi]$ into M equally wide bins. In this case M acts as a smoothing parameter. The probability to obtain an event in any bin is 1/M if H_o is true. For a sample of size n, the expected number of events in any bin is thus (n/M). Let X_i, i = 1, ..., M be the number of events in the bins. The test statistic is then

$$S_{M-1} = \sum_{i=1}^{m} (X_i - n/M)^2/(n/M) = {}^{d}(\chi^2_{M-1}) \text{ under } H_o \qquad (2.27)$$

This test has the following major disadvantages:

(a) The signs of deviations in (2.27) are not taken into account, so that this test is powerful in showing M/2 oscillations - a kind of light curve which is unlikely to occur if M is large. This difficulty can be solved if the Runs-test is combined with Pearson's test (Eadie et al., 1971, Buccheri, 1985). The Runs-test tests for a dependency of the signs of (X_i-n/M) and will give a small probability if the light curve is source-like (i.e. when the signs are not randomly distributed), thus increasing the power of Pearson's test.

(b) A narrow peak may be divided between two bins, which reduces the power of the test.

(c) The choice of the number of bins M: A good choice is $M \approx 1/\delta$ where δ is the FWHM or duty cycle of a peak. However, since the light curve (2.14) with its parameters is not always known, one cannot make this an a priori choice.

(d) In the case of low values of n/M (< 5), the χ^2_{M-1} distribution does not hold anymore (Hoel, 1971, see also Buccheri et al.,1985). In such cases the probability for Type 1 errors is increased.

2.3.3.2. The Z^2_m-test.

Let $\hat{f}_m(\theta)$ be some density estimator of $f(\theta)$ where m is some smoothing parameter. A general test for uniformity which measures the integrated squared distance between the uniform density and the estimator $\hat{f}_m(\theta)$ is

$$Z^2_m = 2\pi n_o \int^{2\pi} (\hat{f}_m(\theta) - 1/(2\pi))^2 d\theta$$

This test statistic is related to Beran's general class of statistics (Beran, 1969). If $\hat{f}_m(\theta)$ is the truncated Fourier series estimator, which can be constructed by using the Fourier expansion (2.15) of $f(\theta)$, replacing R_ℓ with its estimator $\hat{R}_\ell$ in (2.17) and including all the harmonics for ℓ = 1, 2, ..., m, while neglecting all the higher harmonics (ℓ = m+1, ..., ∞), then

$$\hat{f}_m(\theta) = (1+2 \sum_{\ell=1}^{m} (\hat{\alpha}_\ell \cos\ell\theta + \hat{\beta}_\ell \sin\ell\theta))/2\pi \qquad (2.28)$$

and the test statistic reduces to

$$Z^2_m = 2n \sum_{\ell=1}^{m} (\hat{\alpha}_\ell^2 + \hat{\beta}_\ell^2) \qquad (2.29)$$

which was first applied to γ-ray data by the COS-B collaboration (Buccheri et al., 1983). If m is kept fixed, then $Z^2_m \overset{d}{=} (\chi^2_{2m})$ for n > 100. This test shares disadvantage (a) of Pearson's test, in the sense that this test will also be powerful for m oscillations, while one expects only a few source-like peaks to be shown even if m is large. The largest difficulty is the fact that the form of the light curve is not known a priori, so that one either oversmooths or undersmooths the data with a specific choice of m. In Section 2.5 it will be shown how this problem can be dealt with.

However, the advantages of Z^2_m over Pearson's test are important: This test statistic is not dependent on a bin width, so that the danger of splitting a peak between two bins is non-existent. The next advantage is that the distribution of Z^2_m is known even for very small sample sizes. Gerardi et al. (1982) showed this important feature for n > 100 by means

of simulations. For $n < 100$ the distribution of Z^2_m can be determined as follows: Let the Rayleigh power of the ℓ^{th} harmonic be

$$n\bar{R}^2_\ell = n(\hat{\alpha}_\ell^2 + \hat{\beta}_\ell^2) = K_\ell$$

The p-level for each harmonic ℓ can be calculated from (2.26) for any $n > 7$:

$$Pr_\ell = Pr(> K_\ell | H_o)$$

which is valid for all values of $\ell \geq 1$, since $n\bar{R}^2_\ell$ are random variables for all values of ℓ under H_o (Mardia, 1972). Then, under H_o, the statistic (Eadie et al., 1971)

$$-2\ln\left(\prod_{\ell=1}^{m} Pr_\ell\right) = {}^{d}(\chi^2_{2m}) \qquad (2.30)$$

This result is especially useful for PeV astronomers where n is usually small.

2.3.3.3. The Kuiper- and Watson tests.

A complete description of these two tests is given by Mardia (1972). In Paper 1 the relevance of these tests with respect to VHEGRA were discussed. Both these tests differ from the previous mentioned tests in the sense that the cumulative distribution function $F(\theta)$ is tested for uniformity:

$$H_o: F(\theta) = \theta/2\pi \quad \text{against} \quad H_A: F(\theta) \neq \theta/2\pi$$

The sample cumulative distribution function $F_n(\theta)$ is used as an estimate of $F(\theta)$. In the previous cases the density function $f(\theta) = 1/2\pi$ was tested. Since no smoothing is present, one would expect these tests to be more powerful on average than the Pearson- and Z^2_m-tests.

In the case of Kuiper's test, the minimum and maximum deviation of $F(\theta)$ from $\theta/2\pi$ is searched, so that this test will be more powerful for narrow peaks. Watson's test statistic is formed by taking the mean squared distance between $F_n(\theta)$ and $\theta/2\pi$ over the whole phasogram, so that this test is better for broader light curves. These effects are illustrated in Figure 2.3.

The problem with these tests is that one needs to order the phases from small to large so that $\simeq n^2$ steps are necessary to compute the value of the statistic which is undesirable if n is large.

2.3.3.4. The Protheroe test

Protheroe (1985) proposed the test statistic

$$T_n = 2[n(n-1)]^{-1} \sum_{m=1}^{n-1} \sum_{k=m+1}^{n} (\Delta_{mk} + 1/n)^{-1} \qquad (2.31)$$

where

$$\Delta_{mk} = 0.5 - |[|\phi_m - \phi_k| - 0.5]| \qquad (2.32)$$

and $\phi_i = \theta_i/2\pi$ for all events $i = 1, \ldots, n$

Protheroe also tabulated the critical values of this test statistic for different confidence levels and values of n. However, (2.31) forms part of the general U-statistic of Hoeffding (1948). Hoeffding showed that the U-statistic is asymptotically normally distributed, so that (2.31) may be easier to implement on a computer for $n > n'$ where n' is a large number (still unknown) such that the normality property holds for $n > n'$. However, there are still some difficulties:

1. Due to the somewhat difficult form of (2.32), the asymptotic normality property of T_n's distribution may start at large values of n. Expe-

rience with Figure 2.3 showed that normality sets in for $n' > 300$ and it is thus difficult to calculate p-levels for $n' \leq 300$.

2. The number of steps necessary to construct (2.31) is proportional to n^2, so that it would be time consuming for a computer if n is large.

3. This test statistic is also sensitive to a lot of narrow peaks on the phasogram, which is unwanted.

4. In the case of broad peaks, its power diminishes rapidly.

See Figure 2.3 for a comparison of Protheroe's test with other tests for uniformity. It is clear that this test is very powerful for small duty cycles.

2.3.4. SELECTING THE BEST TEST FOR UNIFORMITY

Even if one could specify the parametric equation of $f(\theta)$ for H_A, a likelihood ratio test would be difficult to run on a computer. However, one simple likelihood ratio test is the Rayleigh test which is useful in identifying broad sinusoids, when applied to γ-ray Astronomy. Since it is not known a priori what the form of $f(\theta)$ will be, one has to select the best non-parametric test, or, combine two tests which are sensitive to a broad and narrow peak.

Quesenberry and Miller (1977) compared a number of non-parametric tests and recommended Watson's test as a general test for uniformity. Unfortunately the statisticians never compared tests, using the type of densities obtained in γ-ray Astronomy. The first attempts in this regard came from astrophysicists: In reply to the paper of Gibson et al. (1982b), Leahy et al. (1983) compared Pearson's test to the Rayleigh test and found that Pearson's test is more powerful in detecting narrow peaks while the Rayleigh test is best in detecting broad peaks and sinusoids. Other power studies were done in Paper 1 and by Protheroe (1985). The

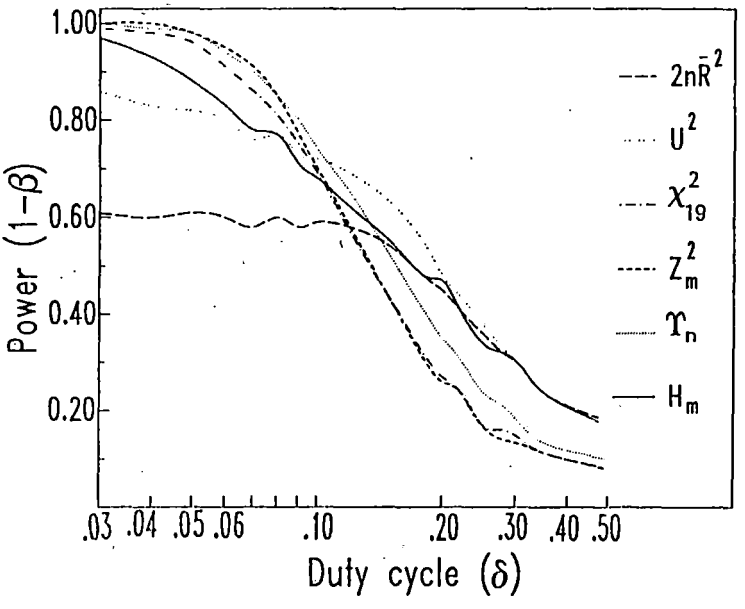

Figure 2.3. (Adapted from Paper 1). The power curve (1 - β) as a function of the duty cycle for different tests for uniformity: The Rayleigh ($2n\bar{R}^2$), Watson's (U^2), Pearson's (χ^2 with 20 bins), Z^2_m (m=10), Protheroe's (T_n with n = 300) and the H_m-test. The alternative density is a Gaussian peak, mixed with a uniform density. The signal strength is 0.1 and the sample size is 300. The level of significance was taken to be 0.05.

results of Paper 1 agreed with those of Leahy et al., but it was also shown that Watson's test is the best general test for duty cycles larger than ≈ 10%. Protheroe made a similar comparison, but showed that his T_n statistic is more powerful than the Rayleigh-, Kuiper-, Watson- and Z^2_2-tests for narrow peaks.

The Rayleigh test is best for sinusoids as mentioned before. The Watson test is best for duty cycles larger than 0.1 while its power seems to equal the power of the Rayleigh test even for sinusoids. According to Figure 2.3 the Z^2_m test is slightly more powerful than Pearson's test with M bins for narrow duty cycles if one lets m = M/2. However, in certain cases Pearson's test with M bins may beat the Z^2_m-test if one chooses a bin position such that the number of pulsed events in one bin is maximised. The latter is discouraged since the Type 1 error rate will increase due to subjective rebinning. The other mentioned disadvantages of Pearson's test and the advantages of the Z^2_m test makes the latter the preferred test. The Z^2_m-test is most sensitive to duty cycles of $\delta = 1/(2m)$.

Protheroe's test seems to be very promising: Its power equals that of the Z^2_{10}-test for $\delta < 0.1$, while its power increases relative to those of Pearson's χ^2_{19}- and the Z^2_{10}-tests for $\delta > 0.1$. Thus, Protheroe's test is more powerful than the other two mentioned tests for deviations of δ from 0.05. However, its power is still smaller than those of the Watson- and Rayleigh tests for large values of δ. The power curve of the H_m-test statistic will not be discussed at the moment, since one first needs to understand the theory of Section 2.4. The derivation of the H_m-statistic and its properties will be discussed in Section 2.5.

The problem in VHEGRA is that one does not always know a priori which kind of light curve to look for. In the case where one tries to confirm another's result which was obtained at the correct radio or X-ray period, the known light curve can be used to decide upon a test statistic. However, if one searches for TeV γ-rays from a new pulsar or wants to confirm a result for which the true period was not known exactly, one has a problem. The logic consequence is to start with one test. If it fails, one switches to another, etc. Be careful: there is a danger to this kind of practice. These efforts tend to raise the Type 1 error rate, or,

in the language of the astrophysicist, he will get more false detections than expected. Unfortunately, very little literature exists on this subject and the only reference to this problem is by Gans (1984). The statement made by Gans is important: If one rejects H_o at the 1% level of significance, one may use three independent tests and stop with one which gives a p-level less than 1%. However, this aspect needs some attention. In this thesis it is suggested that the H_m-test and the Rayleigh test (see e.g. Protheroe, 1987) should be used is nothing is known a priori about the light curve. In Section 3.2 PSR 1509-58 will be identified with the H_m-test and it is doubtful whether this identification could have been done with most other known tests.

2.3.5. SEARCHING IN PERIOD

Periodicity searches are easy to conduct but difficult to evaluate: The main question being how to quantify the significance of an effect considered to be positive. This evaluation is basically done by evaluating the number of independent trials (also called the 'degrees of freedom' by γ-ray astronomers) conducted before the positive effect was found.

In this evaluation the concept of an independent Fourier spacing (IFS) plays an important role and is well known in terms of the frequency domain in the field of time series analysis. It can be defined as follows:

> Let T be the total length of a data sample and let ν_1 and ν_2 be two frequencies. These frequencies are independent if
>
> $$\nu_2 - \nu_1 = x/T \quad , \; |x| \geq 1 \tag{2.33}$$
>
> The value of $|x| = 1$ corresponds to one independent Fourier spacing (IFS) and the set of frequencies spaced 1/T from each other are independent.

■

In the time domain x IFS between the periods P_1 and P_2 is given by the following (using (2.33)):

$$P_1 - P_2 = xP_1P_2/T$$
$$= xP_1^2/(T+xP_1) = xP_2^2/(T+xP_2) \qquad (2.34)$$

and the number x of IFS searched in the period range from P_1 to P_2 is

$$x = (1/P_2 - 1/P_1)T \qquad (2.35)$$

The uncertainty or resolution in the period of any significant radiation found at a specific period is usually one IFS, but depends on the test used. However, certain situations occur where the behaviour of the radiation has to be investigated within one IFS. The influence of such a search on the light curve and significance of the result should be known accurately for each test used. No literature is available on these effects and in the following it will be discussed in detail:

a) It should also be known how the light curve changes when the arrival times are folded at a period which is slightly different from the true period.

b) Due to practical considerations one can plan an experiment so that the known uncertainty in the period is of the same order of, or less than one IFS. However, if the uncertainty is much larger than one IFS, one has to search through many independent periods. A large number (say k) of independent trial periods searched through may cause a significant result to be decreased according to the relation $1-(1-Pr)^k$, where Pr is the p-level obtained for the one apparent significant period.

c) The usual assumption that the number of independent trials equals the number of IFS included in a periodicity search is however false when searches are conducted within an IFS.

In the following the effect on a test statistic and the light curve will be investigated, when the period is shifted with a fraction of x IFS from its true value.

Consider again a data set (see (2.13)) with underlying period P_o such that k_o intervals of length P_o can fit into the total time span T (= $t_{k_o}-t_1$):

$$t_i = iP_o + \varepsilon P_o \qquad , i = 1, \ldots, k_o = T/P_o$$

where i is the total integer number of pulsar rotations within the time (t_i-t_1) and $\theta = 2\pi\varepsilon$ is distributed according to the source function $f_s(\theta)$. Thus, the only contribution to the light curve itself is due to the distribution of ε.

Consider a shift of x IFS from P_o, such that the new period calculated from (2.34) is

$$P = k_o P_o/(k_o+x)$$

Since the trigonometric functions are invariant to additions of multiples of 2π, one may use the wrapped times:

$$\theta_i = 2\pi t_i/P = 2\pi(i+\varepsilon)(k_o+x)/k_o$$

$$= 2\pi(i + xi/k_o + \varepsilon + \varepsilon x/k_o)$$

$$\simeq 2\pi(i + xi/k_o + \varepsilon) \qquad \text{if } \varepsilon x << k_o$$

Approximations of the trigonometric moments can now be formed, which enables one to estimate the mean value of some test statistics. Consider the trigonometric moments of the ℓ^{th} harmonic from (2.17):

$$\hat{\alpha}_\ell = (1/k_o)\sum_{i=1}^{k_o} \cos\ell\theta_i = (1/k_o)\sum_{i=1}^{k_o} \cos 2\pi\ell(\varepsilon + xi/k_o)$$

$$\hat{\beta}_\ell = (1/k_o)\sum_{i=1}^{k_o} \sin\ell\theta_i = (1/k_o)\sum_{i=1}^{k_o} \sin 2\pi\ell(\varepsilon + xi/k_o)$$

Their approximate mean values are calculated by replacing $\ell x(2\pi i/k_o)$ with the variable $\ell x\omega$ and averaging the moments over ω from 0 to 2π. The averaging over ε is done independently by assuming a specific form for $f_s(\theta)$ in (2.14). If $f_s(\theta)$ is taken as the wrapped normal distribution with mean zero and variance σ^2, the moments are

$$\alpha_\ell = p\sin(2\pi\ell x)\exp(-\tfrac{1}{2}\ell^2\sigma^2)/(2\pi\ell x)$$

$$\beta_\ell = p(1-\cos(2\pi\ell x))\exp(-\tfrac{1}{2}\ell^2\sigma^2)/(2\pi\ell x)$$

so that the expected value of the Fourier power of the ℓ^{th} harmonic is given by

$$E(n\bar{R}^2_\ell) = 2(n-1)p^2(1-\cos(2\pi\ell x))\exp(-\tfrac{1}{2}\ell^2\sigma^2)/(2\pi\ell x)^2 + 1$$

where p is the signal strength.

With these analytic expressions for α_ℓ, β_ℓ and the Fourier power, one can determine the behaviour of light curves and those test statistics which make use of the Fourier power, for various duty cycles when the period is gradually shifted away from the true period.

Figure 2.4 illustrates the behaviour of a light curve with $\delta = 0.05$: It is evident that a slight change of x from zero results in a rapid smearing out of the light curve. This effect is reflected by the behaviour of the Z^2_{10}-test - a test which is powerful for narrow duty cycles: For this test $-\log_{10}(Pr)$ has a well defined maximum at $x = 0$ (see Figure 2.5), but drops rapidly when $x \neq 0$. However, for the Rayleigh test $-\log_{10}(Pr)$ is much smaller at $x = 0$ than the corresponding value of the Z^2_{10}-test. Furthermore, in contrast to the behaviour of the Z^2_{10}-test, the value of $-\log_{10}(Pr)$ drops more gradually for the Rayleigh test when $x \neq 0$.

In Figures 2.6 and 2.7 the same is illustrated, but for a signal strength of $3/\sqrt{n}$ and a duty cycle of 30%. For this kind of light curve the Rayleigh test is expected to perform best. Some interesting features can be seen: The light curve and its amplitude does not change drastically when x differs little from zero. This is also reflected in Figure 2.7 where one

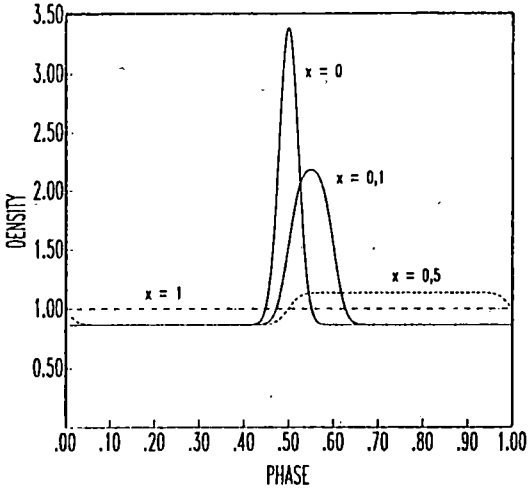

Figure 2.4. The expected behaviour of a light curve with $\delta = 0.05$, $n = 500$ and $p = 2/\sqrt{n}$ for different IFS (x) from the true period.

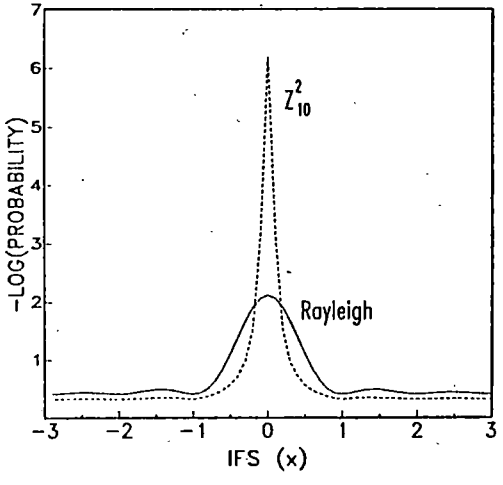

Figure 2.5. The expected behaviour of the Z^2_{10}- and Rayleigh test statistics for various IFS (x) from the true period. The light curve parameters correspond to those of Figure 2.4.

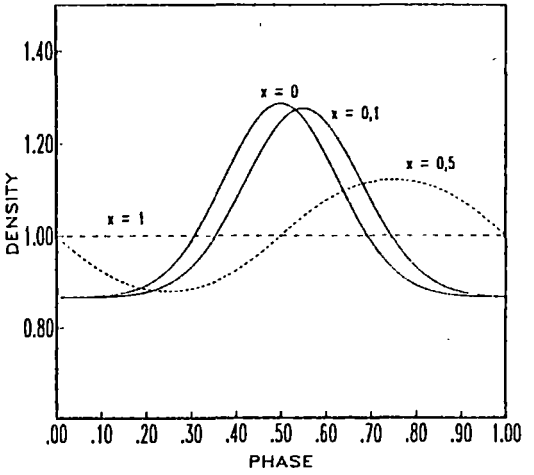

Figure 2.6. The behaviour of a light curve with 30% duty cycle, n = 500 and p = $3/\sqrt{n}$ for various IFS (x) from the true period.

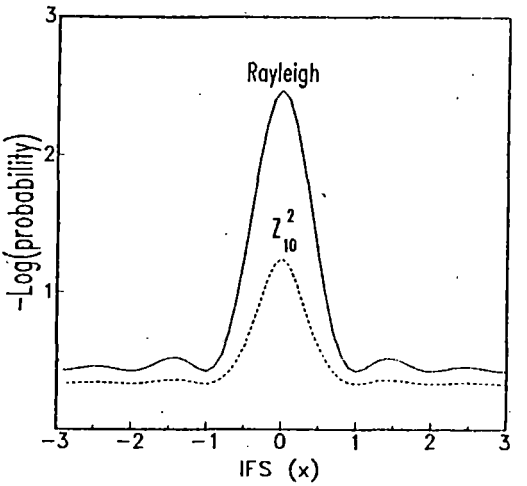

Figure 2.7. The behaviour of the Z^2_{10}- and Rayleigh statistics for various IFS (x) from the true period. The light curve's parameters correspond to those of Figure 2.6.

can see that the resolution of the periodicity is not very well with the Rayleigh test, but the value of $-\log_{10}(Pr)$ is higher for this test than the corresponding value for the Z^2_{10}-test.

From Figure 2.4 and 2.6 one can see that a shift of x results in a peak walk of x/2 on the phasogram. In general, a shift from x = 0 to |x| = 1 results in a peak walk of half a period while the amplitude of the peak diminishes to zero at |x| = 1, so that $-\log_{10}(Pr)$ reduces to a value which is consistent with the distribution of the test statistic under H_o.

Therefore, not only light curve deformation, but also phase shifts occur when the wrong periods are used. If fluctuations create an effect such that the maximum of the statistic is at the wrong period, these effects may result in a wrong interpretation of the results. From Figure 2.5 it is clear that $-\log_{10}(Pr)$ drops rapidly to nearly zero within $|x| < 0.3$ for small duty cycles when a test is used which is sensitive to such narrow peaks. From this and Figure 2.7 one learns that the period resolution is better for narrow peaks than for broad peaks. Consequently one has to conduct more trials per IFS for narrow peaks than for broad peaks to avoid missing a peak.

If the true period is known exactly from contemporary measurements at other wavelengths, such that its error corresponds to an $x \ll 1$, then one should fold the arrival times at that period only. If the uncertainty in the period is ΔP, one should search within that period interval ΔP, allowing a possible extension of at most one IFS at the endpoints of that interval. The method is then to search for the maximum S_{max} of the statistic S within the assumed interval. Let this interval correspond to a shift of x IFS. If a search is conducted within x IFS, where the step length from one period to the next one is an integer number of IFS, the p-level for the x equiprobable periods is

$$1 - (1 - Pr(> S_{max}|H_o))^x \approx xPr(>S_{max}|H_o) \qquad (2.36)$$

The latter assumption is valid if $Pr(> S_{max}|H_o) \ll 1$.

The situation is changed drastically when the search is not limited to integer step lengths in x, but when the maximum value S_{max} of a test statistic S is searched after a number of periods were tested within one or more IFS. There is no literature known on this subject in the case of low counting statistics (i.e. when the period $P < \lambda^{-1}$ where λ is the count rate). It is difficult to study this problem analytically and a few cases will be investigated by means of simulations:

Consider a time series of n events with a duration of T and a reference period P_o such that $P_o << T$. Consider also a search strategy such that k periods are tested within one IFS. The purpose is then to find the real p-level Pr' which will be related to the classical p-level Pr via the effective number of trial periods x^* or the factor of underestimation r according to

$$Pr' = 1 - (1-Pr)^{x^*} = rPr \quad \text{with } x^* \text{ and } r \geq 1 \tag{2.37}$$

Clearly, when $Pr \to 0$, $x^* \to r$. In fact r will be dependent on Pr and a number of parameters

$$r = r(Pr;n,x,S,k) \tag{2.38}$$

It is expected that r will converge to some value ≥ 1 if $k \to \infty$. It will require an enormous amount of computer time to determine r for different values of n, x, k and tests statistics S. Furthermore, $\approx 10^5$ simulations per set of parameters are necessary to determine r for Pr' down to the 10^{-4} level. To illustrate this effect a number of cases will now be discussed:

Exponentially distributed arrival times with a count rate of 1 s^{-1} and a total observation time of 200 s (thus n = 200) were simulated 10^6 times. The maximum value of the Rayleigh and Z^2_{10} statistics were searched within one, two and ten IFS around a reference period of 0.1 s (thus $P_o << T$). The ratios r for k = 20 are plotted in Figure 2.8 for the Rayleigh test and in Figure 2.9 for the Z^2_{10} test. In the case of x = 2 and 10 the p-levels were already corrected with (2.36). One would expect then that the three curves on a graph would lie on each other, but

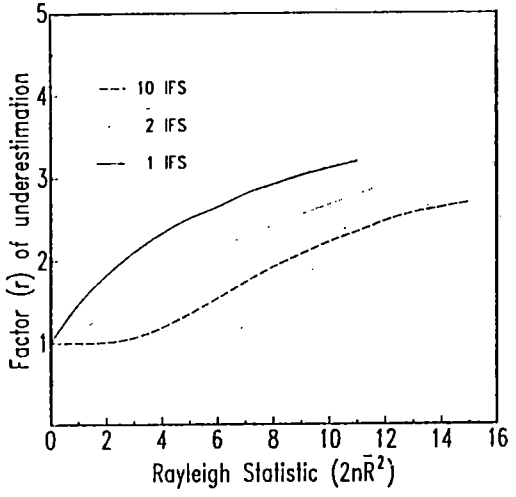

Figure 2.8. The factor of underestimation of the p-level for the Rayleigh test for different values of $2n\bar{R}^2$. The curves for searches within 2 and 10 IFS were already corrected with (2.36) using x = 2 and x = 10 respectively.

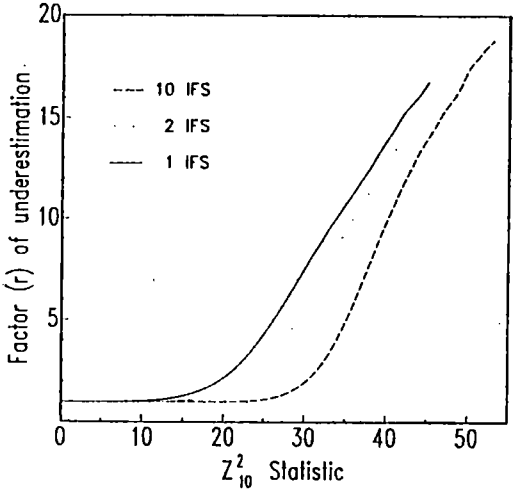

Figure 2.9. The factor of underestimation of the p-level for the Z^2_{10} test. The modus operandi here is similar to that for Figure 2.8.

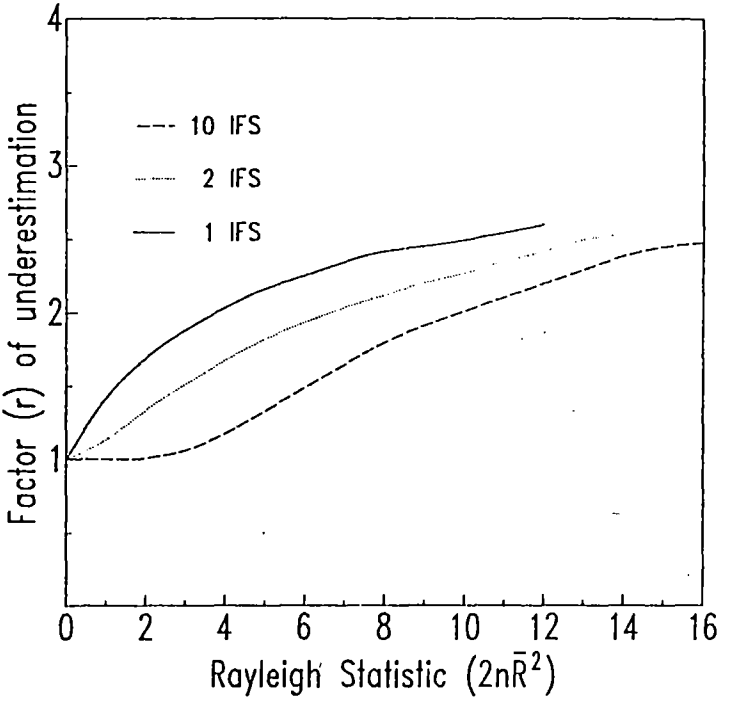

Figure 2.10. The factor of underestimation of the p-level of the Rayleigh test but only for K = 4 steps within one IFS. The modus operandi is further similar to that of Figure 2.8.

this does not seem to be the case: For $x \to \infty$ it seems as if $r \to 1$ so that (2.36) becomes sufficient to evaluate the real significance of a result - independent of the number of steps k conducted within each IFS. However, when a search is conducted within a few IFS, one should be careful when evaluating a result: For $x = 1$ one obtains $r \approx 3$ for large values of the Rayleigh statistic while $r \approx 20$ for the Z^2_{10}-test. In the latter case r depends strongly on the value of Z^2_{10}.

When investigating Figures 2.5 and 2.7, one can see that k should be large when searching for narrow peaks with the Z^2_{10} statistic, but when searching for broad peaks with the Rayleigh test, k need not be that large. One should then also know how (2.38) behaves for small k. In Figure 2.10 the effect of a search with the Rayleigh test within one, two and ten IFS is illustrated for four steps within one IFS (i.e. $k = 4$). One can see that this figure resembles Figure 2.8 closely, i.e. the factor of underestimation decreases if x increases, after (2.36) has been taken into account. However, the factor of ≈ 3 (for $x = 1$) mentioned previously for Figure 2.8, decreased to ≈ 2.5 which is expected: With smaller values of k one is less likely to sample S_{max}.

It is suggested that any researcher should simulate the situation applicable to his own observations to estimate Pr' from Pr. A factor of 3 may be considered as negligible for a single observation. However, when many such results are combined, the ratio r will accumulate, which may prove an apparent significant result to be insignificant (see Section 3.3 for such an example).

2.4. THE ESTIMATION OF LIGHT CURVES

The first step in γ-ray data analysis is hypothesis testing. If one feels satisfied with the obtained confidence level of the test, the next step would be to estimate the light curve and its corresponding parameters. However, the process of estimation is sometimes closely linked with the process of testing. The clearest example of this is the binned histogram

which is an estimate of a light curve while the same light curve is used to calculate Pearson's statistic. The same is also applicable to the Z^2_m-test which is obtained from the Fourier series estimator as illustrated in Section 2.3.

The classic way to estimate a light curve is by means of the histogram. There are the following objections to the use of the histogram:

1. The true light curve barely resembles a 10 or 20 bin histogram.

2. Information within one bin is lost.

3. The choice of the bin width and -position is critical and there is no automatic data based choice for the bin width available yet.

The so-called kernel density estimator (KDE) is therefore introduced to overcome these difficulties. The whole problem of light curve estimation was discussed by De Jager et al. (1986b) (hereafter Paper 2). Only the main aspects will be given here. At first some background on error measures will be given before the KDE is formally introduced. Then the important smoothing parameter will be discussed. A method will also be discussed to construct confidence intervals and -bands for the KDE. Examples of the KDE applied to the COS-B data on Vela pulsar ($E_\gamma > 50$ MeV) will also be given.

2.4.1. SOME ERROR MEASURES OF DENSITY ESTIMATORS

Any density estimator (histogram or kernel) can be denoted by $\hat{f}_h(x;\underset{\sim}{X})$ where $\hat{f}$ refers to the estimator of f and h to the so called smoothing parameter (in the case of a histogram h is the bin width) and $\underset{\sim}{X} = x_1, \ldots, x_n$ is the sample of size n which is used to construct the estimator. The mean squared error (MSE) of an estimator is considered by most statisticians as the best measure of the error and it can also be easily

manipulated mathematically. The MSE for any density estimator in any point x is defined by

$$MSE(x) = E(\hat{f}_h(x;\underset{\sim}{X}) - f(x))^2 \qquad (2.39)$$

$$= [E\hat{f}_h^2(x;\underset{\sim}{X}) - (E\hat{f}_h(x;\underset{\sim}{X}))^2] + [E\hat{f}_h(x;\underset{\sim}{X}) - f(x)]^2$$

$$= \text{variance} + (\text{bias})^2$$

and consists of the well known variance and less known bias terms. Since the square is taken, large deviations become dominant.

The variance indicates fluctuations while the bias can be described as a consistent shift on average of an estimator in a certain direction away from the true value. Scientists seem to be more concerned about the variance than the bias. The reason may be that the variance can be calculated independently of f(x), but not the bias. If $n \to \infty$, both the variance and bias will decrease to zero as the smoothing parameter is decreased to zero in accordance to (2.43). Only in this case will $\hat{f}_h(x;\underset{\sim}{X})$ converge to the true f(x) for all values of x.

A global measure of the error of an estimator is the mean integrated square error (MISE). Integration of (2.39) leads to

$$MISE = \int_0^\infty MSE(x)dx = \int_0^\infty E(\hat{f}_h(x;\underset{\sim}{X}) - f(x))^2 dx \qquad (2.40)$$

The MISE is thus independent of x and gives a single number which is representative of the global performance of $\hat{f}_h(x;\underset{\sim}{X})$. This MISE will play an important role in the following sections. The main aim is to find that h (say h^*) which minimises the MISE for a given data set $\underset{\sim}{X}$. In this case h^* refers to the averaged value over the whole range of x. If one finds that h which minimises the MSE(x) in each point x, h^* will be a function of x. This will give large values of $h^*(x)$ in regions where f(x) changes very slowly with x, but small values of $h^*(x)$ if f(x) shows a very narrow peak at other values of x. This is certainly an improvement on the scheme of finding a single compromising value of h^* from (2.40) for the whole

range of x values. This is beyond the scope of this thesis but should be investigated in future.

2.4.2. KERNEL DENSITY ESTIMATORS (KDE)

The KDE is actually a general moving average procedure and it has certain desirable and optimal properties which is not shared by the classical moving average. For example, the problem with the moving average is the choice of the window-width h. This problem is well known amongst all physicists. This technique is also analogous to the well developed low pass filter technique in Fast Fourier Transforms. However, it will be shown how this very important smoothing parameter can be obtained in an objective way from the data alone without any a priori knowledge. Although the KDE estimates the true light curve with a smooth function such that the MISE is a minimum, one can use other types of analysis procedures complementary to the KDE. The purpose will be to shed more light on specific structures present in the light curve, which may have been smoothed out by a smoothing parameter which is slightly wider than the apparent narrow structures present. The mathematical-statistical concept of the KDE was introduced by Rosenblatt (1956) and Parzen (1962). It is the weighted average over the distribution function $F_n(x)$ of the sample.

The concept of the KDE can be developed as follows: Let $\underset{\sim}{X} = x_1, \ldots, x_n$ be a random sample with probability density function $f(x)$ where x is the random variable on the real line. Let h be the smoothing parameter. The KDE in any point $x \in (-\infty,\infty)$ is given by

$$\hat{f}_h(x,\underset{\sim}{X}) = (1/n)\int_{-\infty}^{\infty} K((x-y)/h)dF_n(y) = (1/nh)\sum_{i=1}^{n} K((x-x_i)/h) \quad (2.41)$$

Here K is the kernel function (evaluated in the point $(x-x_i)/h$) which does the weighting. This function will be assumed to satisfy the following conditions (Swanepoel, 1987):

Table 2.1. Examples of kernel functions and related parameters.

Name of kernel function	Kernel function K(x)	positive/ negative	Fourier transform k(u)[2]	r	k_r	MISE[3] / A	relative[4] CPU time	$\int_{-\infty}^{\infty} K^2(y)dy$
Naive	$\frac{1}{2}$, $\lvert x\rvert \le 1$ 0, $\lvert x\rvert > 1$	+	$\frac{\sin u}{u}$	2	$\frac{1}{6}$	0,463	10^{10}	0.5
Picard	$\frac{1}{2} e^{-\lvert x\rvert}$	+	$(1 + u^2)^{-1}$	2	1	0,948	10^{5}	0.5
Normal	$(2\pi)^{-\frac{1}{2}} e^{-\frac{1}{2}x^2}$	+	$e^{-\frac{1}{2}u^2}$	2	$\frac{1}{2}$	0,454	7	0.282
Epanechnikov	$\frac{3}{4}(1-t^2)$, $\lvert t\rvert \le 1$ 0 , $\lvert t\rvert > 1$	+	$\frac{3}{u^2}\left(\frac{\sin u}{u} - \cos u\right)$	2	$\frac{1}{10}$	0,437	10^{10}	0.6
Fourier integral estimate	$\frac{\sin x}{\pi x}$	+/-	1 $\lvert u\rvert < 1$ $\frac{1}{2}$ $\lvert u\rvert = 1$ 0 $\lvert u\rvert > 1$	-	-	-	~ 6	-
Swanepoel	$\frac{1}{2}(\sin\lvert x\rvert + \cos x)e^{-\lvert x\rvert}$	+ +/-[1]	$\frac{4}{4 + u^4}$	4	$\frac{1}{4}$	0,436	316	0.375

(1) The Swanepoel kernel allows only slight negativity.

(2) $k(u) = \int_{-\infty}^{\infty} \exp(-iuy)K(y)dy$ with $u = h\ell$

(3) $A = \left(\int_0^{2\pi} (f^{(r)}(\theta))^2 d\theta\right)^{1/(2r+1)} n^{-2r/(2r+1)}$

(4) The relative CPU time is defined as the number of terms ℓ necessary for $k(h\ell)$ to decrease to 10^{-10} level if $h = 1$.

(i) K is a bounded density function, symmetric around zero, with support on the interval $[-\omega,\omega]$ for some constant $\omega > 0$ which can be infinity.

(ii) The variance of K should be finite: $0 \leq \int_{-\omega}^{\omega} y^2 K(y)dy < \infty$.

Table 2.1 lists some well known kernel functions. Among them are the well known square wave (naive) and normal density functions. More important than this is the choice of the smoothing parameter h. The choice of this parameter is very critical and ensures the most important 'consistency' property of the KDE - i.e., the KDE should converge to the true unknown density f(x) with a probability of one when the sample size increases to infinity:

$$\lim_{n\to\infty} E(\hat{f}_h(x;\underset{\sim}{X})) = f(x) \qquad x \in (-\infty,\infty) \tag{2.42}$$

if the smoothing parameter h(n) is chosen as a function of n such that

$$\lim_{n\to\infty} h(n) = 0 \quad \text{and} \quad \lim_{n\to\infty} 1/nh(n) = 0. \tag{2.43}$$

Thus, consistency can be obtained if the smoothing parameter decreases to zero as $n \to \infty$.

One can use (2.41) to estimate any density function, e.g. the distribution of pulsars in the sky (see Figure 1.1). One can even extend (2.41) to two dimensions where one can estimate γ-ray sky maps (e.g. on the COS-B data). In this two dimensional case one should choose h such that the kernel function is narrower than the point spread function of the telescope. Again, h will depend on the total sample size involved. In Paper 2 the relevance of the KDE's to periodic γ-ray data was discussed and the naive kernel was used as an example. Although it is not the most efficient KDE, it proves to be better than the histogram on average. In the case of the histogram it was assumed that the optimal bin width could be obtained. However, this is not true, so that the errors for the histogram will always be larger than the errors given in Paper 2.

In order to arrive at expressions for the MSE, MISE and the optimal smoothing parameters, it is best to write (2.41) in terms of a Fourier expansion (Parzen, 1962)

$$\hat{f}_h(x;\underset{\sim}{X}) = (2\pi)^{-1} \int_{-\infty}^{\infty} \exp(-i\ell x) k(h\ell) \hat{R}_\ell d\ell \qquad (2.44)$$

where the Fourier transform of the kernel function K(x) is given by:

$$k(h\ell) = \int_{-\infty}^{\infty} \exp(-i(h\ell)x) K(x) dx \qquad (2.45)$$

Remember that h in (2.45) is measured in radians. Expressions for $k(h\ell)$ for different kernels are given in Table 2.1.

In the case of periodic data one is only concerned with periodic densities. Furthermore the variable x is substituted with $\theta \in [0,2\pi]$, so that ℓ can assume only integer values in (2.44). The latter reduces to a Fourier series expansion

$$\hat{f}_h(\theta;\underset{\sim}{\theta}) = (1 + 2 \sum_{\ell=1}^{\infty} k(h\ell)(\hat{\alpha}_\ell \cos\ell\theta + \hat{\beta}_\ell \sin\ell\theta))/2\pi \qquad (2.46)$$

Here $\underset{\sim}{\theta} = \theta_1, \ldots, \theta_n$ are the folded phases, $\hat{\alpha}_\ell$ and $\hat{\beta}_\ell$ are the trigonometric moments obtained from (2.17) and $\hat{f}_h(\theta;\underset{\sim}{\theta})$ is a normalised density function between 0 and 2π.

Relation (2.46) can easily be programmed on computer. It is also differentiable and integrable. One needs only to calculate the first 50 or 100 trigonometric moments from the data using (2.17), then estimate h (which will be shown later) and calculate (2.46) in as many points θ as one wishes.

At this stage it is appropriate to obtain more explicit expressions for the MSE(θ) and the MISE. The procedure that will be followed here has been motivated by Parzen (1962): Let $u = h\ell$ in (2.45) and let r be a positive number such that

$$0 < k_r = \lim (1-k(u))/|u|^r < \infty \qquad (2.47)$$

then r (which is usually ≥ 2) is called the characteristic exponent of the transform k(u) and k_r is called the characteristic coefficient. In this case the MSE(0) can again be written as the sum of the variance and the bias:

$$MSE(\theta) \approx [f(0)/nh] \int_{-\infty}^{\infty} K^2(y)dy + h^{2r} |k_r f^{(r)}(0)|^2 \qquad (2.48)$$

This expression is only valid for large values of n. The values of r, k_r and $\int_{-\infty}^{\infty} K^2(y)dy$ for different kernels are also indicated in Table 2.1. The MISE can be obtained by integrating (2.48) between 0 and 2π. It is interesting to note that, apart from the constants in (2.48), the variance depends only on the amplitude f(0) of the density, but the bias depends only on the absolute value of the r^{th} derivative $f^{(r)}(0)$ of the light curve. Thus, in regions where the light curve is flat (background) or where the slope of f(0) is constant, can one trust the variance to be a sufficient indicator of the true error. However, where the slope of f(0) changes rapidly (i.e. on the tip of a narrow peak) one can expect the bias to be larger than the variance.

2.4.2.1. The optimal smoothing parameter

The MISE also consists of a sum of the variance and bias components. Figure 2.11 gives a graphical illustration of these components of the MISE. Relation (2.48) illustrates this effect: the variance is inversely proportional to the smoothing parameter while the bias increases with h^{2r}. Consequently there exists an optimal choice for h, say h^*, such that $MISE(h^*) < MISE(h)$ for all $h \neq h^*$. This value can be obtained by differentiating the expression for the MISE with respect to h. By setting this result equal to zero, the optimal value of h is obtained. Densities for which the r'th derivative $f^{(r)}(0)$ of f(0) exists, yields a theoretical expression for the optimal h of

$$h^* = \left[\frac{\int_{-\infty}^{\infty} k^2(y)dy}{2rk_r^2 \int_0^{2\pi} (f^{(r)}(0))^2 d\theta} \right]^{1/(2r+1)} n^{-1/(2r+1)} \qquad (2.49)$$

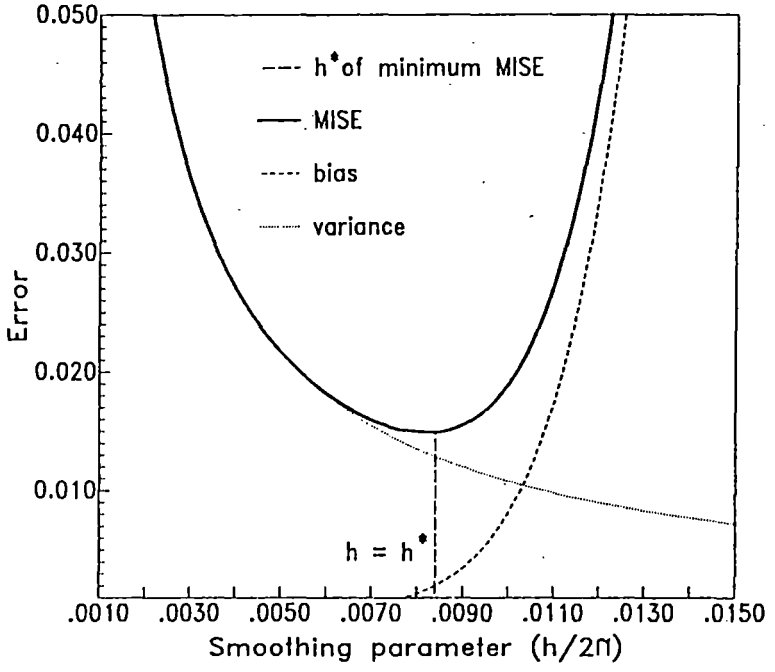

Figure 2.11. The behaviour of the variance and bias components of the MISE as a function of h. Note the unique minimum of the MISE at h^*. This graph is applicable to the Vela pulsar at $E_\gamma > 50$ MeV (see Figure 2.12 for more details).

This yields a minimum MISE of

$$\text{MISE}(h^*) = (2r+1).\left(\int_{-\infty}^{\infty} k^2(y)dy/2r\right)^{2r/(1+2r)}. \left(k_r^2 \int_0^{2\pi} (f^{(r)}(\theta))^2 d\theta\right)^{1/(1+2r)}. \; n^{-2r/(1+2r)} \qquad (2.50)$$

One may argue that these exercises are interesting and informative, but useless for γ-ray Astronomy, since the true underlying light curve is not known a priori. The answer to this is no, since Watson and Leadbetter (1963) showed how the MISE can be written in terms of a Fourier expansion. For periodic data their expression changes from an integral to a sum. Furthermore, one can estimate the h-dependent terms of this MISE from the data alone, so that h^* can be estimated by $\hat{h}$, by minimising the following expression:

$$\hat{h} = \min_h \sum_{\ell=1}^{\infty} [(k(h\ell))^2 \bar{R}^2_\ell - 2k(h\ell)(n\bar{R}^2_\ell - 1)/(n-1)] \qquad (2.51)$$

The minimisation of (2.51) therefore yields a value $\hat{h}$ such that $E(\hat{h}) = h^*$. This method is applicable to any kernel for which $k(h\ell)$ is known.

2.4.2.2. Positive kernel functions.

The majority of kernels can assume only positive values, simply because they have been chosen as density functions. Table 2.1 indicates which kernels are positive. In Paper 2 the properties of the simplest kernel in this class was discussed, i.e. the 'naive' kernel which results in the well known moving average technique. De Jager et al. (1987) (Paper 3) proposed the use of the normal kernel which results in an estimator with a smaller MISE than that for the naive estimator (see Table 2.1 for a MISE comparison between different kernels). Furthermore, with the normal kernel one saves an enormous amount of computer time relative to the time required for the naive kernel. The computer time is determined by the rate at which (2.51) converges (see Table 2.1 for a comparison of the relative computer times necessary for different KDE's).

For the positive kernels one has that r = 2 yields a finite positive value for k_r from (2.47). Consequently the rate at which the MISE decreases to zero is proportional to $n^{-4/5}$ from (2.50). In Paper 2 the expression for h^* was calculated for unimodal light curves of the form of (2.14) from (2.49). For $f_s(\theta)$ the Gaussian source function with duty cycle δ was assumed. The optimal value of h^* for a signal strength of p is then

$$h^* = q\delta(p^2 n)^{-1/5} \text{ radians} \qquad (2.52)$$

where q is some constant which depends on the kernel used. For the naive kernel q = 4.917 (Paper 2) while q = 2.826 for the normal kernel. Thus, if one knows a priori what p and δ should be, h^* can be calculated using (2.52). Note that this expression is valid for large n but is invalid for bimodal light curves. It is important to realise that $h^* \to \infty$ if $p \to 0$, which is desired. This means that a horizontal density estimate will be obtained if $\underline{\theta}$ is uniformly distributed.

2.4.2.3. Mixed kernels

In the case of mixed kernels, K can assume both negative and positive values in (2.41). In this regard the Fourier Series Estimator and Swanepoel kernel will be considered.

(i) The Fourier series estimator

The Fourier Integral Estimator (FIE) is obtained by using the kernel function $(\sin x)/(\pi x)$. For periodic data, this results in the Fourier Series Estimator (FSE). In Section (2.3.3.2) the relevance of this estimator to γ-ray Astronomy was shown with respect to the Z^2_m-test. It may be necessary to quote this estimator again:

$$\hat{f}_m(\theta;\underline{\theta}) = (2\pi)^{-1}[1 + 2\sum_{\ell=1}^{m}(\hat{\alpha}_\ell \cos \ell\theta + \hat{\beta}_\ell \sin \ell\theta)] \qquad (2.53)$$

In this case m is the smoothing parameter and is equivalent to 1/h where h is the smoothing parameter of the general KDE. This m is also the number of harmonics which should increase to infinity if $n \to \infty$. Only then will (2.42) hold for the FSE. However, when f(0) is cardioid (see relation (2.22)), $m^* = 1$ for all values of n. This means that m = 1 is sufficient for all n when all the power is in the fundamental. However, it is not for the experimenter to decide what the optimal m, namely m^* should be if f(0) is unknown.

For this density estimator an admissible value of r cannot be found from (2.47) so that relations (2.49) and (2.50) are not applicable to the FSE. However, in Paper 2 it was shown that the optimal number of harmonics (which minimises the MISE) for a unimodal Gaussian source function with the same parameters as given by relation (2.52), is given by

$$m^* = 0.375[\ln(p^2(n+1))]^{\frac{1}{2}}/\delta \qquad (2.54)$$

This result also suggests how many harmonics should be used for the Z^2_m test, if one knows the light curve parameters p and δ a priori. From (2.54) it is evident that m^* decreases as p decreases, which supports the findings of Gerardi et al. (1982). According to this equation the smallest acceptable signal strength is $p = 1/\sqrt{n}$ which corresponds to a DC excess of one sigma.

Hart (1985) proposed a method to estimate m^* if f(0) is unknown: the estimator of m^* is that value of m, say $\hat{m}$, which maximises the expression

$$(n+1) \sum_{\ell=1}^{m} \bar{R}^2_\ell - 2m \qquad (2.55)$$

Condition (2.55) will be called the 'Hart-rule'. The correspondence between the Hart-rule and the Z^2_m-test is striking: In terms of the Z^2_m-statistic one can rewrite the Hart-rule as follows:

$$\hat{m} = \max_m (Z^2_m - 4m) \qquad (2.56)$$

The importance of the Hart rule will become evident when a new but 'objective' test (the H_m-test) for uniformity will be derived in Section 2.5.

(ii) The Swanepoel kernel

Very recently Swanepoel (1987) proposed the kernel function

$$K(x) = \tfrac{1}{2}(\sin|x| + \cos x)\exp(-|x|), \quad x \in (-\infty,\infty)$$

He showed that this kernel function yields the best KDE (w.r.t. all other kernels) if f(x) is continuous while f'(x) is discontinuous in any point x. It is also approximately the optimal kernel if f(x) itself is discontinuous. These features may be desirable for γ-ray Astronomy in those cases where the regions of γ-ray emission on a pulsar are sharply defined.

Consider the more general case where both f(x) and f'(x) are continuous. Relation (2.47) yields r = 4 so that the MISE decreases to zero at a speed of $n^{-8/9}$ in (2.50) - a rate which is faster than the $n^{-4/5}$ rate for the positive kernels and the $n^{-2/3}$ rate for the histogram. This result is very surprising and implies that the Swanepoel kernel is asymptotically the best to use for all possible light curves. Furthermore, if the fourth derivative of a light curve is zero in all points $\theta \in [0,2\pi]$, the bias will be zero and the variance will be a true indicator of the error of $\hat{f}_h(\theta;\underline{\theta})$.

2.4.3. CONFIDENCE BANDS AND -INTERVALS FOR KDE'S

Kernel density estimators are consistent in the sense that $E\hat{f}_h(x) \to f(x)$ as $n \to \infty$ (relation (2.42)) (The notation of $\hat{f}_h(x)$ instead of $\hat{f}_h(x;X)$ is used for the sake of simplicity). Another important aspect is that $\hat{f}_h(x)$ is asymptotically normal (Parzen, 1962): If $\sigma[\hat{f}_h(x)]$ is the standard error of $\hat{f}_h(x)$, the variable

$$(\hat{f}_h(x)-E\hat{f}_h(x))/\sigma[\hat{f}_h(x)] = z = {}^{d}(N(0,1))$$

for all x and large values of n. Using this and the consistency property, one can at least give an approximate confidence interval for f(x) in any point x. Let $\pm Z_\alpha$ correspond to those ordinates of the N(0,1) density such that the area under this density between the values $[-Z_\alpha, Z_\alpha]$ is $(1-\alpha)$ (i.e. the confidence level). A confidence interval for the true density is then

$$f(x) = \hat{f}_h(x) \pm Z_\alpha \sigma[\hat{f}_h(x)]$$

The standard error of $\hat{f}_h(x)$ is approximated by the variance component of the MSE (2.48), so that

$$f(x) = \hat{f}_h(x) \pm Z_\alpha(\hat{f}_h(x)_{-\infty}\int^{\infty} K^2(y)dy/nh)^{\frac{1}{2}} \qquad (2.57)$$

A '2 sigma' or 95% confidence interval is characterised by $Z_{0.05} = 1.96$. Although a plot of (2.57) gives graphically a band for all values of x, it cannot be considered as a confidence band for f(x). The meaning of a real confidence band can be illustrated as follows: Let $x_1, x_2, \ldots, x_\ell$ be a set of values at which (2.57) is evaluated. Since the latter gives confidence intervals it means that f(x) cannot be simultaneously within the ℓ intervals at a confidence level of $(1 - \alpha)$. However, one may say this if (2.57) describes a confidence band. According to Bickel and Rosenblatt (1973) an inflation of the interval described in (2.57) yields a confidence band. Inspection of their inflation factor (which increases with n at a very slow rate of $(\ln(n))^{\frac{1}{2}}$) indicates that $Z_{0.05}$ should be multiplied by a factor of = 1.5 to give an approximate 95% confidence band for f(x).

However, their method is applicable to the case $r \leq 2$ in (2.47) and (2.48) so that the inflation factor of = 1.5 is only applicable to the positive KDE. A method should still be worked out for $r > 2$ to be valid for Swanepoel's kernel. It is interesting to note that the error bars for a histogram (which is calculated from Poisson statistics) represents only confidence intervals and not a confidence band. The inflatory factor for the

histogram may be much larger than 1.5 which is due to the large inherent bias in the histogram technique.

In relation (2.57) only the variance of the MSE was used to obtain the error of $\hat{f}_h(x)$. The bias was neglected, but is proportional to $|f^{(r)}(x)|^2$ so that (2.57) is a perfect estimator of the true error in those regions of the phasogram where the r^{th} derivative of the light curve equals zero. For the histogram r = 1 so that the bias is nonzero if $f'(\theta) \neq 0$. For the positive KDE, r = 2 so that $f^{(2)}(\theta) \neq 0$ will yield a bias, while $f^{(4)}(0)$ is the decisive parameter for the Swanepoel kernel. It is interesting to note that for those light curves where an Epanechnikov-type source function (see Table 2.1) is mixed with the uniform background, $f^{(2)}(0)$ will be nonzero for some θ, so that the positive KDE's will yield a certain amount of bias. However, Swanepoel's kernel yields $f^{(4)}(0) = 0$ for all $\theta \in [0,2\pi]$ for such kind of light curves, so that no bias will be present for his kernel. This illustrates again the general superiority of the Swanepoel kernel.

2.4.4. IMPLEMENTING THE KDE FOR GAMMA RAY DATA

For the reader not familiar with KDE's, the previous sections may have been tiresome, but it was necessary to explain their properties and behaviour. Scientists neglected KDE's to a large extent mainly because they were educated in the use of the histogram, the literature around the KDE's are unknown to them and it was difficult to obtain an optimal smoothing parameter. Presently, the histogram still shares the latter difficulty. However, advanced computing techniques resolve this problem for KDE's i.e. the general expression for an estimator of the MISE for the densities defined on the interval $(-\infty,\infty)$ can be calculated by means of numerical integration to yield $\hat{h}$, an estimate for h^*.

However, gamma ray astronomers cannot afford such time consuming techniques, since they are often confronted with large data samples which have to be analysed on a very frequent basis. Fortunately their work

is mainly concerned with periodic data which reduces the integration problem for the MISE given by Watson and Leadbetter (1963) to that of a mere sum given by (2.51). Consequently the field of KDE's should be of interest to them since it can be easily implemented in practice and because they are keen on getting the best representation of light curves. Since one obtains a continuous function which can be easily manipulated by mathematics, theoreticians will also find it better to work with the KDE.

The KDE technique is now well established. One should only select that kernel which results in the smallest MISE while the computer time necessary is relatively small. The best kernels in regard to computer time are the FSE-, the normal- and Swanepoel-kernels. The second and most important aspect is the sensitivity of the technique: In this case one should select that kernel function which results in the smallest MISE. Among the class of positive kernels, one finds that the Epanechnikov-kernel yields the smallest MISE, while its computer time is relatively large. Davis (1975, 1977 and 1981) showed that the FSE is asymptotically better than the positive KDE's when $f(0)$ belongs to certain classes. However, a γ-ray astronomer cannot rely on such a result due to the large uncertainties in the form of $f(0)$. In Paper 2 the viewpoint of Davis (1975, 1977, 1981) was supported by stating that the FSE should be used for broad and smooth light curves. It was also illustrated that the efficiency of the FSE increases with increasing signal strength. Since the light curves in VHEGRA deviate only slightly from uniformity, the FSE will not be the best general γ-ray light curve estimator. However, the Hart-rule which yields the optimal number of harmonics, leads to an excellent test for uniformity which will be discussed in the next section.

The purpose of Paper 3 was to propose the use of the normal kernel as a general technique which is fast to implement on a computer while its MISE is of the smallest of all positive kernels. The most recent development in the field of KDE's came from the proposed kernel by Swanepoel (1987). His kernel results in an estimator which is optimal for nearly any kind of density. It is then suggested that the Swanepoel kernel should be used to obtain a γ-ray light curve estimate and its approximate confidence band. Better estimators may still emerge, but they will only be

useful to VHEGRA if they can be easily implemented in practice. However, the success of the KDE can be ascribed to a number of desirable properties which is not shared by the old fashioned histogram. They are (a) consistency, (b) the optimal smoothing parameter is obtained in an automatic way, (c) a smooth function is obtained which can be manipulated mathematically, (d) an approximate confidence band can be constructed and (e) if the data sample $\underset{\sim}{\phi}$ is uniformly distributed, the chances are ≈ 60% to obtain a horizontal line (since $\hat{h} \to \infty$) as a density estimate, i.e. the KDE usually decides whether a peak is significant or not. A FORTRAN program of the KDE (with Swanepoel's kernel) is included in Appendix A. The program accepts the phases $\underset{\sim}{\phi} = \phi_1, \ldots, \phi_n \in [0,1]$ (i.e. $\phi = 0/2\pi$) and estimates h^*, $f(\phi)$ and the corresponding confidence interval at each selected phase.

2.4.5. EXAMPLE: THE VELA PULSAR AT E > 50 MEV

The purpose of this section is to illustrate the use of the KDE. The COS-B data on the Vela pulsar at energies E > 50 MeV were selected. See Kanbach et al. (1980) and Mayer-Hasselwander (1985) for a detailed description of the observation periods and pulsar parameters. The selection criteria of events from the database were suggested by Buccheri (1986).

This data were chosen because the light curve of Vela is very complicated with large variations and near-discontinuities. Figure 2.12 shows the Swanepoel KDE of nearly all the Vela data, normalised to the sample size of $n = 3\,462$ on the phase interval $\phi \in [0,1]$. Figure 2.11 illustrates the optimal choice of $\hat{h} = 0.0085$ for this light curve. The band around the density estimate defines 95% confidence intervals at each selected phase ϕ. The most important parameters of this light curve are shown in Table 2.2 and differ in phase mostly with ≈ 0.02 from the estimates given by Kanbach et al. (1980). Using the estimate of the background region, a signal strength of 58.3% is calculated. According to the Hart-rule (2.56) the optimal number of harmonics is $\hat{m} = 22$.

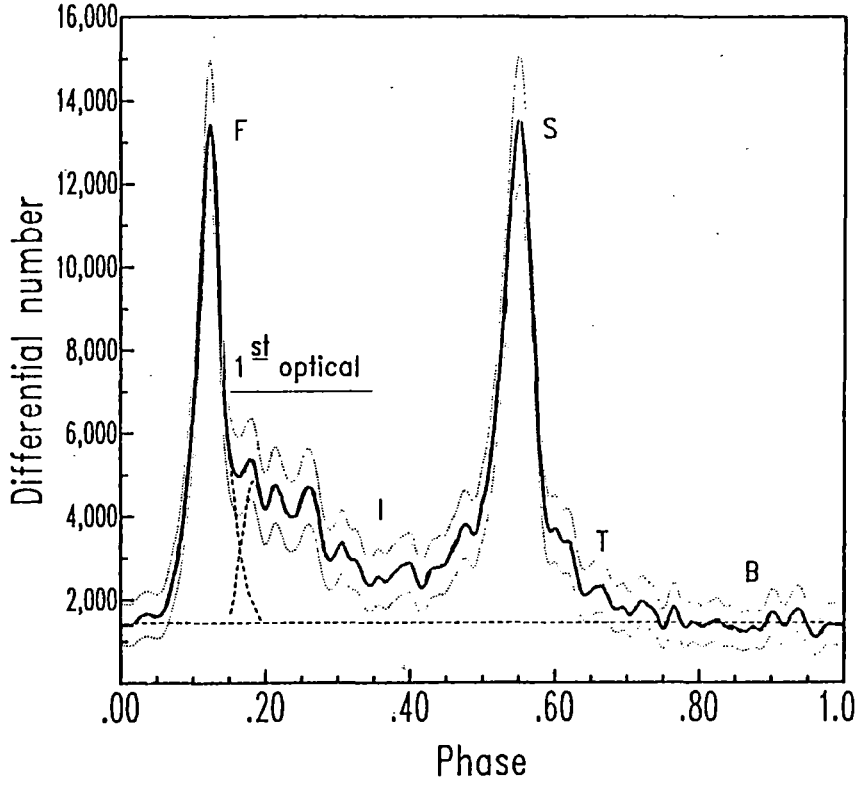

Figure 2.12. A Swanepoel kernel density estimate of the Vela light curve for $E_\gamma > 50$ MeV for observations C, L, U and 45. The total sample size is 3462 and the optimal smoothing parameter is $\hat{h} = 0.0085$. The band shown represents 95% confidence intervals. The position of the first optical peak and the identified first- and interregion pulses are also shown. The symbols indicate the phase regions identified in Table 2.2. Phase zero corresponds to the radio pulse. The horizontal dashed line represents the estimated background level.

To illustrate the KDE using different kernels, the same data were analysed by using the naive-, normal- and Swanepoel kernels and the results are indicated in Figure 2.13. The naive kernel required ≈ 10 000 harmonics before (2.46) converged, while the normal and Swanepoel kernels required only 100 and 250 harmonics respectively, which illustrates the preference of the Swanepoel and normal kernels above the naive kernel with respect to computer time. The histogram with 100 bins is also shown for comparison. However, this choice of bin size for the histogram is subjective and has no theoretical basis. Consequently one cannot evaluate and compare the histogram with the KDE. The zig-zag nature of the naive kernel is quite evident and is due to the discontinuous square wave nature of this kernel (i.e. the classic moving average). Using the optimal choices of $\hat{h}$ (as estimates of h^*) and relation (2.49), the MISE's of these KDE's are calculated from (2.50) as 0.018, 0.016 and 0.014 for the naive, normal and Swanepoel KDE's respectively, showing that the Swanepoel KDE has the smallest MISE although not significantly less than the other errors. Observe also Figure 2.13 (a, b and c) - the graphs nearly look the same although the amplitude of the Swanepoel KDE is largest in Figure 2.13a, suggesting that it has the smallest bias.

From the KDE (Figure 2.13a) it follows that the first pulse is symmetric between phases 0.096 and 0.150 around phase 0.123. Such an interpretation cannot be made from the histogram. If the radiation regions for the first pulse and interregion are different as suggested by Smith (1986), it means that the observed light curve around phase 0.164 is a mixture of three densities: the known background level, the first pulse and the interregion pulse. If the first pulse is also symmetric between phases 0.050 and 0.196, one can estimate the interregion pulse alone: It starts at phase 0.15 and follows the observed light curve at phases larger than 0.196. These components are also shown on Figure 2.12 and 2.13a and an interregion structure can be identified in Figure 2.12 which is approximately in phase with the first optical pulse. The second pulse (Figure 2.12) is unsymmetrical but it may be due to contamination from interregion- and trailer γ-rays. The effect of fluctuations in the second pulse can be ruled out since the confidence band there is already very narrow. If the trailer component extends into the region of the second

pulse, the slope of $f(\phi)$ at phase $\phi \approx 0.555$ may be nearly infinite, which suggests a very sharply defined emission region at that phase.

The effect of smaller sample sizes on the KDE is illustrated in Figures 2.12, 2.14 and 2.15. Comparing the three Swanepoel kernels it is clear that $\hat{h}$ increases with decreasing sample size as is expected from (2.49). The effect of this is that the widths of the peaks increase (i.e. they become oversmoothed), the reason being that the increasing variance (or fluctuations) are compensated for at the cost of the bias. A further consequence of such an oversmoothing is a decrease in the amplitude of the peaks. From Figure 2.15 it seems as if the naive KDE is best for small sample sizes. This is not yet certain since Statisticians have not investigated the distribution of $\hat{h}$ for a given light curve and sample size yet. Some attention was given to this problem in Paper 2. It is intuitively expected that the variance of $\hat{h}$ is large for small n but small for large n. Consequently one can expect a wide range of h-values for $n < 50$ so that the scatter of $\hat{h}$ around the theoretical h^* may be quite large. The best one can do then in the case of small sample sizes is to be subjective and choose an h-value which gives the light curve the best appearance, or, to be more objective, one can use the Hart-rule (2.56) and use $h = 2\pi/(6\hat{m})$ in the light curve estimator (2.46).

Description of region	phase position
Mode of first pulse	0.123 ± 0.006
FWHM of first pulse	0.037 ± 0.008
Mode of second pulse	0.551 ± 0.010
FWHM of second pulse	0.051 ± 0.009
Phase difference between two pulses	0.428 ± 0.011
Background (B)	0.750 - 0.050
First pulse (F)	0.050 - 0.164
Interregion (I)	0.164 - 0.488
Second pulse (S)	0.488 - 0.594
Trailer (T)	0.594 - 0.750

Table 2.2. The parameters of the Vela light curve in Figure 2.12. The errors indicated are at an approximate confidence interval of 95%.

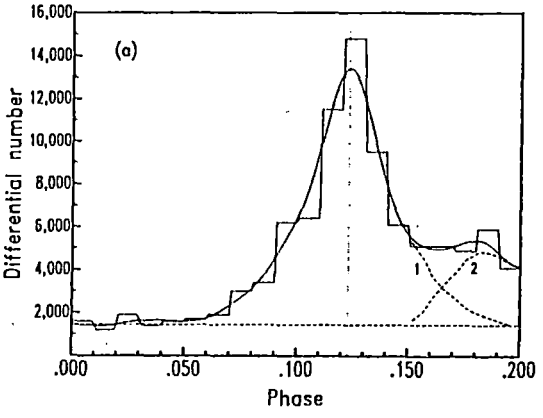

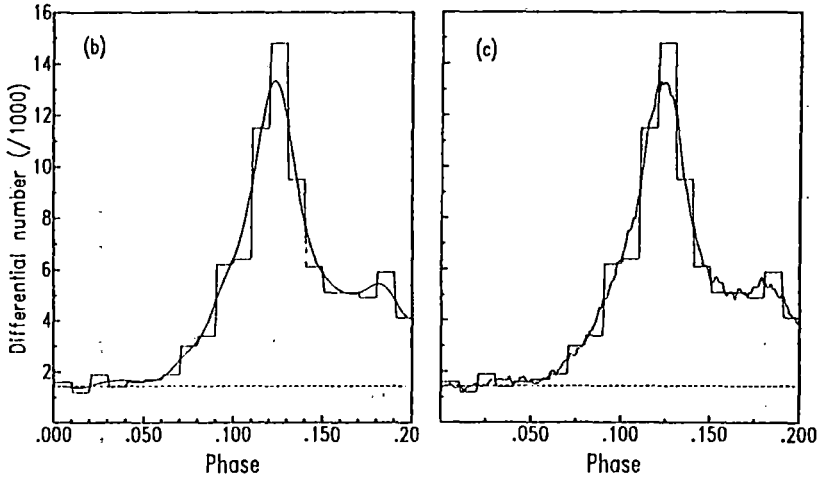

Figure 2.13. Kernel density estimates of the same data used to construct Figure 2.12. Only the phase region 0 to 0.2 is shown. For (a) the Swanepoel kernel was used with $\hat{h}$ = 0.0085. The observed symmetry around phase 0.123 was used to complete the first (1) and interregion (2) pulses. For the normal kernel (Figure (b)) $\hat{h}$ = 0.0064 while $\hat{h}$ = 0.01 for the naive kernel (Figure (c)).

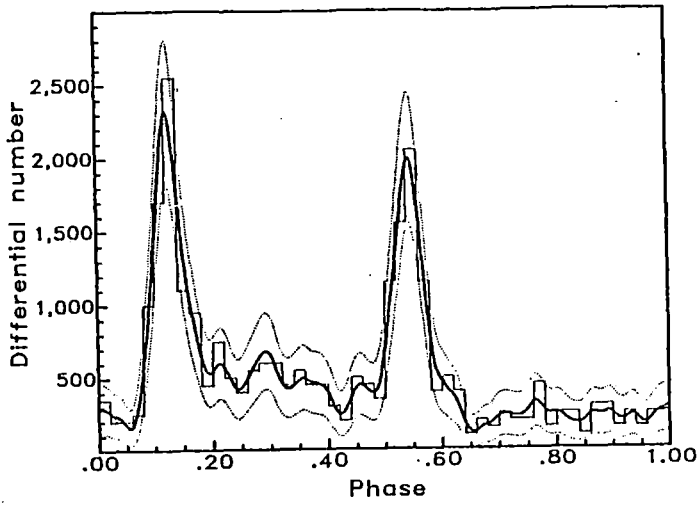

Figure 2.14. A Swanepoel kernel density estimate of the data of observation C_1 only (n = 540). A 50-bin histogram is also shown for comparison. The band shown represents 95% confidence intervals.

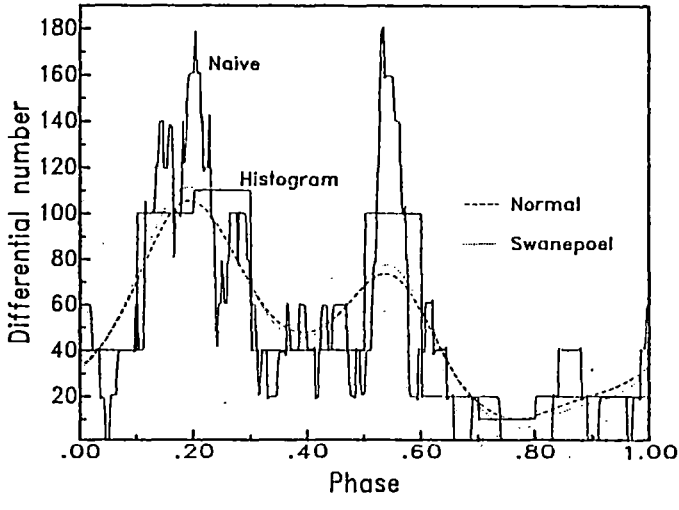

Figure 2.15. Density estimates of the first 50 events of observation C_1, using the Naive, Normal and Swanepoel kernels. A 10-bin histogram is also shown for comparison.

2.5. THE H_m-TEST FOR UNIFORMITY

In Section 2.3 it became clear that most tests are biased towards certain forms of light curves. The only test which seems to be a good general test is Watson's test, but it requires $\approx n^2$ steps to calculate. What is needed is a test like Z^2_m which is fast to compute, while m is variable. The choice of m should be an objective but optimal one. The best choice of m is given by the Hart-rule (relation (2.56)) which minimises the difference between the Fourier Series Estimator and the true unknown light curve. Furthermore, the test should be nearly as powerful as the Rayleigh test for broad peaks and nearly as powerful as the Z^2_{10} or Protheroe's tests for narrow peaks. It should also be like the Runs test combined with Pearson's test, which discriminates against many oscillations on a light curve which are supposed not to be source-like. A test which answers these requirements was developed and is called the H_m-test:

The Hart-rule sums the power in the first m harmonics and stops when $Z^2_m - 4m$ reaches a maximum at some m. Consequently the following test statistic for uniformity is suggested:

$$H_m = Z^2_{\hat{m}} - 4(\hat{m}-1) \geq 0 \qquad (2.58)$$

The hypothesis of uniformity should be rejected for large values of H_m. Since $\hat{m}$ is a random variable, depending on the data, $Z^2_{\hat{m}} \neq {}^{d}(\chi^2_{2\hat{m}})$ for $n > 100$ and the probability distribution of H_m had to be determined from simulations. Some 10^7 simulations of ≈ 50 χ^2_2-variables were done and the distribution of H_m was estimated for $\hat{m} = 1, \ldots, 20$.

Even the 10^7 simulations of random noise were too few to determine the probability distribution of H_m for $\hat{m} > 20$ since the probability to find $\hat{m}$ harmonics decreases rapidly to zero as $\hat{m}$ increases to infinity. For example, the probability to find $\hat{m} = 1$ is 80% while the probability to find $\hat{m} = 20$ is 2×10^{-5} for noise.

Fortunately the distributions of H_m could be parameterised, so that tables are unnecessary to calculate the p-level given an experimental value of H_m. The simulated distributions were fitted on twenty Gamma distributions using the parameters

$$\theta(m) = \bar{H}_m/\text{variance}(H_m)$$

$$r(m) = \bar{H}_m^2/\text{variance}(H_m)$$

so that the p-level for an experimental outcome can be calculated from the relation:

$$Pr(> H_m|H_o) = {}_x\int^{\infty} e^{-t}t^{r(m)-1}dt/\Gamma(r(m)) \qquad (2.59)$$

where $x = \theta(m)H_m$. Since γ-ray astronomers are mostly interested in the tail of probability distribution functions where small p-levels are expected, the accuracy of (2.59) was tested as follows: Another set of 10^5 H_m values were calculated, each from 300 uniformly distributed phases on the phasogram. These values of H_m were converted with (2.59) to p-levels (Pr) and again converted to Rayleigh powers by using the relation $Z = -\ln(Pr)$. The variable Z should follow the well known e^{-Z} probability distribution if Pr is uniformly distributed on the interval [0,1]. Through a minimum χ^2-fit, the distribution of e^{-Z} was confirmed - even for large values of H_m. Using (2.59), one can have confidence in the calculated p-levels. A very important feature showed up: If $\hat{m} = 1$, then $H_{\hat{m}=1} \overset{d}{=} (\chi^2_2)$. In other words: The H_m-test 'searches' through all harmonics. If it finds only the fundamental, it is just as powerful as the Rayleigh test. Appendix B gives a Fortran program to calculate (2.59) from IMSL routines given a set of phases on the interval [0,1].

There is one advantage: If there is only power in the m^{th} harmonic which is sufficiently strong to be picked up by the Hart-rule, the noise content of all m-1 harmonics will be added to H_m and the larger this m, the more likely it will be that H_o will be accepted. If this m is large ($m > 5$), which is unlikely for real sources, the value of H_m will be nearly consistent with the null hypothesis and the H_m-test will act like a combination of the Runs test and Pearson's test which is desired. Thus, it

is more likely that the H_m-test will see many peaks and holes in the data as 'noise' and not as a 'signal'.

According to its power curve in Figure 2.3, this test is very important if one has no a priori information about the true light curve: For duty cycles larger than 0.3 it is just as powerful as Watson's and the Rayleigh tests. For $0.1 < \delta < 0.3$ its power curve is slightly lower than Watson's power curve. In this same region it is more powerful than Protheroe's test, the Z^2_{10}- and Pearson's χ^2_{19}-test. However, when $\delta < 0.1$, H_m is more powerful than Watson's U^2-test but less powerful than the Protheroe-, Z^2_{10}- and χ^2_{19}- tests.

Note also that the distribution of H_m is known for $n > 100$ which is applicable to VHEGRA. If this test is applied to sample sizes less than 100, one is apt to overestimate a p-level, i.e. the significance of a positive result will be underestimated.

The following may be concluded if nothing is known a priori about the form of the light curve:

1. Large sample sizes ($n > 100$)

   In VHEGRA one usually has $n > 100$ which represents sample sizes for which the distribution of H_m is known. Protheroe's and Watson's tests are impractical since they require $\approx n^2$ steps on a computer. Here H_m is the proposed statistic since it is quite powerful and much less time consuming on an computer. If this test fails to yield a p-level less than $\approx 10^{-3}$ at $\delta < 0.1$, one can think about implementing Z^2_{10} without significantly raising the probability of making a Type 1 error.

2. Small sample sizes ($n < 100$)

   In this case the distribution of H_m is unknown. First use Watson's test to test for broad duty cycles. If this test fails to reject H_o at a significance level of 10^{-2} to 10^{-3}, switch to either the Protheroe- or the Z^2_{10}-tests to test for narrower duty cycles. The study made

by Gans (1984) assures one that retesting with a second test will not raise the probability of making a Type 1 error significantly. In PeV Astronomy one usually has $n < 100$ so that these prescriptions can be followed in extensive air shower experiments.

2.6. SIGNAL STRENGTH ESTIMATION

There are three methods of estimating signal strengths: by means of (a) ON-OFF comparisons, (b) direct calculation from the light curve estimate and (c) harmonic analysis. The second and especially the third method will receive some attention: If the light curve has a sufficiently well defined background region such that this level can be estimated from the light curve alone, one can estimate the ON-regions from the KDE as illustrated in Table 2.2 and estimate the signal strength as suggested in Papers 1 and 2. This method can be called the 'light curve method'.

The light curve method is quite easy to implement when the pulsed region is narrow. However, when the radiation pattern is broad, the background cannot be reliably estimated unless one has OFF-source measurements available. If the latter is not available, one has to use other methods to estimate the background. In such cases most of the power will be concentrated in the lower harmonics. It is then necessary to plot the Fourier power versus ℓ for $\ell = 1, \ldots, \hat{m}$ where $\hat{m}$ is obtained from the Hart-rule. The form of the light curve and the behaviour of the Fourier power as a function of ℓ will give an indication of the functional form of $f(\theta)$. If a single harmonic ℓ dominates the light curve, the method outlined in principle by Middleditch and Nelson (1976), Gibson et al. (1982a and b), Chadwick et al. (1985b) and Gorham et al. (1986a and b), can be used to estimate the signal strength:

Consider the case where $f(\theta)$ is a pure sinusoid at the ℓ^{th} harmonic of the period:

$$f(\theta) = (1 + p\cos\ell\theta)/2\pi \qquad (2.60)$$

The case $\ell = 1$ implies the well known cardioid density (2.22) which seems to represent most light curves obtained in VHEGRA. The case $\ell = 2$ seems to have occurred once on 23 May 1984 when Gorham et al. (1986a) observed Her X-1 at $E_\gamma > 250$ GeV. The case $\ell = 3$ will be discussed in Chapter 3 for PSR 1509-58. For any ℓ it can be shown from (2.16) and (2.19) that

$$n\bar{R}^2_\ell \simeq (n-1)p^2/4 + 1 \tag{2.61}$$

so that an unbiased estimator for the total signal strength and its standard error (Mardia, 1972) is

$$\hat{p} = 2\left(\frac{n\bar{R}^2_\ell - 1}{n-1}\right)^{\frac{1}{2}} \pm (2/n)^{\frac{1}{2}} \tag{2.62}$$

For large n, $\hat{p}$ is asymptotically normally distributed with a mean value of κ (see relation (2.22)) and a variance of 2/n. This variance was derived from the variance of κ given by Mardia (1972) on page 125. Chadwick et al. (1985b) assumed that $\hat{p}$ has the same distribution as $\bar{R}$ which is incorrect. This leads to an underestimation of both the signal strength and its standard deviation by a factor of two.

The next case is where the light curve contains a single Gaussian peak with a standard deviation of $\sigma = 2.668\delta$ (radians) (where δ is the duty cycle) and a signal strength of p. Then

$$n\bar{R}^2_\ell \simeq (n-1)p^2 e^{-\frac{1}{2}\ell^2\sigma^2} + 1 \tag{2.63}$$

If $(n\bar{R}^2_\ell - 1)$, $\ell = 1, \ldots, \hat{m}$ converge to zero with increasing ℓ at a rate of $\exp(-\frac{1}{2}\ell^2\sigma^2)$, one can confirm the existence of such a Gaussian peak. One then has a system of m equations and two unknowns (σ and p) and the determination of these parameters would be a numerical problem.

In general, if one has a good guess of the general parametric form $f(\theta)$ of a light curve (up to the unknown parameters), one can estimate the parameters as follows: Construct a system of $\hat{m}$ equations

$$\frac{n\bar{R}^2_\ell - 1}{n-1} \simeq \int_0^{2\pi} e^{i\ell\theta} f(\theta)\, d\theta, \quad \ell = 1, \ldots, \hat{m} \tag{2.64}$$

Examples of (2.64) are (2.61) and (2.63). As long as $\acute{m}$ is more than the number of unknown parameters, (2.64) can be solved with numerical techniques.

One therefore has to be very careful when estimating signal strengths. The wrong choice of $f_s(\theta)$ may result in a wrong estimation of p. This is why a plot of the Fourier power as a function of the harmonics may lead one to a choice of $f_s(\theta)$, since the behaviour of $E(n\bar{R}^2_\ell)$ is known as a function of ℓ for any known form of $f_s(\theta)$. In the case of low signal strengths the negligence of the bias term '-1' in relations (2.62), (2.63) and (2.64) results in an overestimation of the signal strength.

2.7. CONCLUSION

The analysis of VHE γ-ray data rests on two aspects in statistics which are hypothesis testing and estimation. This applies to both DC and periodic sources. The purpose of hypothesis testing is to identify a source while estimation theory is used to estimate the light curve, signal strength and other geometrical parameters of radiation.

In Section 2.2 the Gini-test was proposed to test whether the time differences in DC data are exponentially distributed. The advantage of this test is the fact that it is scale free, bin-free and the Gini-statistic is N(0,1) distributed for sample sizes as small as 10. The use of the method developed by Dowthwaite et al. (1983) and reviewed by Li and Ma (1983) is suggested to evaluate the significance of an excess number of counts. If it is proved for a DC analysis from the method of Dowthwaite et al. (1983) and the Gini-test that the count rates of the two OFF-regions are identically distributed for all scans, there seems to be no reason to reject those scans where the OFF-source count rates differ by more than 2σ. In fact $\approx$ 5% of all scans should show effects of 2σ and more for a given test.

In Section 2.3 it was stressed that all the information in a light curve is contained in the characteristic functions. The purpose of using optimal hypothesis testing procedures is stressed: although the likelihood ratio test is theoretically the best for any data, it cannot be applied to VHE data, which is very unfortunate. The reason being: (a) it is difficult to obtain a parametric form for f(θ), (b) even if the latter could be done, the numerical problem of finding the maximum likelihood estimates of the parameters of f(θ) would be difficult and (c) the sample sizes involved are usually large. One simple likelihood ratio test is the Rayleigh test which enjoys much attention in VHEGRA. It is an important test since it tests for power in the fundamental. The theoretical distribution of the Rayleigh test is known for very small sample sizes ($n > 7$). This advantage is not shared by Pearson's test and is one of the reasons why the claim of the 59 s periodicity of Geminga A is questionable (Buccheri et al., 1985). The Rayleigh test can be extended to the Z^2_m-test of Gerardi et al. (1982) where m is chosen a priori. Even the distribution of Z^2_m is also known for $n > 7$. The latter property is useful for UHEGRA where one usually searches for narrow duty cycles.

If one knows a priori what the form of a light curve should be, one can select one of the following tests: The Rayleigh test for cardioid densities, Watson's test for duty cycles larger than 10% (if the sample size is not too large) and the Z^2_m-test for duty cycles of the order of (1/2m). If it is known that the light curve has two peaks separated by $\Delta\phi$ in phase, one can calculate the most intense harmonics from the characteristic functions and include only them in the calculation of Z^2_m. However, the H_m-test should not be used if one is certain about the form of f(θ).

In Section 2.3.5 the effect of a period of analysis that differs slightly from the true period, was discussed. In the case of broad light curves, the form and the amplitude of the light curve do not change rapidly if the period of analysis differs slightly from the true period. However, this change is much more significant if the light curve has a narrow duty cycle. This illustrates that the resolution of the true period is good if the duty cycle is narrow and if the proper test statistic (e.g. Z^2_{10}) is used, whereas the period resolution is poor for broad duty cycles. From Figures 2.5 and 2.7 it is clear that one needs to test less periods within

one IFS with the Rayleigh test than with a test like Z^2_{10}. Furthermore, with the Rayleigh test one is more likely to identify a signal at a period which differs slightly from the true period than with the Z^2_{10}-test. This even applies to narrow peaks on the light curve. Finally, a very important aspect is brought forward: If one searches for the maximum value of the Rayleigh test statistic within one IFS, the obtained p-level should be multiplied by a factor of between 2 (for small values of $n\bar{R}^2$) and 4 (for large value of $\hat{n\bar{R}^2}$). This multiplication factor may go up to 20 if the Z^2_{10} or Pearson's x^2_{19}-tests are used for the same purpose.

Another very important contribution to the analysis methods in VHEGRA is the estimation of light curves. The use of the histogram to estimate a light curve is discouraged due to its subjectivity and the large errors inherent in this method. It is shown that the error of any estimator consists of a variance and a bias component. The variance is well known among astronomers but the bias is somewhat neglected. Any estimator of a density function is dependent on a smoothing parameter. The choice of this parameter is very critical in VHEGRA due to the weak γ-ray signals usually encountered. A wrong choice for this parameter may easily smear such a peak out. The use of the kernel density estimator, which is aimed at a reduction of the bias, is proposed. For this estimator the optimal smoothing parameter h^* can be estimated from the data alone without any ad hoc assumptions. It is also shown that the process of estimating h^* is very convenient for periodic data from a computational viewpoint. There is a multitude of kernels which can be chosen for the KDE. According to statisticians the choice of a specific kernel is not as critical as the choice of h. This was also illustrated in Section 2.4.5. However, the Swanepoel kernel is nearly optimal if $f'(\theta)$ or $f(\theta)$ is discontinuous in any point θ and also seen from a computational viewpoint, although it requires a factor three more computer time than the normal kernel in the case of large sample sizes.

One should bear the following limitations in mind: In the case of very small sample sizes ($n < 50$) the KDE may oversmooth the data (see Figure 2.15), fine structures with a width less than $\approx 2\hat{h}$ cannot be identified by the KDE. However, if a narrow fine structure contributes to more than one sigma DC-excess, an $\hat{h}$ value will be found which is less than the

width of that fine structure (see Paper 3), so that the latter can be identified. From Paper 3 it also follows that a broad structure will be 'seen' by the KDE if its corresponding DC-excess is more than 3 sigma (compare these conditions with Figure 1.2). The latter requirements can also be seen as an advantage: The KDE 'decides' objectively whether a structure is significant. If there are no significant structures on the light curve, it is likely that (2.51) will give $\hat{h} \approx 2\pi$, i.e. a horizontal line for a light curve. Thus, according to Figure 1.2 and Table 1.1 many of the observations on Crab would have yielded negative results with the KDE, since the DC-excesses were sometimes less than one sigma.

Another KDE, the Fourier series estimator, cannot be considered as a good general light curve estimator. However, its method (the 'Hart-rule') of obtaining the optimal smoothing parameter yields an estimate of the number of harmonics present in a given data set. This information was used to adapt the Z^2_m-test proposed by Gerardi et al. (1982). This resulted in the 'H_m-test' with H_m as test statistic. It was shown that this test statistic is just as powerful as the Rayleigh test for broad light curves and nearly as powerful as Z^2_{10} and Protheroe's test for small duty cycles. Thus, when $n > 100$ (which is applicable to VHEGRA) and if nothing is known a priori about the light curve, H_m will be the best test statistic to use. If the H_m-test fails to reject uniformity, one may use another test on the same data without significantly raising the probability of making a Type 1 error, but one should not apply more than two different tests on the same data.

An important aspect in the analysis of periodic data is the estimation of the signal strength p. It is always best to have OFF-source comparison available when doing this. However, if not available one should go back to the KDE of the light curve. The KDE and its confidence band can be used to estimate the mean background level. This method is quite accurate if the periodic signal is confined to a narrow duty cycle. If the duty cycle is large, it may be difficult to estimate the background level and one may resort to the Fourier power as a function of the different harmonics when estimating p.

Change point procedures (see e.g. Lombard and Schultz, 1986) did not receive any attention in this study. These procedures will prove to be very valuable for X-ray and γ-ray Astronomy and can be used to identify the pulsed regions of a light curve and changes in the form of a light curve with time and space. Changes in the count rate with time and space can also be identified. In the lower energy regions one can also identify changes of energy spectra with space, time or phase on a light curve. However, there is not much literature on all these subjects, but more techniques can be developed by Statisticians (Lombard, 1987).

CHAPTER 3

THE ANALYSIS OF VHE DATA

Two aspects concerning the analysis of γ-ray data were prominent in Chapter 2: These were hypothesis testing, which is concerned with the identification of a source and estimation procedures, which is concerned with estimation of radiation characteristics. In Section 2.2 the steps to follow in the analysis of DC data were discussed. Sections 2.3 to 2.6 were concerned with the analysis of periodic data. The application of these procedures will be illustrated when the data obtained from observations of a few sources is analysed: A DC source (Centaurus A) and two periodic sources (PSR 1509-58 and PSR 1802-23) will be discussed. In the case of PSR 1509-58 the radio parameters are known for an epoch which does not bracket the VHE observation times, so that the radio parameters have to be extrapolated to the epoch of observations, allowing a limited amount of searching. The light curve and corresponding parameters will also be estimated. In the case of the pulsar suspect PSR 1802-23 a short review of the published results by Raubenheimer et al. (1986) will be be given. For this pulsar the radio parameters are very uncertain, so that a searching procedure in period has to be conducted. The purpose here is to re-evaluate the significance of Raubenheimer et al.'s claim in the light of developments in Section 2.3.

3.1. THE EXTRAGALACTIC SOURCE CENTAURUS A

Centaurus A (NGC 5128 or CEN A) is the nearest active galaxy and is situated at a distance of $\approx$ 5 Mpc from Earth. A summary of the characteristics of NGC 5128 was compiled from the review of Ebneter and Balick (1983): X-ray observations of the nucleus shows time variability on a time scale of days superimposed on long term variations. Jet like

features are observed at X-ray, optical and radio wavelengths. The X-ray jet is ≈ 4 arc min in length and 20 arc sec wide and is at its brightest at the nucleus. The disk contains gas, dust and hot young stars. The elliptical component of CEN A appears to be a normal giant elliptical galaxy which shows some unusual features. The galaxy contains some 20 spectroscopically confirmed globular clusters. Two large radio lobes are found which extend some 10 degrees in declination. The balloon Compton telescope of MPE observed an approximate 4σ effect from CEN A in the 0.7-20 MeV region (Von Ballmoos, Diehl and Schönfelder, 1985). They obtained a differential spectral index of -1.4 ± 0.4. At higher energies (E_γ > 35 MeV) SAS-2 and COS-B obtained no positive results from CEN A. Grindlay et al. (1975a) observed CEN A from 1972 to 1974 in Narrabri (New South Wales) at γ-ray energies larger than 300 GeV. He claimed the detection of CEN A at VHE γ-ray energies at a significance of 4.5σ. Only one other extragalactic source, M31 (Dowthwaite et al., 1984a) seems to emit TeV γ-rays.

Grindlay (1975) modelled two synchrotron and two inverse Compton components for CEN A: the two synchrotron components predicts the energy spectrum from the GHz region up to the optical regions quite well. The one inverse Compton component predicts the MPE observations quite well and shows a drastic break in the spectrum at approximately 10 MeV, which explains the upper limits obtained from the SAS-2 and COS-B observations. The second but higher energy inverse Compton component dominates at E_γ > 50 MeV. This component has a spectral index of -1.7 and also lies below the sensitivity levels of SAS-2 and COS-B. It also fits excellent to Grindlay's TeV data, but the spectrum breaks at around 4 TeV.

Grindlay obtained a flux of $(4.4 \pm 1)\times10^{-11}$ cm^{-2}.s^{-1} at E_γ > 300 GeV. Assuming this spectral index of -1.7 one obtains a predicted flux of $F_\gamma(> 1\ \text{TeV}) < 1.9\times10^{-11}$ cm^{-2}.s^{-1} for the Potchefstroom facility. The 'less than' symbol is due to the predicted spectral break.

3.1.2. OBSERVATIONS

The VHE γ-ray telescope of Potchefstroom was officially switched on on 23 May 1985 and the intention was to perform test runs to investigate the performance and stability of the telescope. The best information could be obtained from drift scan runs: The candidates selected were 2CG006-00 (Swaneburg et al., 1981), the radio burster CIR X-1 and the X-ray source SCO X-1. The most important source considered was CEN A due to the positive VHE results obtained by Grindlay and its favourable declination.

CEN A was observed during the dry winter months when sky conditions were favourable. Observations of CEN A started on 23 May 1985 and ended on 16 July 1985. A total of 92 drift scans across the nucleus of CEN A were undertaken with two to five scans per night. The zenith angles covered ranged between 16 and 40 degrees. The average count rate at an average zenith angle of 30 degrees was $\approx 40\ min^{-1}$. The number of scans necessary to confirm the predicted inverse Compton component above ≈ 1 TeV at the 4σ level would be approximately 90, so that the total of 92 scans seems to be sufficient.

The mean phototube count rates for all mirrors and all 92 scans gives the status of the NSB and is shown as a function of the time after the start of a scan (or right ascension) in Figure 3.1. The effect of a number of 5th magnitude stars at $\approx$ 10 min after the start of the scan and two 3rd magnitude stars slightly beyond 36 min can be seen. At that time no padding lights had been installed to stabilise the NSB. The consequence of the absence of padding lights is that the threshold energy of the system becomes time dependent as well as NSB correlated. Consequently one can expect difficulties with the identification of CEN A using this data. However, it would be interesting to see how the absence of such stabilisers would manifest in the Cerenkov data. The method outlined in Section 2.2.3 was followed to analyse the data of the 92 scans:

The first step is to identify those scans for which either the system malfunctioned or when clouds were seen overhead. During the 37th scan

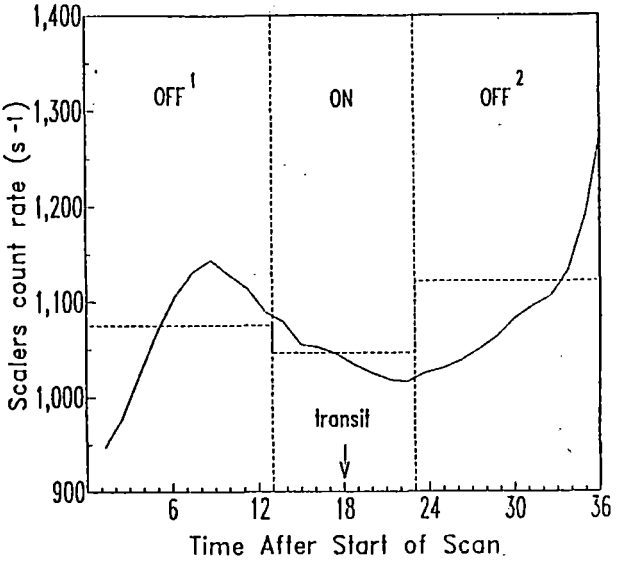

Figure 3.1. A plot of the mean scalers count rate for all phototubes as a function of the time after the start of a scan.

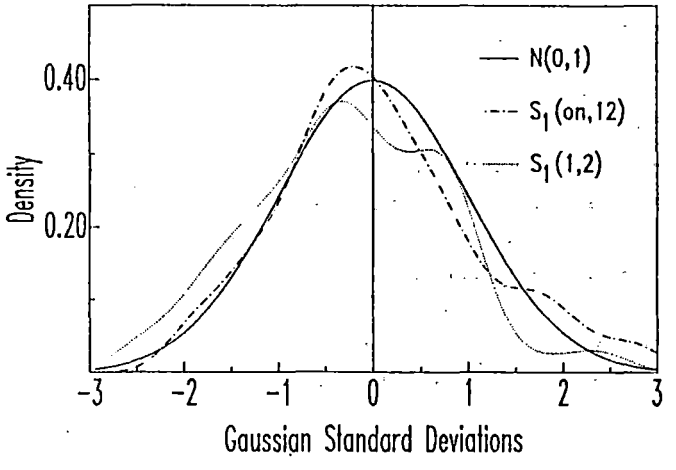

Figure 3.2. A density estimate of the S_1 statistic for N_{off^1} vs N_{off^2} and N_{on} vs N_{off} (= N_{off^1}+N_{off^2}). The heavy line is the theoretical N(0,1) density function. Negative values for $S_1(1,2)$ indicate that $N_{off^1} < N_{off^2}$ and vice versa while negative values of $S_1(on,12)$ indicate that the ON-source count rate is lower than the OFF-source count rate.

the Cerenkov registering system failed, while clouds were seen overhead during scan 42 and partly during scan 43. Consequently, only 89 scans were usable. A significant deviation of duration of ≈ 0.1 s was observed only once, when the count rate increased to $\approx 1000\ s^{-1}$. This event was also removed from the data. Such events were never seen again during the 1985/1986 observations.

The next step is to test whether the time differences for each OFF-source data set are exponentially distributed (i.e. a test for Poisson homogeneity). The Gini-test is used here since it is bin-free, scale-free and the test statistic given by equation (2.1) is standard normally distributed for sample sizes even as small as 10. The Gini-test is two-tailed in the sense that the hypothesis for exponentiality can be rejected for large values of $|G|$ and not G only.

It was decided to test for Poisson homogeneity at a significance level of $\pm 1.96\sigma$ which corresponds to a probability of making a Type 1 error of 0.05. For the 89 scans one expects 4.5 scans to be rejected on average if the data are truly exponentially distributed. For the first OFF-region the number of rejections was three which, is close to what one would expect for stable random data. However, for the second OFF-region the number of rejections was 8, which is unacceptably high and the latter occurrence corresponds to a binomial chance probability of 0.04, so that the hypothesis of Poisson homogeneity for the second OFF-region can be rejected at a confidence level of 96%. This can be understood if one considers Figure 3.1: In the first OFF-region the change in NSB is not as drastic as the corresponding change during the second OFF-region. Since the threshold energy will be affected by a change in the NSB (Jelley, 1986), one will expect the Cerenkov count rate to be correlated with the NSB in the absence of stabilisers like padding lights.

The next step was to compare the Cerenkov count rates in the two OFF-regions with each other. The number of standard deviations $S_1(1,2)$ of N_{OFF^1} above N_{OFF^2} was calculated using equation (2.6). A density estimate of the 89 calculated $S_1(1,2)$ values is indicated in Figure 3.2. The combined significance of $S_1(1,2)$ for all 89 scans (as described in Section 2.2.3) yields a value of $(89)^{\frac{1}{2}}\bar{S}_1(1,2) = (-3.0 \pm 1.2)\sigma$, which means

that the count rate in the second OFF-region is significantly higher than that in the first OFF-region. This is also illustrated by the combined light curve of all 89 scans (Figure 3.3), where one can see that $N_{OFF^2} > N_{OFF^1}$.

The classic approach in DC-analysis is to reject those scans where the one OFF-region differs by more than 2 to 3σ from the other OFF-region. Even this did not work here, because the density estimate of $S_1(1,2)$ (in Figure 3.2) would still be unbalanced on the left side, leaving an ON-OFF comparison to be unreliable. No further attempt was made to reject the two data sets with a duration of three minutes for each scan as shown on Figure 2.1.

Also shown in Figure 3.2 is a density estimate of the number of standard deviations $S_1(on,12)$ of the ON-source count rate above the OFF-source ($OFF^1 + OFF^2$) count rate. Due to the behaviour of Figure 3.1, one should expect this density to have a negative mean in the absence of TeV γ-rays from CEN A. In fact, the density estimate is shifted to the left, but there is an unusually high tail on the positive side which is unexplainable in terms of Figure 3.1. The combined significance $(89)^{\frac{1}{2}}\bar{S}_1(on,12)$ of all the scans is $(0.5 \pm 1.1)\sigma$. This value may either be due to an unusually high fluctuation in the ON-source region, or it may be due to γ-rays from CEN A. This can be understood when considering Figure 3.3 where one can see that the ON-source region is higher than the first OFF-region, which is not expected according to Figure 3.1. To quantify the positive tail of the density function of $S_1(on,12)$, one can calculate the probability due to chance of obtaining 5 scans which shows $S_1(on,12) > 1.96$, while the expected number of scans is less than 1.9. This probability is less than 4.8%. The 'less than' is applicable since the two OFF regions are supposed to be higher than the ON region (in the absence of a source).

This somewhat abnormal behaviour of the ON-source count rate can be understood if one observes the two large peaks in the ON-region in Figure 3.3. However, those peaks are not close to the transit position at 18 min and it is questionable whether they can even be attributed to transient effects from CEN A.

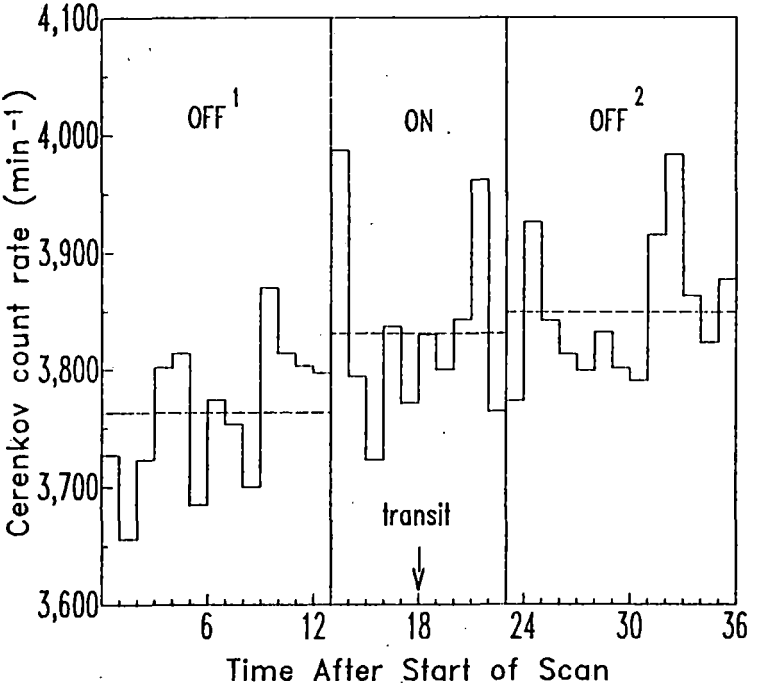

Figure 3.3. The combined light curve of CEN-A where all 89 scans have been used. The two vertical lines at 10 and 23 minutes define the ON-source region while the horizontal dotted lines correspond to the mean Cerenkov level for each region indicated.

De Jager et al. (1986a) attempted to correct for the effect of a varying NSB. A regression of the Cerenkov count rate versus NSB yielded a correlation coefficient of ≈ 0.5. The OFF-source Cerenkov count rates were corrected to the expected ON-source Cerenkov count rates (in the absence of a source of γ-rays) and the significance of the ON-source excess was calculated as 2.4σ. However, such a scheme is not very reliable due to the weak correlation found between the Cerenkov- and NSB-rates, but it still gives an indication of some enhancement from the direction of CEN A.

Consequently, one can make no conclusive statement about the reality of VHE γ-rays from CEN A for the 1985 observations. This vexing problem can only be solved by introducing padding lights in future, or by tracking CEN A for 10 minutes and also two adjacent OFF-regions for 5 minutes each, while the NSB should be checked to be similar in all three regions - the modus operandi of Grindlay et al. (1975a).

3.2. THE ISOLATED PULSAR PSR 1509-58 IN THE SUPERNOVA REMNANT MSH 15-52

Observations of the supernova remnant or synchrotron nebula MSH 15-52 by the Einstein satellite (Seward et al., 1983) revealed two compact objects. One revealed pulsations at a period of ≈ 0.150 s in both the radio (1.4 GHz) (Manchester, Tuohy and D'Amico, 1982) and X-ray (0.2-4 keV) (Seward and Harnden, 1982) bands. Due to the radio identification of this pulsar, it was named PSR 1509-58. This pulsar has a small characteristic age, i.e. $P/2\dot{P}$ ≈ 1600 years, so that one would also expect MSH 15-52 to be a young SNR. However, the age of MSH 15-52 is probably ≈ 10^4 years which does not agree with the age of the pulsar (Seward et al., 1983).

PSR 1509-58 (hereafter 'MSH') can be placed in the same category as the Crab and Vela pulsars, in the sense that the pulsars are young and clearly identified with their radio and/or X-ray synchrotron nebulae.

Only the Crab nebula of the three nebulae does not show a shell of radio and X-ray emission from an expanding supernova shock front surrounding the synchrotron nebula (Helfand and Becker, 1984). MSH is unique in the sense that its $\dot{P}$ ($\approx 1.54 \times 10^{-12}$ s.s^{-1}), is the largest of all radio pulsars known. The result is a large rate of kinetic energy loss: $\approx 1.4 \times 10^{37}$ erg.s^{-1}.

It is interesting to note that the light curve of MSH exhibits a single peak with a duty cycle of $\approx 9\%$ in the radio range. The X-ray light curve also shows a single peak, but with a duty cycle of $\approx 25\%$. Greenstein and Hartke (1983) explained the X-ray pulse profile by means of a polar cap model and their fit fixes the angle between the magnetic and rotation axis at ≈ 40 degrees. There is no evidence that the X-ray emission is due to non-thermal magnetospheric emission (as it is for the Crab pulsar) (Helfand, 1982). Unfortunately, there is no information about the relative phases of the radio and X-ray peaks.

COS-B did observations in the direction of MSH and the position of this pulsar was included in the error circle of a source listed in the first catalogue of COS-B γ-ray sources (Wills et al., 1980), but the source was excluded in a following revision (Swaneburg et al., 1981). The reason for the exclusion is that the 'point source' observed was not significant enough. According to Buccheri (1986) the COS-B data with 50 MeV $< E_\gamma <$ 3 GeV was searched for pulsations from MSH using the newest parameters supplied by Manchester, Durdin and Newton (1985). No evidence for pulsed emission was found. Nevertheless, MSH is an important object to study at γ-ray energies due to its very large $\dot{P}$ and relatively small value of P. The only difficulty with this source is its large distance of 4.2 kpc which is twice the distance to the Crab pulsar and 8 times more distant than the Vela pulsar. Cheng, Ho and Ruderman (1986) also predicted that this pulsar may be capable of forming an energetic outer gap in the magnetosphere which can generate γ-rays ($E_\gamma < 3$ GeV) through synchrotron emission and VHE γ-rays through inverse Compton processes (see Chapter 4).

3.2.1. OBSERVATIONS

Observations of MSH in the tracking mode started on 10 June 1985 and ended on 21 June 1985. Observations started at approximately 21h00 each night and the observation time for each track was approximately 1.75 hours. On 14 June 1985 no observations were done due to bad weather conditions and on the last night the observation time was extended to more than three hours. The total number of tracks ON-source is 11 with a total number of events registered ON-source of 37 334 within a time of 20.89 hours. The zenith angles covered ranged between 32 and 42 degrees.

There was no malfunctioning of the registering system at that time. In Figure 3.4 a plot a of the single photomultiplier count rate as a function of the time after the start of the eleventh run is shown. The Cerenkov count rate per minute for the same time interval is displayed on the same graph. The average zenith angle of the observations was ≈ 35 degrees so that an estimate of the mean threshold energy is ≈ 1 TeV/$\cos^{3.5}$(35) ≈ 2 TeV. At that zenith angle the collection area may also be larger than 9×10^8 cm^2. Since one is looking for short periodicities, the long term behaviour of the NSB is negligible in a timing analysis.

The 10 MHz clock worked satisfactorily in the sense that the drift of the local clock time with respect to the atomic clock time in Johannesburg could be measured within 0.1 μs (see Figure 3.5). The drift of the atomic clock with respect to UTC was 87 μs within this 11 days. Being 200 times smaller than the local drift, it was not corrected for. A quadratic function was fitted through the measured drifts. The time interval ΔT which should be subtracted from each arrival time is

$$\Delta T = 13.32 + 0.19t + 0.041t^2 \quad \text{(ms)} \qquad (3.1)$$

where t is measured in days and t = 1 corresponds to 0h UT on the first of June 1985. The rms residual of the fit in (3.1) is 0.22 ms which would correspond to a scatter of 0.1% of the phases on the light curve of MSH. Unfortunately, no absolute UTC match-up was available, so that a direct

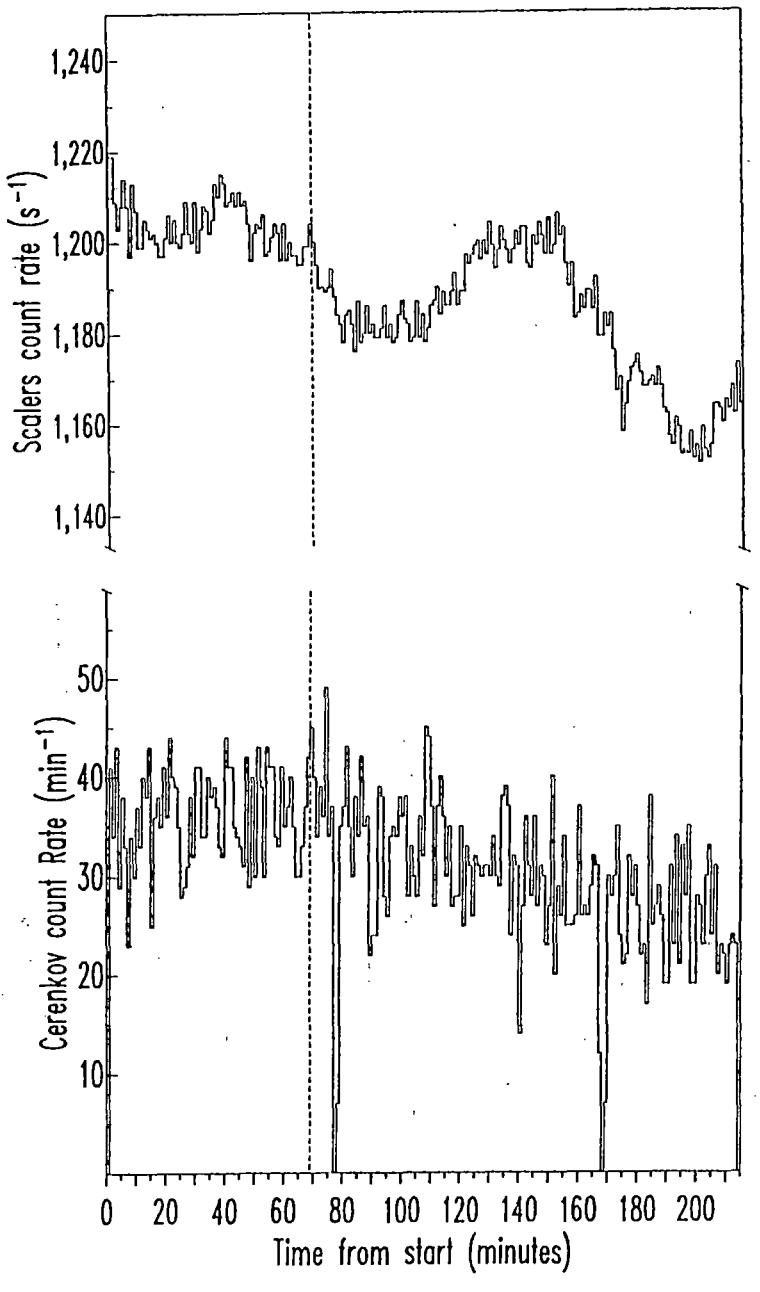

Figure 3.4. The PMT count rate and Cerenkov count rate as a function of the time after the start of the eleventh track. The vertical dashed line indicates the upper culmination of the pulsar. The two data gaps in the Cerenkov rate at 75 min and 168 min are due to limitations of the registering system.

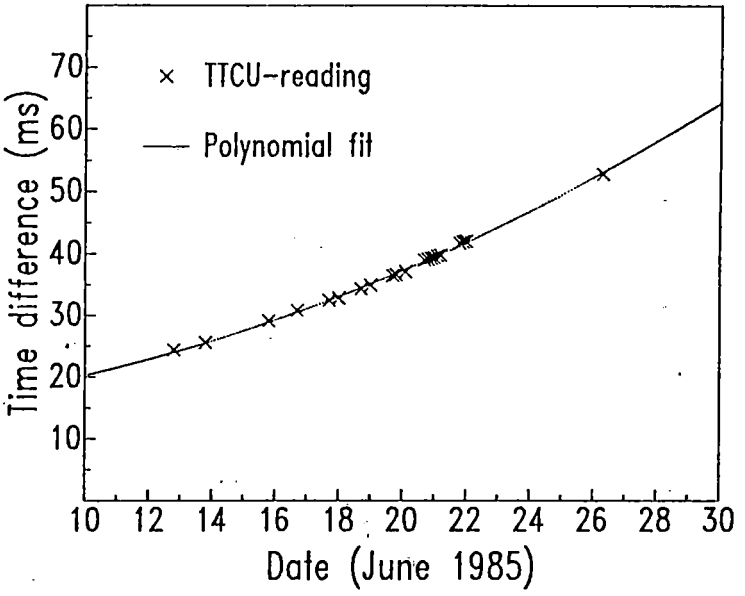

Figure 3.5. The drift of the local clock with respect to an accurate atomic clock during the period of observations of PSR 1509-58. The crosses represent the measured drifts while the smooth line represents a second order polynomial fit through these data points.

comparison of the radio and VHE γ-ray pulse phases was impossible. The site coordinates in Geocentric Cylindrical coordinates were calculated from the Geodetic coordinates given in Section 1.4. The inaccuracy of the latter coordinates is ≈ 1.3 arc seconds. The source position is given by Manchester, Durdin and Newton (1985) and the maximum inaccuracy amounts to ≈ 1 arc second.

After the arrival times have been corrected with ΔT, they were transformed to the solar system barycentre using the newest version of the program 'BARTIM' as supplied by Chandler (1985) of the Smithsonian Astronomical Observatory. This program uses the PEP 740R ephemeris which takes the inner planets into account and the resulting accuracy is ≈ 0.1 ms which is approximately on the same level of accuracy as the corrections implied by (3.1). The output time is Ephemeris time (ET) and not UTC. Using the inaccuracies in the site and source positions, the maximum differences introduced by the barycentric corrections were less than 1 ms, so that these uncertainties cannot influence the timing analysis appreciably, when a source periodicity of 150 ms is searched for.

The parameters of MSH (Manchester, Durdin and Newton, 1985) is

Frequency:	ν_o = 6.656 424 796(3) s^{-1}
Frequency derivative:	$\dot{\nu}_o$ = -6.824 27(3)x10^{-11} s^{-2}
Second derivative:	$\ddot{\nu}_o$ = 1.982(9)x10^{-21} s^{-3}
Epoch (Julian day):	T_o = 2 445 144.743 7
R.M.S. residual:	= 2.8 ms

A digit in brackets refers to two standard errors. One should remember that the time span between the quoted epoch and our observations is 3 years and the time interval between the last published radio observation and our observations is 1.2 years. It is thus informative to quote Buccheri (1981):

> "The high precision timing required in the pulsar parameters for long duration gamma ray experiments is not guaranteed by extrapolation from far epochs. Therefore only pulsar parameters

obtained simultaneously in the radio and γ-ray range are directly usable."

To illustrate this point one can refer to the X-ray observations of MSH which led to the identification of this pulsar. Remember that this pulsar was not known as a radio emitter at the time of the X-ray observations. Consider for example the first and last X-ray observations of MSH by the Einstein Observatory (Weisskopf et al. (1983)): In Table 3.1 the epochs T_e, the observed X-ray periods P_{obs}, their errors σ_{obs} and the predicted radio periods P_{rad} are indicated. One can see that the quoted X-ray errors σ_{obs} do not quite bracket the predicted radio periods. Consequently one has to search within at most one IFS around the predicted radio period.

The phase ϕ_i of each arrival time t_i is given by the fractional part of the relation (2.12):

$$\phi_i = \phi_o + \nu_o t_i + \tfrac{1}{2}\dot{\nu}_o t_i^2 + (1/6)\ddot{\nu}_o t_i^3 \qquad (3.2)$$

Since an arrival time could not be fixed with respect to UTC within ≈ 1 s, the inclusion of ϕ_o is arbitrary. Before the complete set of arrival times were folded using (3.2), a similar set of pulsed arrival times with the parameters of Manchester, Durdin and Newton (1985) were simulated with the accurate formula used by Downs (1981):

$$t = NP + \tfrac{1}{2}N^2\dot{P}P + (1/6)N^3(\dot{P}P^2+\dot{P}^2P) + (1/24)N^4(4\ddot{P}\dot{P}P^2+\dot{P}^3P)$$

Here N is the integer number of pulsar rotations since t = 0. The application of (3.2) to these arrival times yielded the desired Dirac delta light curve which proves that the analysis program is working satisfactory.

Since the clock maintained phase from night to night, the data could be treated as a single continuous set of arrival times. Consequently, one can test for coherent pulsed emission. Although the X-ray light curve shows a single broad pulse due to polar cap emission, the γ-ray emission is expected to occur near the light cylinder (Cheng, Ho and Ruderman, 1986, see also Chapter 4), so that the γ-ray profile does not need to resemble the X-ray light curve. One cannot select a statistical test unambiguously due to the uncertainty in the form of the light curve. It was therefore decided to select the H_m-test as discussed in Section 2.5 since this test seems to be powerful for a wide variety of light curves.

The value of one independent Fourier spacing due to 11 days of observations equals $\Delta\nu_{11} = 1/(86400 \times 11.04)$ Hz = 1.048 μHz. The parameters $\dot{\nu}_o$ and $\ddot{\nu}_o$ were kept fixed at their published values while ν was allowed to vary within the interval $(\nu_o \pm \frac{1}{2}\Delta\nu_{11})$, which corresponds to a search interval of one IFS. The results are illustrated in Figure 3.6 and at $\nu = \nu_o - 0.25\Delta\nu_{11}$ a p-level of 10^{-4} is evident. The effect of oversampling within one IFS as described in Section 2.3.5 was simulated for the H_m-test under the same circumstances whereby the reported effect was found. The ratio r of underestimation was = 10 so that the real p-level is 10^{-3}. One can thus reject the hypothesis for uniformity at a confidence level of 99.9%.

The period of detection which corresponds to $\nu_o - 0.25\Delta\nu_{11}$ is P_{obs} = 0.150 374 813(3) s for the epoch T_e = 2 446 227.38 JED. The approximate standard error σ_{obs} = 3 refers to the HWHM of the peak in Figure 3.6, so that P_{obs} can be considered as being shifted with approximately $\sigma_p = (P_{obs} - P_{rad})/\sigma_{obs}$ = 2 standard errors from the predicted radio period. One can see from Table 3.1 that σ_p for the X-ray and VHE measurements are similar and positive. In fact, only one of the five observations reported by Weisskopf et al. yielded a negative σ_p. For the last (and longest) X-ray observation, the difference between the X-ray and radio positions caused a shift of only 1.6×10^{-4} IFS, while the 95% confidence interval for the observed IFS between the X-ray and radio periods is

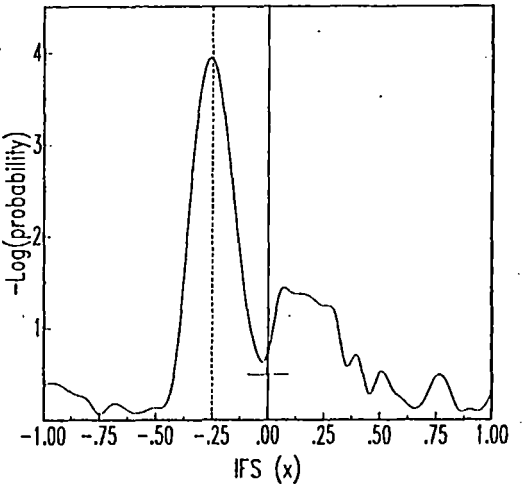

Figure 3.6. The p-level calculated from the H_m-test transformed to the significance $-\log_{10}(Pr)$ for all eleven tracks (combined in time) as a function of the number of IFS $x = (\nu - \nu_o)/\Delta\nu_{11}$. The period corresponding to $\nu_o - 0.25\Delta\nu_{11}$ is the identified period P_{obs}. The bar at $x = 0$ gives the error of the predicted radio period. The x-scale can be transformed to a period scale if one takes $P = 0.150\ 374\ 807 + (23.7\ ns)x$.

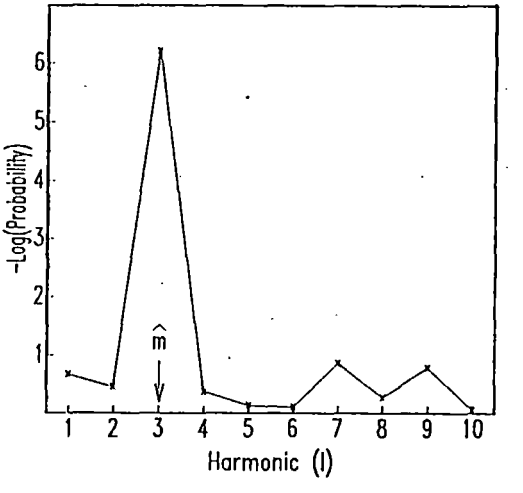

Figure 3.7. The parameter $-\log_{10}(Pr)$ for each harmonic ℓ plotted at the period P_{obs}. The optimal number of harmonics is three which were used to evaluate the p-level of the peak in Figure 3.6.

[0.003 - 0.083] IFS. This illustrates that the positional differences may not necessarily have contributed to the observed shifts in period.

The absolute error (P_{obs} - P_{rad}) is smallest for the VHE measurements which is due to the single data set with a duration of eleven days and the IFS is then much smaller than the smallest IFS of the X-ray observations.

Consequently one can have confidence in the identified VHE periods but follow up radio observations are necessary to confirm this effect.

3.2.3. THE FREQUENCY SPECTRUM.

To investigate the geometrical characteristics of the radiation, the p-level (transformed to $-\log_{10}$(p-level)) for each harmonic ℓ was plotted as a function of ℓ in Figure 3.7. It is evident that all the power is concentrated in the third harmonic, which corresponds to a p-level of 6×10^{-7} for that harmonic alone. The power in all the other harmonics corresponds to those of a uniform density. Furthermore, one can see how conservative the H_m-test really is: the act of searching through the harmonics causes the p-level to be changed from 6×10^{-7} to 1.1×10^{-4} - a change of a factor of nearly 200. The main reason for this is that there is very little power in the first harmonic and no power in the second harmonic and one actually sums noise at ℓ = 1, 2 to the signal at ℓ = 3 when calculating the H_m-statistic.

To investigate the frequency spectrum further, the p-level for the third harmonic alone was plotted for the frequency range $\nu_o \pm 30\Delta\nu_{11}$ in Figure 3.8. This range corresponds approximately to one third IFS for a single track at this period. This structure was also observed by Chadwick et al. (1985b) and North et al. (1987) and illustrates a few facts with which VHEGRA has to be contented:

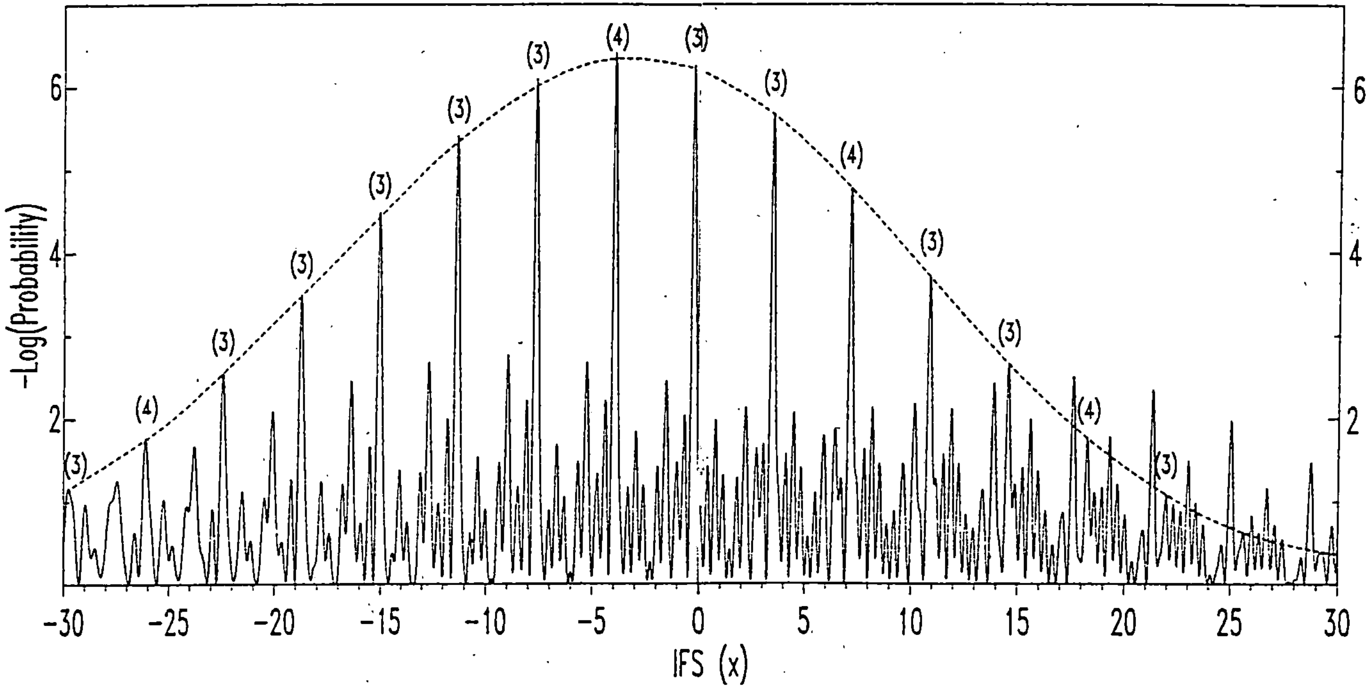

Figure 3.8. A graph of the parameter $-\log_{10}(Pr) = 0.43n\bar{R}^2{}_3$ for the third harmonic alone as a function of the number of IFS $x = (\nu - \nu_o)/\Delta\nu_{11}$ for a range which covers approximately a third of the IFS for a single tracking run. A number in brackets above each peak represents the optimal number of harmonics obtained from the Hart rule (2.56) at that period.

(i) The broad structure is exactly the width expected from a single track alone and it specifies the underlying period resolution of such an experiment when no external information is available

(ii) Due to the eleven repetitions of the experiment an interference pattern in period space resulted in a pattern which allows the resolution of the experiment to increase dramatically, provided the external information can pinpoint the correct peak. Still, quite a number of peaks have a similar significance, illustrating the leaking of Fourier power to adjacent peaks due to data gaps. Due to the ≈ 7 hour limitation of observations per night and the apparent weakness of the sources, this type of picture will be seen quite often in the future.

As to the properties of MSH, it is clear from the numbers in brackets above the main peaks that this radiation is mainly at the third harmonic. The pattern of Figure 3.8 can be simulated quantitatively by referring to the theory of a diffraction grating (see e.g. Hecht and Zajac, 1980). The relative intensity produced by eleven equidistant slits on a screen is given by

$$I(x;b,d) = \left[\frac{\sin 3\pi x b/d}{}\right]^2 \left[\frac{\sin 3\pi x}{3\pi x/11}\right]^2$$

where x is the distance perpendicular to the beam of light, b is the slit width and d is the distance between slits. The factor of 3 compensates for the third harmonic.

The whole data set corresponds to b = 180 minutes and d = 11 days and Figure 3.9 with these parameters resembles Figure 3.8 clearly. However, the secondary maxima in Figure 3.8 are not as clear as those in Figure 3.9, which is due to the contamination of the data by the strong uniform background. Small differences also occur since not all tracks were equal in length and equidistantly spaced.

The frequency spectrum was investigated further for all the data combined by examining the distribution of $2n\bar{R}^2_3$ for 9 461 equally spaced (spacing = 1/3 IFS) periods around ν_o, but excluding the pulsed region

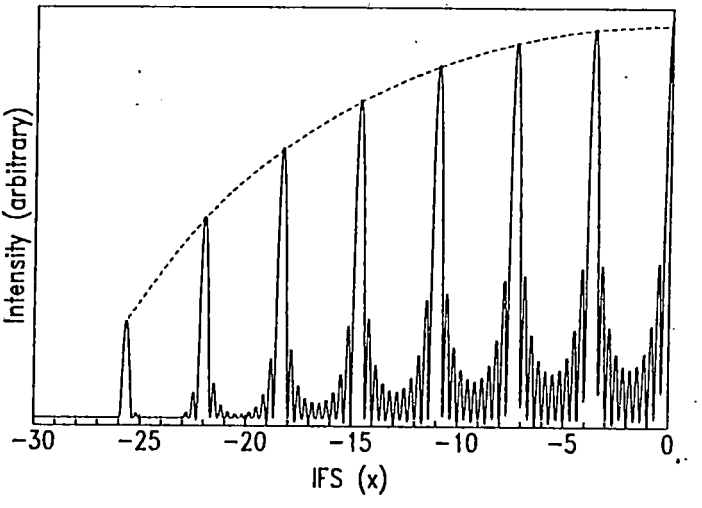

Figure 3.9. The intensity profile for a diffraction grating with eleven equally spaced slits. The parameters of the grating were selected to approximate the parameters of the eleven tracks on PSR 1509-58 as close as possible. The scale of x is closely related to the corresponding scale in Figure 3.8.

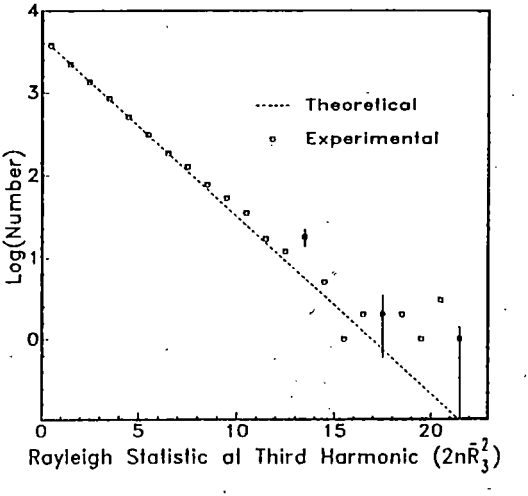

Figure 3.10. The differential number distribution of $2n\bar{R}^2{}_3$ calculated from 9461 selected frequencies around the expected frequency ν_o, but excluding the region $\nu_o \pm 30\ \Delta\nu_{11}$. The spacing between the frequencies is (1/3) IFS.

described by Figure 3.8. The differential number distribution of the $Z = 2n\bar{R}^2_3$ values were investigated via a minimum χ^2-fit on the expected distribution of exp(-bZ) where b = 0.5 is expected for uniformly distributed events. The result of the fit obtained was $b = 0.487 \pm 0.17$ at a confidence level of 95%, which includes 0.5. The fit for b = 0.5 is shown in Figure 3.10 and the excess events at $Z > 16$ are not significant and are possibly due to power leakage from the main radiation region. However, the fit is acceptable, ensuring that the data used were indeed uniformly distributed.

3.2.4. THE SIGNAL STRENGTH AND FLUX

According to Figure 3.7 all the power is concentrated in the third harmonic. The best parametric approximation for the light curve is a triple sinusoid (equation (2.60) with $\ell = 3$):

$$f(\theta) = (1 + p\cos 3\theta)/2\pi, \quad \theta \in [0, 2\pi]$$

An unbiased estimator of the total signal strength according to (2.62) is

$$\hat{p} = 2[(n\bar{R}^2_3 - 1)/(n - 1)]^{\frac{1}{2}} \pm (2/n)^{\frac{1}{2}}$$

The Fourier power of the third harmonic at P_{obs} in Figure 3.7 is given by $n\bar{R}^2_3 = 14.5$ which corresponds for the 37 334 events to a signal strength of $p_c = (3.8 \pm 0.7)\%$. With a mean threshold energy of ≈ 2 TeV, an effective collection area of $\approx 9 \times 10^8$ cm^2 and a total observation time of 20.89 h, the flux of VHE γ-rays from MSH can be estimated as

$$F_\gamma(> 2 \text{ TeV}) = (2.1 \pm 0.4) \times 10^{-11} \text{ cm}^{-2}.\text{s}^{-1}$$

where the error is statistical only. However, the error may be larger due to uncertainties in the collection area.

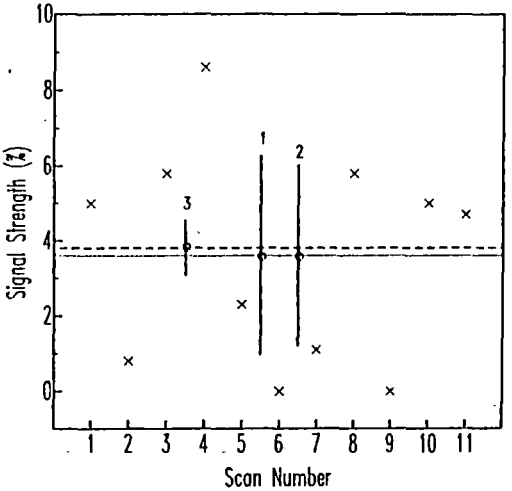

Figure 3.11. The estimated signal strength of the eleven tracks (crosses). The solid horizontal line at $\bar{p}$ = 3.6% corresponds to the average signal strength calculated from the 11 observations. The dashed horizontal line at p_c = 3.8% corresponds to the signal strength calculated from all the data combined in time (i.e. the 'coherent analysis'). The three vertical bars represent one sigma confidence intervals which were calculated as follows: (1) the standard error σ of the eleven values, (2) the expected average standard error σ' for a single tracking run and (3) the expected standard error for all eleven tracking runs combined in time.

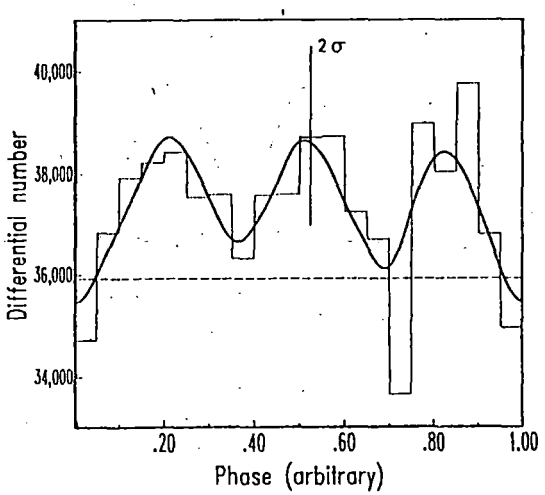

Figure 3.12. An estimate of the γ-ray light curve of PSR 1509-58 with P = P_{obs} for all 37 334 events. The KDE technique with Swanepoel's kernel was used, yielding $\hat{h}$ = 0.054. Also shown is a 2σ confidence band and a 20-bin histogram estimate. The dotted horizontal line is the estimated background level.

3.2.5. COHERENCY AND TIME VARIABILITY

The eleven tracks were searched for evidence of time variability at the identified frequency of $\nu_o - 0.25\Delta\nu_{11}$ using the third harmonic alone. The signal strength p_i for each track $i = 1, \ldots, 11$ was calculated from (2.62) and is shown in Figure 3.11 as a function of the scan number. The mean value of these signal strengths is $\bar{p} = (3.6 \pm 0.8)\%$ which is very close to the value of $p_c = (3.8 \pm 0.7)\%$ obtained from the coherent analysis. Since $p_c \simeq \bar{p}$, one can believe that the TeV radiation from night to night is coherent.

The status of time variability can be determined if one compares the standard error of p_i

$$\sigma = \sqrt{[(1/11) \sum_{i=1}^{11} (\bar{p} - p_i)^2]}$$

with the mean expected error of p_i for steady emission

$$\sigma' = (1/11) \sum_{i=1}^{11} (2/n_i)^{\frac{1}{2}}$$

where n_i, $i = 1, \ldots, 11$ are the sample sizes of the individual tracks. The results on MSH yielded $\sigma = 2.7\%$ while $\sigma' = (2.5 \pm 0.1)\%$. Observe also that the central limit theorem yields $\sigma/\sqrt{11} = 0.8$ and $\sigma'/\sqrt{11} \simeq 0.7$ which are respectively the errors on $\bar{p}$ and p_c. The errors σ and σ' of p_i are shown as bars on Figure 3.11. Since $\sigma \simeq \sigma'$ it may be assumed that the observed VHE emission from MSH was steady with NO EVIDENCE OF TIME VARIABILITY.

The fact that the emission from MSH was steady is very important, since reports of high energy transients (in contrast to steady emission) from isolated pulsars are difficult to identify with the observed steady radiation at lower energies (Smith, 1986).

Table 3.1. A comparison of observation period P_{obs} relative to the predicted radio period P_{rad} for different epochs T_e.

Epoch T_e (JD 2 444 000+)	Epoch difference $(T_e - T_o)$ days	Observed Period $P_{obs} \pm \sigma_{obs}$	Predicted [c] Period (P_{rad})	Relative [d] error (σ_p)
107.88[a]	- 1036.9	0.150 092 885(75)	0.150 092 781(2)	+1.4
470.66[a]	- 674.1	0.150 141 100(13)	0.150 141 072(1)	+2.2
2227.38[b]	1082.6	0.150 374 813 (3)	0.150 374 807(2)	+2.0

a X-ray observations by HEAO-2.
b TeV observations by the Potchefstroom group.
c Extrapolated radio period from epoch T_o.
d $\sigma_p = (P_{obs} - P_{rad.})/\sigma_{obs}$ (standard deviations).

Table 3.2. A list of the pulsars found in the 2CG006-00 error box.

PULSAR [a]	Right Ascension(1950.0) h m s	Declination (1950.0) degrees	Period [b] (ms)	Dispersion measure ($cm^{-3}.pc$)	Mean flux density (mJy)
1758-23	17 38 15(20)	- 23.08 (7)	415.7644(20)	1140 (50)	5
1755-23?	17 56 00(45)	- 23.53(17)	60.7308 (5)	550(100)	2
1802-23?	18 02 45(45)	- 23.37(17)	112.5343(20)	400(100)	3

a A question mark indicates that the pulsar is a suspect.
b The periods correspond to November 1981.

3.2.6. THE VHE GAMMA RAY LIGHT CURVE.

The phases $\theta_1, \ldots, \theta_{37\ 334}$ were used to estimate the light curve with the Swanepoel kernel and is shown in Figure 3.12. The estimated smoothing parameter was $\hat{h} = 0.054$ which is close to the theoretical value of $h^*_r = 0.049$, calculated from (2.49) with $r = 4$ and the triple sinusoid with $p_c = 0.038$. A histogram with $M = 20 \approx 1/\hat{h}$ bins is also shown. The bin positions were chosen only once.

One can see that the histogram agrees quite well with the KDE but its scatter is quite large. The large deviations of the histogram between phase 0.7 and 0.8 can be cancelled by a readjustment of the bin positions. This illustrates how misleading a histogram may be. Also shown is a band of approximate 2σ confidence intervals on the KDE. These are slightly narrower than the confidence intervals calculated from the histogram.

The percentage background is $100(1 - p_c) = 96.2\%$ and this level is also shown in Figure 3.12. It can be considered as a good estimate since all the power is in the third harmonic, which implies that the characteristic functions $R_\ell = 0$ for all ℓ except $\ell = 3$. Consequently the light curve is a triple sinusoid and the method used to estimate p_c is correct. Furthermore, some parts of the light curve lies below this line, so that there is no evidence that p_c was overestimated using relation (2.62). One can also see that the three minima are not at the same height, so that one cannot conclude that the fundamental period is 50 ms.

3.3. A YOUNG PULSAR IN THE ERROR BOX OF THE GAMMA RAY SOURCE 2CG006-00

The COS-B satellite detected some 25 high energy γ-ray sources at $E_\gamma > 50$ MeV. Only four of them are clearly identified with well known objects. They are PSR 0531+21, PSR 0833-45, 3C273 and ρOph (Swaneburg et al., 1981). There is a possibility that 2CG065+00 may be associated with

the 6 ms pulsar PSR 1953+29 (Chadwick et al., 1985a). However, the majority of 2CG objects remain unidentified due to the large field of view of COS-B and the belief is that many of them may be associated with short period pulsars which have been missed in previous radio surveys due to the limiting sensitivities of radio search techniques and interstellar scattering. This motivated a sensitive search for short period pulsars in three relatively strong unidentified COS-B point sources by Manchester, D'Amico and Tuohy (1985) at the Parkes radio telescope and four other 2CG point sources with the Arecibo experiment (Boriakoff, Buccheri and Fauci, 1983). Three pulsars were found in the 2CG006-00 error circle and none in the other two γ-ray point sources observed at Parkes. This makes 2CG006-00 an important object for further γ-ray studies. However, it should be mentioned that only one pulsar in 2CG006-00 is confirmed and the two others need confirmation although they have strong signal to noise ratios. Table 3.2 lists these pulsars, their status and corresponding parameters.

The dispersion measures quoted are quite high and may be due to an intervening HII region in the direction of Right Ascension = 18^h and Declination = -23 degrees (Manchester, D'Amico and Tuohy, 1985). According to Manchester and Taylor (1977) the mean electron density n_e in that direction is large and variable. According to D'Amico (1986) it is difficult to estimate n_e in the direction under consideration. Assuming a density of $n_e \approx 0.12$ cm^{-3} one obtains a distance of $\approx$ 10 kpc for PSR 1758-23 which is the same distance postulated by Manchester, D'Amico and Tuohy, (1985). For PSR 1755-23 the distance is $\approx$ 5 kpc and for PSR 1802-23 it is $\approx$ 3 kpc. The latter two suspects may be considered as better candidates for γ-ray emission than the confirmed one, due to the smaller distances and periods involved.

These pulsars in 2CG006-00 were discovered during November 1981. Up to the present time there has been no follow up observations at a similar sensitivity level, so that no attempt has been made to measure a $\dot{P}$ for any of those pulsars. Consequently, observations at other epochs in the γ-ray bands are only useful if the γ-ray count rates are high while the observation time ON-source is small. Consequently the information in Table 3.2 is insufficient to search for periodicities in the COS-B data,

but for VHEGRA the situation is better. To illustrate this, one can use the well known Taylor expansion for the frequency around a reference epoch t_o

$$\nu(t) = \nu(t_o) + \dot{\nu}(t-t_o) + \tfrac{1}{2}\ddot{\nu}(t-t_o)^2$$

Let t_1 and t_2 denote the beginning and end times of an observation (with $t_1 > t_o$). If one neglects $\dot{\nu}$ and $\ddot{\nu}$, the shift in frequency from time t_1 to t_2 due to this assumption is

$$\Delta\nu = \nu(t_2) - \nu(t_1) = \dot{\nu}(t_2 - t_1)$$

If a maximum shift of $\frac{1}{2}$IFS (which corresponds to a "peak walking" of 25%) is allowed (see Section 2.3.5) the maximum total observation time $(t_2 - t_1)$ must be

$$\dot{\nu}(t_2-t_1) \leq (2(t_2 - t_1))^{-1} \text{ or } t_2-t_1 \leq P/(2\dot{P})^{\frac{1}{2}} \qquad (3.3)$$

Buccheri and Sacco (1984) first arrived at the above relation. Assuming that these pulsars are isolated (no evidence for binary motion had been found), one can roughly assume that 10^{-15} s.s^{-1} < $\dot{P}$ < 10^{-13} s.s^{-1} according to the standard model of magnetic dipole radiation (see Chapter 4), so that the maximum observation times range between 10 and 100 days for PSR 1758-23, between 2 and 15 days for PSR 1755-23 and between 3 and 30 days for PSR 1802-23. Unfortunately one cannot search at the moment for those pulsars in the COS-B data base, since the observation time of COS-B for a certain source was ≈ 20 days during which only ≈ 500 photons were collected. A second problem is the large number of IFS which would be necessary to cover all possible $\dot{P}$ values. The situation is different for VHEGRA: The observation time necessary to collect ≈ 500 events is ≈ 10 minutes. It is thus possible to use the information in Table 3.2 for VHE γ-ray observations and a negligence of $\dot{\nu}$ and $\ddot{\nu}$ will not cause the light curve to smear out during 10 minutes of observations.

3.3.1. OBSERVATIONS

Being one of the strongest COS-B sources, it was observed in the drift scan mode during two dark moon periods during June and July 1985. The observations were spread over 22 separate nights which resulted in the registration of 36 213 events within the COS-B error box and 89 770 events in the two adjacent OFF-regions. De Jager et al. (1986a) reported a 7.6σ DC excess in the ON-region, but corrected this significance to a value of 1.9σ which was necessary due to the presence of the Trifid Nebula and other stars close to the position of 2CG006-00 in the absence of padding lights. However, they stressed that this result may not be reliable due to the weak correlation found between the Cerenkov count rate and starlight background.

Although the data base cannot be used for spatial analysis (see Section 3.1), it is still very useful for timing analysis. Raubenheimer et al. (1986) searched for the pulsars listed in Table 3.2 at their radio positions. At that time only the Rayleigh test was used to search for power in the fundamental. It was also assumed that the period derivative of each pulsar was less than 422×10^{-15} s.s^{-1} - the value for the Crab. Evidence for pulsed emission at p-levels less than 10^{-2} was found in seven scans of PSR 1802-23, while the Right Ascension profiles for six of them resemble Figure 2.1. Taking all the degrees of freedom into account, PSR 1802-23 could be identified as a possible transient source at a confidence level of 99.8%.

At this stage it is important that one should take notice of three kinds of analyses. These are the 'transient'-, 'persistent'- and 'coherent' methods of analysis on data which consist of more than one independent observation: Let there be k such observations:

(a) With a transient analysis those scans (or tracks) are identified which show p-levels less than a prescribed level of significance of 10^{-2} or 10^{-3}. Let there be ℓ such observations. The binomial probability of obtaining ℓ successes out of k trials is then calculated. This method is sensitive if the ℓ observations contain transients while

(k - ℓ) observations are 'dead'. The transient method was used by Raubenheimer et al. (1986), Lamb et al. (1986), Gorham et al. (1986a) and Fegan et al. (1986). Observe their confidence levels - they were usually less than 99.9%. However, if the emission is steady and non-variable, the transient method may underestimate the significance and one should use the more powerful .

(b) persistent method whereby the Rayleigh powers of the k observations are summed. In this case each scan will contribute to the significance of the result - no matter how small the contribution from each observation is. If $k \to \infty$, the confidence level will converge to one. Examples of this kind of analysis is the identification of PSR 1953+29 by Chadwick et al. (1985a) and the reanalysis of the data on PSR 1802-23 in this section. Note that coherency is not a condition for the success of this method, but if the emission is also coherent, one should use the most powerful

(c) coherent method whereby all observations are treated as a single set of arrival times. This method will be successful if all the relevant pulsation parameters are known. For examples of the coherent analyses see Chadwick et al. (1985b), North et al. (1987) and the analysis of MSH in the previous section. Note the respective p-levels obtained by these authors before the extra trials were taken into account: 5×10^{-7}, 2×10^{-6} and 6×10^{-7}. They are much less than the values of $> 10^{-3}$ obtained from the transient analyses.

It is interesting to see that the transient-, persistent- and coherent methods give for MSH 'chance probabilities' of 5×10^{-3}, 10^{-4} and 6×10^{-7} respectively for the third harmonic alone. Observe the increase in the significances when improving the analysis methods.

If the radiation from PSR 1802-23 is at least steady, a 'persistent' analysis will give a larger confidence level than that obtained from the transient analysis. A coherent analysis cannot be done for PSR 1802-23, since no $\dot{P}$ information is available at the moment. The transient analysis will be repeated by taking the mentioned effect of oversampling within an IFS

into account. A persistent analysis will then be done to see whether the confidence level can be improved.

Raubenheimer et al. (1986) investigated the distribution of the Rayleigh statistic for scan 37 for only 250 IFS around the radio period, but did not quantify that distribution further. The distribution for two scans which showed evidence for pulsed emission (numbers 22 and 37) will be quantified: The first ten minutes of each data set were used to calculate the Rayleigh statistic for 10^6 IFS (where the independent periods ranged between 0.6 ms and 1 s). The Rayleigh statistics for each scan were binned into 28 intervals and are shown on Figure 3.13 for scan 22. The expected differential number distribution for uniformly distributed events is again exp(-bZ) where b = 0.5. From a minimum χ^2-fit, b was found to be 0.501(2) and 0.498(2) for scans 22 and 37 respectively. A number in brackets refers to a 95% confidence interval for the estimated b. Consequently $2n\bar{R}^2$ follows the expected distribution quite well.

3.3.2. THE STATUS OF TRANSIENT EMISSION

The probability of obtaining 7 out of 75 scans at a detection threshold of α is given by the binomial probability:

$$Pr(\alpha) = \left(\frac{75!}{7!(75-7!)}\right)\alpha^7(1-\alpha)^{69} = 2\times10^9\ \alpha^7(1-\alpha)^{68}$$

Raubenheimer et al. (1986) searched for those scans which showed a p-level less than the chosen significance level of $\alpha = 0.01$, but since 2 IFS were searched, the effective threshold is changed to

$$\alpha = 1-(1-0.01)^2 \approx 0.02$$

giving a chance probability of $Pr(0.02) = 7\times10^{-4}$. However, when taking the results of Section (2.3.5) into account, the p-level of the Rayleigh distribution is underestimated by a factor of ≈ 5.7 when searching within 2 IFS for the maximum value of the Rayleigh power equal to or larger

than 9.21 (which would have corresponded to $\alpha = 0.01$). The resulting threshold is then $\alpha \approx 0.057$ so that the real binomial probability for chance occurrence is $Pr(0.057) = 0.072$. Consequently the real confidence level for the detection of emission from PSR 1802-23 in these three pulsar searches is only 80% and not 99.8%. Thus, one cannot consider the seven scans as indicative of radiation from PSR 1802-23. However, additional evidence of radiation from PSR 1802-23 was found: A $\dot{P}$ of $\approx 10^{-13}$ $s.s^{-1}$ was found for scan 37 which (together with P = 112 ms) agrees approximately with the $\dot{P}$ and P values of the Vela pulsar. Furthermore, some evidence of coherency was found when two sets of data over periods of three days were combined in time for a coherent analysis. At that stage no $\dot{P}$ was introduced and according to equation (3.3) a smearing of only $\approx$ 25% would have resulted on the light curve if the real $\dot{P}$ is $\approx 10^{-13}$ $s.s^{-1}$. The introduction of a P-term in the analysis may therefore improve the confidence level.

3.3.3. SEARCH FOR STEADY, NON-COHERENT PULSED EMISSION

As mentioned previously, a 'persistent analysis' on data from a steady and non-variable source will provide a much better confidence level than that obtained from a transient analysis: The data from each of the 75 scans was split into 31 overlapping sections, each with a length of 6 min. The number of IFS which fits into the assumed period range equals 1.3 in this case. At each of the 31 Right Ascension positions the maximum $(2n\bar{R}^2)_i$ of the Rayleigh statistic was searched within the 1.3 IFS. For each position the 75 maximum values were summed. The ratio r (factor of underestimation) as a function of $2n\bar{R}^2$ was calculated for 1.3 IFS from Figure 2.8 by means of interpolation. Using this relation, the distribution of the sum of 75 such maximum values were simulated. The distribution was found to be

$$\sum_{i=1}^{75} 2n\bar{R}_i^2 \approx {}^{d}(\chi^2_{273}) \approx {}^{d}(N(273,23))$$

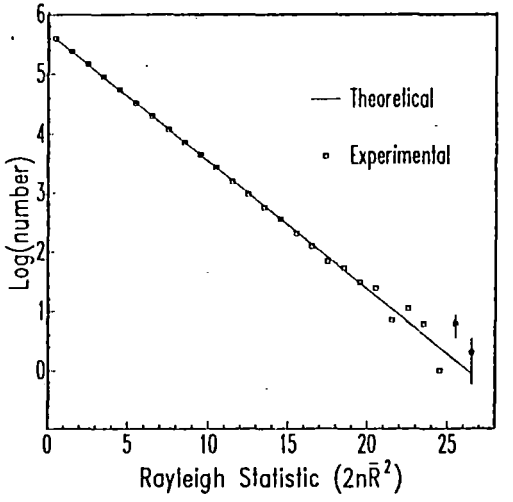

Figure 3.13. The theoretical and experimentallv determined differential number distributions for the first 10 min OFF-source data of scan 22 on the γ-ray source 2CG006-00. 10^6 independent periods ranging between 0.6 ms and 1 s were sampled to draw up this distribution.

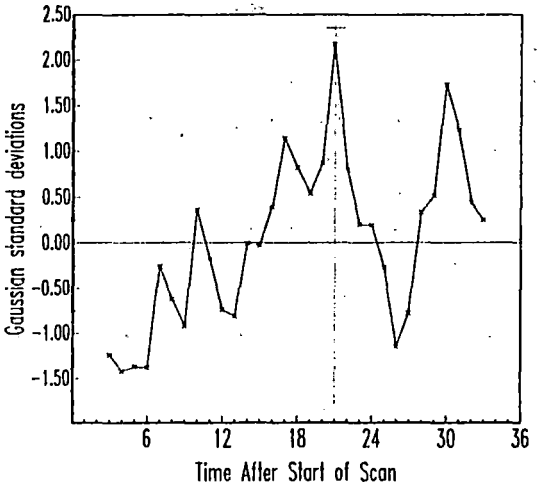

Figure 3.14. The significance (Gaussian standard deviations) for each overlapping section of 6 min for all 75 scans on PSR 1802-23. The vertical dotted line corresponds to the pulsar position while the bar gives the error in the radio position.

This result on PSR 1802-23 is shown in Figure 3.14, where the summed values had been transformed to standard normal variables. At the position of the pulsar a peak with a significance of 2.2σ is visible. It is disturbing to see the 1.7σ peak at 28 min also. However, the standard deviations in Figure 3.14 are identically N(0,1) random variables under H_o, but they are not independently distributed due to the overlapping data sections. Consequently neither the Right Ascension profile nor the 1.7σ peak at 28 min can be evaluated with respect to all the data in this figure.

Consequently the evidence for steady pulsed emission is more significant than the indications for transient emission, since it is a low level contribution from each scan which gives rise to the observed 2.2σ peak in Figure 3.14. Thus, the identification of persistent emission from PSR 1802-23 can be considered at a confidence level of 98.6%.

This result is a typical illustration of an analysis which was hampered by too little information resulting in the introduction of too many 'degrees of freedom' (especially in view of Section 2.3.5).

If one assumes that the radiation from PSR 1802-23 is real, some characteristics of the radiation can be determined: The 2.2σ significance corresponds to a p-level of 0.017 which corresponds to a signal strength of $\bar{p} = (2.5 \pm 1.0)\%$ calculated from (2.62) for ≈ 21 700 events in the six minute window ON-source. This is indicative of a flux of steady emission of $\approx 2.2 \times 10^{-11}$ cm^{-2}.s^{-1}. Raubenheimer et al. (1986) identified a signal strength of ≈ 28% for scan 37 alone. This signal strength corresponds to a 3.8σ Gaussian standard deviation from the level of steady emission which was calculated as follows: Consider a sample of size n from the data base which alone yields a signal strength of p'. The number of Gaussian standard deviations z of p' above the steady level of $\bar{p}$ is calculated from the property of asymptotical normality of the random variable p':

$$p' = \bar{p} + z(2/n)^{\frac{1}{2}}$$

Consequently scan 37 cannot be considered as a statistical fluctuation from the steady emission level and it must be a transient if the radiation is real.

3.4. CONCLUSION

The failure to make any conclusive statement about CEN A illustrates again the importance of stabilising the illumination of the phototubes during the course of a scan. However, one important purpose of the analysis of the CEN A data was to illustrate the use of the scale-free and bin-free Gini-test. This test seems to be able to identify slow trends in the count rate and it can be used for many applications in experimental astrophysics - even if the sample sizes are as small as 10.

The case of MSH is unique in the sense that it is the first time that such a triple peaked light curve showed up for an isolated pulsar. The Rayleigh test and a test for the second harmonic would have failed to identify this pulsar. Without the H_m-test, one would have been forced to adopt a test like Z^2_{10}. However, the H_m-test was able to identify this pulsar once, without having to resort to other tests. The outcome of the H_m-test is two dimensional: apart from giving a p-level, it also gives the best estimate of the optimal number of harmonics. In the case of MSH, $\hat{m} = 3$. Extra information was gained when the Fourier power as a function of the harmonics showed that all the power is concentrated in the third harmonic. Consequently a good estimate of the signal strength could be made. The information gained from the analysis on MSH is the following:

(a) The radiation from MSH is coherent.

(b) There is no evidence that the radiation is time variable, since the signal strength remained constant from night to night within acceptable statistical fluctuations.

The period P_{obs} at which MSH was identified in this study, deviated from the extrapolated radio period with the same amount as the corresponding deviations of the observed X-ray periods from their extrapolated radio periods. One must also keep in mind that this pulsar was first identified as an X-ray pulsar. Consequently, P_{obs} obtained from the TeV observations can be considered as being consistent with the radio parameters and the detection of pulsed coherent and steady VHE γ-rays from MSH is claimed at a confidence level of 99.9%.

Due to the results of Section 2.3.5, the results on PSR 1802-23 are not as significant as presented by (Raubenheimer et al., 1986). This shows how careful one should be when searching for pulsed emission within one IFS especially when the results from different observations are combined. The result obtained is a good illustration of the dependence on input from other astronomies and the effect of allowing too many independent trials in the search. However, when searching for steady pulsed emission from PSR 1802-23, evidence thereof showed up at a confidence level of 98.6%. Although much lower than the published confidence level of 99.8% for transient emission, this indication of persistent emission is considered to be more valuable, since transient emission is unlikely to occur for isolated pulsars (Smith, 1986). Furthermore, some indication of coherency was found between some scans (Raubenheimer et al., 1986) which may enhance the significance of the result. The value of $\dot{P} \approx 10^{-13} \cdot s.s^{-1}$ found for this object by Raubenheimer et al. is acceptable according to the standard model of magnetic dipole radiation. If this period derivative is correct, PSR 1802-23 is a prime candidate for VHE γ-radiation according to the outer gap model (see Chapter 4), indicating follow up observations and analysis on this object.

CHAPTER 4

GAMMA RAYS FROM ISOLATED PULSARS.

In view of the two isolated pulsars discussed in Chapter 3 and the others found to radiate in the TeV region, it is important to know whether these pulsars are able to radiate VHE γ-rays via the known physical processes. Secondly, it is also important to know which other pulsars may be VHE radiators.

After a discussion of the standard model for pulsars and the important parameters like the energy loss rate and the estimation of a magnetic field strength, the production of γ-rays in two models will be investigated: It will be shown that most pulsars can produce polar cap γ-rays with E_γ < 1 GeV while only some millisecond pulsars can provide observable VHE polar cap γ-rays. It is only the more complex model of Cheng, Ho and Ruderman (1986) (hereafter CHR) which can produce all radiation from optical up to VHE γ-rays for a larger sample of pulsars. Both these models invoke synchrotron, inverse Compton and curvature radiation as the mechanisms involved and differs only as to the regions where the emission originates.

4.1. THE RATE OF ENERGY LOSS AND MAGNETIC FIELD STRENGTH ESTIMATION.

It is well known that the total rate of kinetic energy loss of an isolated pulsar which is spinning down, is given by

$$\dot{E} = -I\Omega\dot{\Omega} = -(2/5)mR^2\Omega\dot{\Omega} \simeq -3.2\times10^{-46}\ \dot{P}P^{-3} \qquad (4.1)$$

where typical quantities are

moment of inertia	$I \simeq 8\times10^{44}$ g.cm^2
mass of a pulsar	$m \simeq 2\times10^{33}$ g (one solar mass)

radius of a pulsar	$R = 10^6$ cm
angular velocity	$\Omega = 2\pi/P$
angular acceleration	$\dot{\Omega} = -2\pi\dot{P}/P^2$

This energy equation plays a critical role in pulsar physics since it gives the maximum amount of energy which is available for the production of any type of radiation. Since it is only dependent on P and $\dot{P}$, it is known for most of the known pulsars.

A second quantity which plays an important role in pulsar models is the magnetic field - especially when the efficiency of γ-ray production is evaluated. In general the magnetic field of a pulsar cannot be measured, except for those X-ray pulsars which exhibit a cyclotron line feature (Trümper, et al., 1978). In the case of isolated pulsars, the surface magnetic field strength should be estimated from the spindown equation. In this case one models the energy loss rate from the pulsar and set it equal to relation (4.1).

Ostriker and Gunn (1969) set (4.1) equal to the energy loss rate due to magnetic dipole radiation.

$$I\Omega\dot{\Omega} = -(2/3)M^2(\sin^2\chi)\Omega^4/c^3 \qquad (4.2)$$

Here $M = \frac{1}{2}B_s R^3$ is the magnetic dipole moment and χ is the angle between the rotation and magnetic axis. Setting $\chi = 90^0$ they obtained the following estimate of B_s (see also Harding, 1981):

$$B_s = 10^{15}(I/R^6)^{\frac{1}{2}}(P\dot{P})^{\frac{1}{2}} \text{ (gauss)}$$

However, magnetic dipole radiation is not the only mode of energy loss from a pulsar. The streaming of particles from the polar cap along the open field lines also contributes to the spindown of pulsars (Goldreich and Julian, 1969). The spindown equation for particles resembles relation (4.2), except that $\sin^2\chi$ is substituted by $\cos^2\chi$ and the constant of 2/3 is substituted by a constant $\alpha = 1$ (see e.g. Smith, 1977 and Muslimov and Tsygan, 1985). The summation of these two terms yields a term $\approx M^2\Omega^4/c^3$ which is approximately independent of χ.

It is known that the standard model $I\Omega\dot{\Omega} = M^2\Omega^4/c^3$ alone cannot explain the distribution of pulsar periods (Huang et al., 1983). Various authors tried to incorporate a decaying magnetic field of the form $B_s\exp(-t/\tau_M)$ to explain some of the observed properties (see e.g Gunn and Ostriker, 1969 and Lyne, Manchester and Taylor, 1985). Here t is the age of the pulsar and $\tau_M \approx 10^7$ year is the time scale for magnetic decay. Chanmugan and Gabriel (1971), Kundt (1981) and Kulkarni (1986) argued against magnetic decay. Fan et al. (1982) showed that Ohmic heating in the magnetosphere of a pulsar leads to a spindown equation of the form $KM^2\Omega^2/Rc^2$ but they neglected the $M^2\Omega^4/c^3$ term, since as they argued, Bode's law for planetary magnetism (which states that $M = I\Omega$) contradicts the existence of the $M^2\Omega^4/c^3$-term. De Jager and De Jager (1987) showed that Bode's law cannot be valid for pulsars, but supported the basic Ohmic heating spindown equation of Fan et al.. De Jager and De Jager also showed that $K \approx 0.01$ is consistent with the differential number distribution of pulsar periods, the P-$\dot{P}$ distribution for pulsars and with the observed luminosity of high energy particles from Jupiter as recorded by the Pioneer spacecraft (Fan et al., 1982). The hybrid spindown equation proposed by De Jager and De Jager is given by:

$$I\Omega\dot{\Omega} = M^2\Omega^4/c^3 + 0.01M^2\Omega^2/Rc^2 \qquad (4.3)$$

which also explains the observed luminosity from Jupiter, since the first term can be neglected for small Ω. The second term dominates for long period pulsars ($P > 0.5$ s) so that the calculated magnetic field strength is proportional to $1/\sqrt{\tau}$, where $\tau = P/2\dot{P}$ is the characteristic age of the pulsar. Kundt (1981) also predicted this $1/\sqrt{\tau}$ dependence for old pulsars, although he could not illustrate this explicitly by using a spindown equation.

However, for short period pulsars ($P < 0.4$ s), the effect of Ohmic heating in (4.3) is negligible (since Ω is large) so that one can use the standard model $I\Omega\dot{\Omega} \approx M^2\Omega^4/c^3$ alone. This approximation is sufficient for γ-ray astronomy since one is then only concerned with short period pulsars. The estimated surface magnetic field strength is then

$$B_s = 4.7\times10^{19}(P\dot{P})^{\frac{1}{2}} \text{ (gauss)} \qquad (4.4)$$

4.2. CONSTRAINTS ON THE OBSERVATION OF ISOLATED PULSARS.

Consider a typical VHEGRA experiment where a flux of $F_\gamma(>E_o)$ was measured above a threshold energy E_o. The mean energy of the γ-rays is $\bar{E}$. Consider also the case where the light curve exhibits a single pulse with a duty cycle δ and a total beamwidth β ($\simeq 1.7\delta$ if the source function is a Gaussian). The pulsar geometry factor for a cone of emission is given by Buccheri (1981) and Graser and Schönfelder (1983) as

$$\Delta\Omega/\beta = 2\pi(1 - \cos\pi\beta)/\beta \qquad (4.5)$$

The multiplication by $\Delta\Omega$ corrects for the total radiation in a solid angle since one measures only along the line of sight to the pulsar and the division by β corrects for the effect that the observer is stationary with respect to the rotating beam. One should actually multiply $\Delta\Omega/\beta$ by two to take the radiation from the opposite pole also into account.

In the case of polar cap γ-rays it is relatively easy to evaluate $\Delta\Omega/\beta$ from (4.5) given β. In the case of outer gap γ-rays, one can re-evaluate $\Delta\Omega/\beta$ to a zeroth order as follows: Consider Figure 4.1 in spherical co-ordinates (r,θ,ϕ) such that $\theta = 0$ and π define the spin axis $\underline{\Omega}$. Let $\Delta\theta$ be the angle subtended by any beam marked by 1, 2, 3 or 4. Let $\Delta\phi = \beta$ be the azimuthal angle (not visible on Figure 4.1) of a gap. The gap is thus considered as a rectangular slab. A Southern observer (shown on the figure) will see only beams 1 and 3 and one has to take the energy loss from beams 2 and 4 also into account by multiplying by two. If the observer sees t ($\simeq 2$) peaks (i.e. gaps), one should multiply the answer by t also. Thus, to a zeroth order

$$\Delta\Omega/\beta = 4\pi(2(\Delta\theta/\pi)(\Delta\phi/2\pi)t)/\Delta\phi$$

$$= 1.3\Delta\theta t \qquad (4.6)$$

For longer gaps (denoted by g1 and g4) $\Delta\theta \simeq 40°$ but for shorter gaps (g2 and g3) $\Delta\theta$ may be much smaller. One can see that the estimate given by (4.6) is independent of β due to the assumption of a slablike gap.

In principle one can have four gaps but an average value of $\Delta\Omega/\beta = 3$ will be assumed for all pulsars.

If the distance to the pulsar is d, the mean luminosity of the observed γ-radiation is

$$L_\gamma(>E_o) = F_\gamma(>E_o)\bar{E}d^2\Delta\Omega/\beta \qquad (4.7)$$

A very important constraint is that the observed luminosity L_γ cannot exceed E in (4.1), or, that the observed conversion efficiency η_γ should be less than one:

$$\eta_\gamma = L_\gamma(>E_o)/\dot{E} < 1 \qquad (4.8)$$

In general one must have that the sum of the conversion efficiencies in all energy bands (from radio through to UHE) should be less than one. This constraint requires that the energy extracted per second cannot exceed the kinetic energy loss.

4.4. THE STANDARD MODEL OF A PULSAR.

The main features of the model of a pulsar and its electrodynamics were developed by Goldreich and Julian (1969): In the derivation of the electromagnetic field equations one assumes that a pulsar is a highly conducting and magnetised neutron star. It can be shown that the electric force on an electron in the star's crust in the direction of $\underline{B}$, is much larger than the gravitational forces, so that a vacuum state is unstable. Consequently electrons and positrons must be stripped from the crust. These leptons in the magnetosphere redistribute themselves in a state of lowest energy such that $\underline{E} + \underline{v}\times\underline{B} = 0$ or $\underline{E}.\underline{B} = 0$ almost everywhere. The resulting charge density calculated from the theorem of Gauss $\underline{\nabla}.\underline{E} = 4\pi e(n_- - n_+)$ is

$$e(n_- - n_+) = \underline{\Omega}.\underline{B}/(2\pi c(1 - |\underline{\Omega} \times \underline{r}/c|^2)) \qquad (4.9)$$

where n_- and n_+ are the number densities of the electrons and positrons respectively. The whole magnetosphere is divided by the null surfaces $\underline{\Omega}.\underline{B} = 0$ into regions where there exists charges of one sign only, where the sign of the region is determined by the sign of $\underline{\Omega}.\underline{B}$. These regions and some quantities which are discussed in the following paragraphs are illustrated in Figure 4.1.

The magnetosphere corotates with the pulsar up to a distance where the corotation velocity $\underline{\Omega}x\underline{r} = \Omega r\sin\theta = c$. The surface defined by such r and θ values defines the light cylinder and the perpendicular distance from $\underline{\Omega}$ to this surface is called the light cylinder radius which is given by

$$R_L = c/\Omega = 4.8\times10^9 P \text{ (cm)} \tag{4.10}$$

It is always useful to know the magnetic field strength at a radial distance $r = \rho R_L > R$ where ρ is the radial distance in terms of light cylinder radii. For a dipole field geometry this magnetic field strength is given by

$$B = B_s(R/r)^3 = 4.2\times10^8\rho^{-3}(\dot{P}P^{-5})^{\frac{1}{2}} \text{ (gauss)} \tag{4.11}$$

where B_s is the surface field value given by relation (4.4).

For the aligned rotator ($\underline{M}.\underline{\Omega} = \pm M\Omega$) the equation of any dipolar field line is given by $r = (\text{const})\sin^2\theta$. The equation of the last closed field line, for which corotation still holds everywhere along this line, is given by

$$r = R_L\sin^2\theta \tag{4.12}$$

The last closed field lines define the two so-called polar caps. The angular extent θ_p of such a cap is derived from (4.12) at r = R and is small for all pulsars:

$$\theta_p = \sin\theta_p = (R\Omega/c)^{\frac{1}{2}} = 0.0145P^{-\frac{1}{2}} \text{ (radians)} \tag{4.13}$$

For the aligned rotator the field lines are closed if $\theta_p < \theta < \pi-\theta_p$ at the stellar surface and the particles rotate rigidly in this zone. For $\theta_p > \theta > \pi-\theta_p$ the field lines are open and particles can stream from the polar

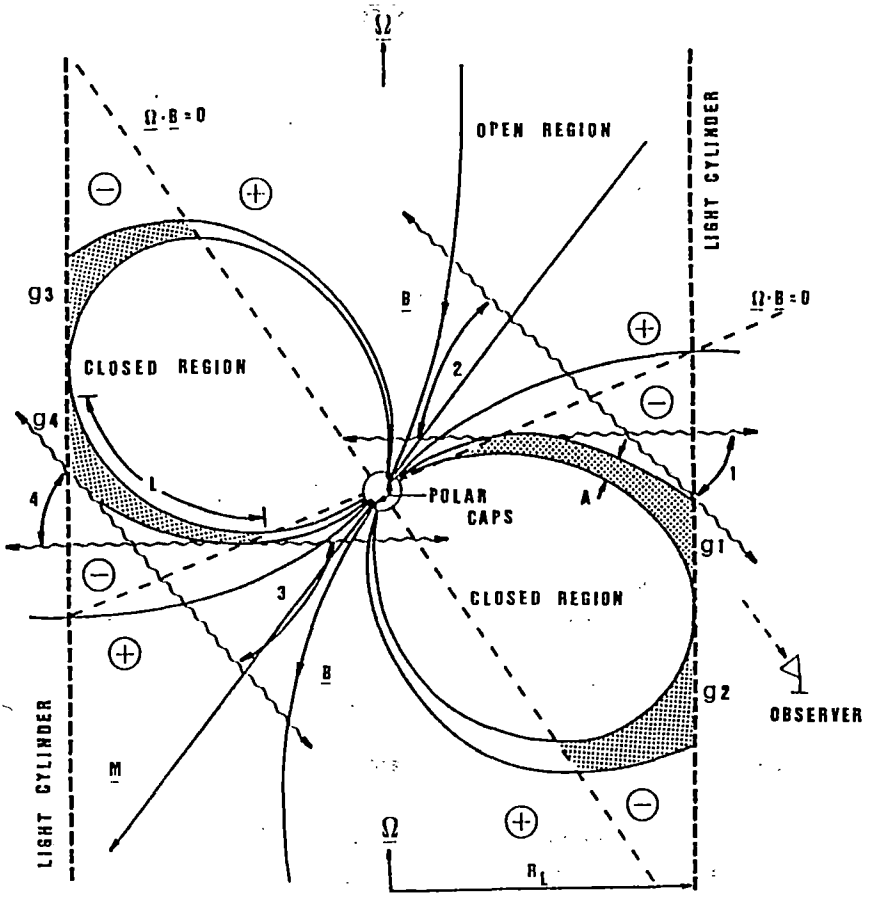

Figure 4.1. (Adapted from CHR). A model magnetosphere of a pulsar. The magnetic axis M is tilted with respect to the spin axis Ω. The shaded areas are the outer gaps g1, g2, g3 and g4. The indicated observer will see radiation from beams 1 and 3. The observed radiation from an outer gap originates at a height A above the last closed field line (for the main pulse) or a height A above the last closed field line. The second pulse must traverse the whole magnetosphere before reaching the observer. Consequently it may be modulated due to absorption along its way through the magnetosphere.

caps to infinity along these field lines. The maximum available potential difference over a polar cap (between $\theta = 0$ and $\theta = \theta_p$) to accelerate such particles is

$$\Delta V = \Omega^2 B_s R^3/c^2 \simeq 6.2\times10^{20}(\dot{P}P^{-3})^{\frac{1}{2}} \ (V) \qquad (4.14)$$

The number of particles N_p emitted per second from a polar cap is

$$N_p = \pi(\theta_p R)c(n_- - n_+) = \Omega^2 B_s R^3/2ec = 6.4\times10^{33}(\dot{P}P^{-3})^{\frac{1}{2}} \ (s^{-1}) \qquad (4.15)$$

and the associated energy loss rate through the light cylinder (or luminosity) is maximally

$$\dot{E}_p = e(\Delta V/2)N_p = M^2\Omega^4/c^3 = 3.2\times10^{46}\dot{P}P^{-3} \ (erg.s^{-1}) \qquad (4.16)$$

which balances the rate of kinetic energy loss given by (4.1). It is these leptons streaming from the polar caps which provides the necessary fuel for γ-radiation. The mechanisms for γ-radiation will be discussed in the two following sections.

4.5. GAMMA RAYS FROM THE POLAR CAP

The simplest model for the production of γ-rays by means of any process (curvature, synchrotron or inverse Compton) due to the streaming of leptons from a polar cap with a rate N_p given by (4.15), is by assuming that the energy E_o of emitted γ-rays is independent of P and B (see e.g. Harding, 1981). Consequently, the luminosity of produced γ-rays will be proportional to $E_o N_p$ or

$$L_\gamma \propto E_o B_s/P^2 \qquad (4.17)$$

The conversion efficiency calculated from (4.8), (4.17) and the pulsar's characteristic age $\tau = P/2\dot{P}$ is

$$\eta \propto P\sqrt{\tau} \qquad (4.18)$$

Schönfelder (1985) illustrated that (4.18) is consistent with the measured values of Crab, Vela and the upper limits obtained from various other pulsars.

Harding (1981) showed in a detailed analysis that curvature radiation from the streaming electrons yields γ-rays which can be attenuated due to pair production. An estimate of the number of observable γ-rays produced per second above 100 MeV is (with $B_{12} = B_s/10^{12}$ gauss)

$$N_\gamma(>100\text{MeV}) = 1.2\times10^{35} B^{0.95} P^{-1.7} \ (s^{-1}) \qquad (4.19)$$

which gives a conversion efficiency of

$$\eta \propto P^{1.3}\sqrt{\tau} \qquad (4.20)$$

Harding argued that the difference between (4.18) and (4.20) is due to the latter's inclusion of the effect of pair production. It was stressed by both Harding (1981) and Heyvaerts and Signore (1981) that such polar cap models cannot explain the origin of observed VHE γ-rays and they suggested that such γ-rays must be produced closer to the light cylinder where the absorption of γ-rays is less important due to a smaller B-field (see 4.11). However, one should remember that their statements were made before the discovery of PSR 1937+214 - a millisecond pulsar with a low B-field (Backer et al., 1982) and one can expect higher energy γ-rays to escape absorption in the open magnetosphere of such pulsars with low values of both P and $\dot{P}$.

Ruderman and Sutherland (1975) proposed a mechanism whereby a charge depleted gap is formed just above the polar cap. Inside this gap $\underline{E}.\underline{B} \neq 0$ while $\underline{E}.\underline{B} \approx 0$ in the rest of the magnetosphere (here $\underline{E}$ is the electric field strength). The height of this gap is

$$H \approx 5\times10^3 (R_c/10^6) P^{3/7} B^{-4/7}$$

$$= 10^7 (P/\dot{P})^{2/7} \ (\text{cm}) \qquad (4.21)$$

where the radius of curvature of a magnetic field line near the polar cap is R_c where

$$R_c = R(c/\Omega R)^{\frac{1}{2}} = 6.9\times10^7 P^{\frac{1}{2}} \text{ (cm)} \qquad (4.22)$$

The potential difference across this gap which acts as a battery to accelerate electrons is given by Ruderman and Sutherland (1975)

$$\begin{aligned}\Delta V &\simeq 1.6\times10^{12}(R_c/10^6)^{4/7}P^{-1/7}B^{-1.7} \\ &= 1.4\times10^{12}\ (P/\dot{P})^{1/14} \text{ (V)}\end{aligned} \qquad (4.23)$$

Usov (1983) estimated the expected energy and luminosity of γ-rays emitted by electrons which are accelerated through such a polar gap: The Lorentz factor of these electrons is calculated from (4.23):

$$\gamma_b = 3.4\times10^7(P/B_{12})^{1/7} = 2.7\times10^6(P/\dot{P})^{1/14} \qquad (4.24)$$

Curvature and synchrotron photons with energies larger than

$$E^{abs} = 4\times10^{10}P/B_{12} = 851(P/\dot{P})^{\frac{1}{2}} \text{ (eV)} \qquad (4.25)$$

are absorbed due to pair production in the strong magnetic field. At a distance $r >> R$ (far from the stellar crust) the primary particles will have a Lorentz factor of

$$\gamma = 10^7(R_c/10^7)^{2/3} = 3.6\times10^7 P^{1/3} \qquad (4.26)$$

The larger the difference $(\gamma_b - \gamma)$, the more energy is emitted in the form of γ-rays with a radiation maximum centred near E^{abs}. Using (4.15) one can estimate an upper limit to the γ-ray luminosity

$$\begin{aligned}L_\gamma &\leq (\gamma_b - \gamma)mc^2N_p \\ &= 10^{24}B_{12}(\gamma_b - \gamma)P^{-2} \\ &= 3.4\times10^{31}(P^{-0.19} - B_{12}^{0.14})B_{12}^{0.86}P^{-1.67} \text{ (erg.s}^{-1}\text{)}\end{aligned} \qquad (4.27)$$

The resemblance between (4.17), (4.19) and (4.27) is striking - they are all of the form B_s/P^2. The difference between Harding's luminosity equation (4.19) and Usov's equation (4.27) is quite pronounced: Usov's model gives an explicit cutoff for γ-rays for those pulsars for which $\gamma \geq \gamma_b$ in (4.27). According to Usov's model γ-rays with $E_\gamma < E^{abs}$ are observable only if (using (4.24), (4.26) and (4.27))

$$P \lesssim 0.74B^{-0.75} \qquad \text{or} \qquad \dot{P}P^{3.67} \lesssim 2\times10^{-16} \tag{4.28}$$

An equal sign in (4.28) describes the 'death line' for polar cap emission. This line is shown on the $\dot{P}$-P diagram of Figure 4.2. Consequently all pulsars on the left of this line are considered to be candidates for polar cap γ-ray emission. The equation for the maximum γ-ray energy E^{abs} from (4.25) is of the form P = (const)P. Three such lines are shown on Figure 4.2 for $E^{abs} = 10^{8}$, 10^{10} and 10^{12} eV. The radiation maxima for Crab and Vela are E^{abs} = 240 and 720 MeV respectively. The fact that E^{abs} for Vela is larger than that for Crab is qualitatively in agreement with Vela's harder observed spectrum. The radiation maximum of PSR 0950+08 is ≈ 30 GeV which is just too small to explain reports of VHE γ-rays from this pulsar (see e.g. Gupta et al., 1978). One can also see that E^{abs} increases with decreasing $\dot{P}$, so that PSR 1937+214 is a candidate VHE γ-ray emitter. However, there is another requirement for such a pulsar to be observable: The luminosity in (4.27) and thus $\dot{E}$ in (4.1) should be large enough to yield an observable flux of γ-rays on Earth. Consequently one should also have $\dot{P} >$ (constant)P^3 from (4.1) where the constant should be large enough. The line 'DLOG' on Figure 4.2 is such a line with $\dot{E} = 10^{34}$ erg.s^{-1} (the motivation for this line will be discussed in the next section). Lines parallel to 'DLOG' are lines of constant $\dot{E}$ and if one moves to the left on such lines, $\dot{E}$ and the luminosity (4.27) also increase.

It can now be understood that the best candidates for VHE γ-rays from a polar cap should be pulsars with P ≈ 1 ms and $\dot{P} \approx 5\times10^{-20}$ s.s^{-1}. Only PSR 1937+214 has such parameters. Thus, only millisecond pulsars with $\dot{P} < 10^{-19}$ s.s^{-1} can produce observable polar cap TeV γ-rays, but the smaller $\dot{P}$ is, the smaller the distance to the pulsar should be for it to be observable by means of the ACT. The outer gap model of CHR which

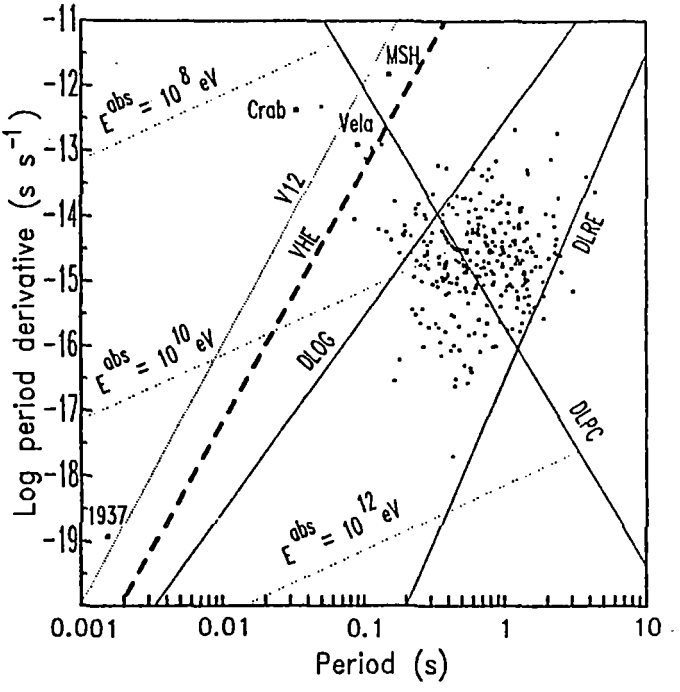

Figure 4.2. A $\dot{P}$ - P diagram for all isolated radio pulsars. The death lines for radio (DLRE) (De Jager and De Jager, 1987), polar cap (DLPC) and outer gap (DLOG) emission are shown. All pulsars lying to the right of those lines will not be observable with respect to the emission under consideration. The contours E^{abs} = 10^{8}, 10^{10} and 10^{12} eV represent the maximum observable γ-ray energies for polar cap emission. The division line between V1- and V2-parameters is shown by the line 'V12'. The line marked 'VHE' represents the ideal VHE γ-ray pulsars.

will be discussed in the next section, provides another set of VHE γ-ray emitters, i.e. the Crab- and Vela-like pulsars.

All the aforementioned results assume curvature radiation as the main source of the γ-rays. Xia et al. (1985) indicated that inverse Compton scattering near the stellar surface can be more efficient. This could change the luminosity equations for polar cap γ-rays.

4.6. THE OUTER GAP MODEL OF CHR FOR GAMMA RAY EMISSION.

Most 'gap' models (Ruderman and Sutherland, 1975, Cheng, Ruderman and Sutherland, 1976 and CHR) are similar in the sense that a self sustaining charge depleted region is formed in some part of the magnetosphere. According to CHR, gaps can be formed just above the polar cap and in the open magnetosphere close to the light cylinder. It is these gaps which can generate electromagnetic radiation over a wide range of energies - up to the VHE region. One reason for the success of CHR's model is that VHE γ-rays are produced near the light cylinder and these γ-rays would not be absorbed by the weaker B-field. Another model which places the γ-ray production site close to the light cylinder is that of Morini (1983). His model may also be able to predict observable VHE γ-rays. However, in this section only the detailed model of CHR will be investigated with the aim of explaining VHE γ-ray production.

4.6.1. THE CONDITION FOR OUTER GAP FORMATION

According to CHR an outer gap can be formed if $B_s\Omega^2$ is large enough, the reason being that the potential drop along such a gap and the rate of particle flow through it are proportional to $B_s\Omega^2$ or some power of it. Furthermore, $\dot{E}$ in (4.1) should be larger than 10^{34} erg.s^{-1}. The spindown equation (4.3) for $P \lesssim 0.5$ s (i.e. $I\Omega\dot{\Omega} \approx M^2\Omega^4/c^3$) yields a de-

pendence of $\dot{E}$ on $B_s\Omega^2$ of the form $I\Omega\dot{\Omega} = (B_s\Omega^2)^2R^6/4c^3$ so that the condition for outer gap formation is

$$B_s\Omega^2 \gtrsim 10^{15} \text{ or } \dot{P}P^{-3} \gtrsim 2.9\times10^{-13} \qquad (4.29)$$

An equal sign in (4.29) yields the 'death line' for outer gap formation and is indicated on Figure 4.2 by the line marked as 'DLOG'. Only pulsars lying to the left of this line are candidates for outer gap formation. Furthermore, this line also describes a contour of constant $\dot{E}$ (calculated from (4.1)). One can also see that the sample of outer gap pulsars is smaller than the sample of pulsars which can produce observable polar cap γ-rays.

4.6.2. THE FORMATION OF THE GAP.

Consider Figure 4.1 again: An outer gap is formed in the outer magnetosphere between the $\underline{\Omega}.\underline{B} = 0$ null surface and the light cylinder, along the last closed field line. Four such gaps are shown in Figure 4.1: two long ones denoted by g1 and g4 and two shorter ones denoted by g2 and g3. Since $\underline{M}.\underline{\Omega} < 0$ was chosen, the gaps are in negatively charged regions of the magnetosphere. If $\underline{M}.\underline{\Omega} > 0$, all the signs will change, but the basic physics will be the same.

The leptons in the closed magnetosphere corotate rigidly with the pulsar in a force free state so that no charges leave the closed region. However, nothing prevents electrons to leave the open magnetosphere through the light cylinder. Electrons leave the marked gaps in Figure 4.1 which cause those regions to have a nett positive charge. This nett positive charge pushes the positrons on the starward side of the null surface back towards the star and leaves a growing gap. Such a gap will grow and fill the entire open magnetosphere unless interrupted or modified. In fact, this growth is limited via copious pair production such that the gap has a width $A = aR_L$ (indicated on Figure 4.1) with R_L the light cylinder radius given by (4.10) and $a \approx 0.1$. The length of the gap is indicated

by $L = \ell R_L$ with $\ell < 1$. The azimuthal width $W = wR_L$ (with $w = 1$) of the gap cannot be shown on the figure, but it is assumed to be somehow limited by the tilt angle x between $\underline{M}$ and $\underline{\Omega}$.

In this way a self sustaining gap in a near vacuum state is formed with $\underline{E}.\underline{B} \neq 0$ inside the gap and $\underline{E}.\underline{B} \approx 0$ outside. The maximum potential drop along B from the beginning to the end of the gap is proportional to $B_s\Omega^2$ and ranges between 10^{12} and 10^{15} V for pulsars lying to the left of the 'DLOG' line in Figure 4.2. Consequently, a typical gap is capable of accelerating leptons to energies greater than 10^{12} eV. The primary electrons (with a production rate given by (4.15)) will be accelerated through the gap and will not slow down to terminate the gap. The needed return current to the star is provided by positrons which are pulled in through the light cylinder and accelerated towards the star, or, by positrons which are formed by the pair production process just above the gap (where a small remnant $\underline{E}.\underline{B}$ still exists) and accelerated along $\underline{B}$ towards the star.

The key to the outer gap model is the pair production mechanism which sustains the gap and limits its growth. It also provides the observed radiation. There seems to be three distinct regions which can be associated with the gap.

4.6.3. THE THREE CONTROLLING REGIONS OF AN OUTER GAP.

CHR suggested a 'bootstrap' magnetosphere in which three important regions can be identified (see Figure 4.3).

(1) The outer gap itself: Primary electrons from the star and positrons from outside the light cylinder are accelerated due to the large $\underline{E}.\underline{B}$ through the outer gap, radiating either curvature γ-rays or boosting soft photons via the inverse Compton process to very high energies. These photons move into the convex side of $\underline{B}$ (away from the closed region). These energetic primary γ-rays collide with

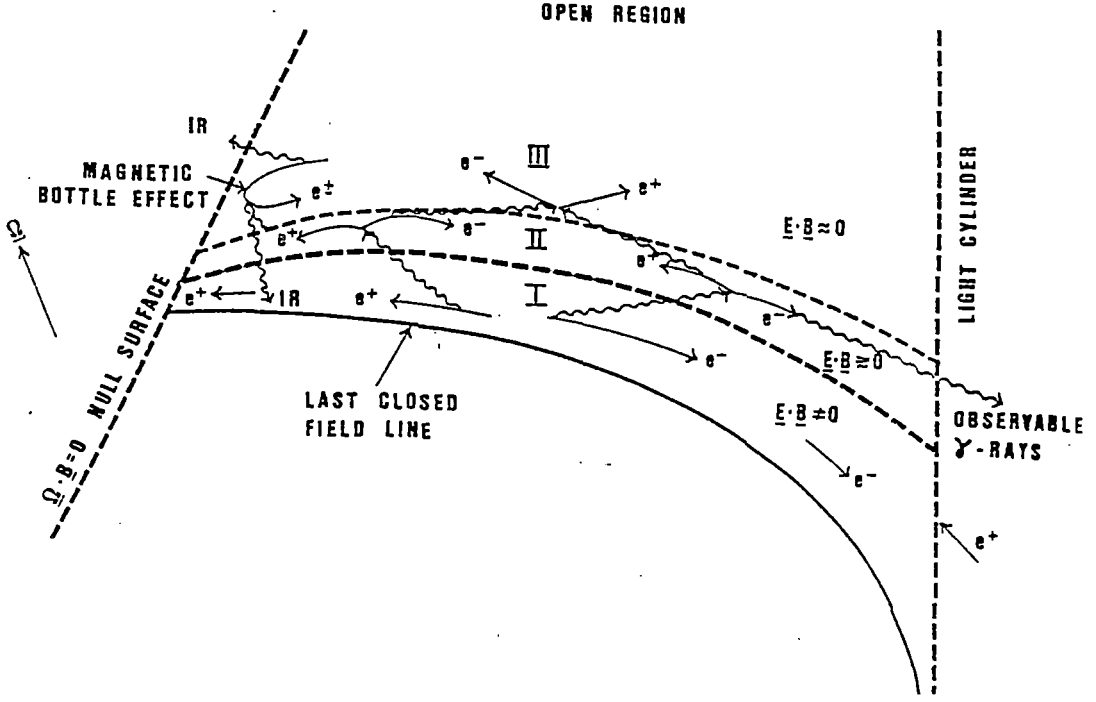

Figure 4.3. A two dimensional drawing of the (r,θ) plane of the outer gap (region (I)), its charged upper boundary (region (II)) and the tertiary region (III). Gamma rays from region (I) feeds region (II) by means of the creation of secondary pairs. Crossed beams of secondary γ-rays from these secondary leptons create the tertiary pairs in region (III). Some tertiary leptons drift towards the star in a magnetic mirror, reverse direction of speed parallel to B and radiate soft (mainly infrared) photons in all directions including the direction of the gap. This is the main scheme for a Vela-type pulsar. A Crab-type pulsar may have a slightly different scenario.

photons to create highly energetic secondary lepton pairs which form region II just above region I:

(II) The secondary pairs are separated into e^+ and e^- beams parallel to the primary beams due to a small remnant $\underline{E}.\underline{B}$. These leptons radiate secondary photons from the optical to the VHE γ-region via synchrotron and/or inverse Compton processes. Consequently, the gap has a charged 'roof' (i.e. region (II)) of crossed lepton and secondary γ-ray beams which limits the height of the gap at a value of $A = aR_L$ above the last closed field line. However, these secondary γ-ray beams can move beyond (II) and cross to create tertiary pairs in the third region.

(III) This region is still further away from the last closed field line than (II). The tertiary pairs have too low an energy to radiate γ-rays and X-rays. However, soft tertiary infrared and optical photons are radiated from these pairs via the synchrotron process to illuminate the entire open magnetosphere. The gap itself is illuminated via a magnetic mirroring effect whereby the velocity component $v_{\parallel}$ of leptons parallel to $\underline{B}$, (but in the direction of the converging $\underline{B}$-field lines towards the star) is reversed in direction so that soft tertiary synchrotron photons are emitted in all directions including the direction of the outer gap. Consequently, the outer gap is also refuelled with these tertiary photons so that the mechanism in (I) can be repeated.

Thus, in this self consistent bootstrap scenario, (I) controls (II) which controls (III) which controls (I). In this way the gap remains in a dynamic balance. However, the important aspect is that the growth of the gap should be limited by the formation of (II) via pair production: This latter mechanism can differ from pulsar to pulsar. CHR identified four such pair production mechanisms:

4.6.4. THE FOUR POSSIBLE LIMITING MECHANISMS OF AN OUTER GAP.

The gap needs a pair production mechanism which can limit its growth. The four possible mechanisms of producing leptons in region (II) are (CHR)

(a) Curvature γ-rays with energy $\hbar\omega = \gamma_c m_e c^2$ from the primary lepton flow may materialise as 'Sturrock pairs' on the gap magnetic field lines, provided that $\gamma_c B_{12} \phi \geq 1$, where ϕ is the angle between the incident γ-ray and $\underline{B}$. However, the outer gap B-field strength for typical pulsars is too small for Sturrock pairs to materialise in region (II).

(b) Thermal X-rays from the polar cap of the neutron star can act as target photons for the primary γ-rays from region (I) to give the necessary secondary leptons.

(c) Non-thermal secondary X-rays created in region (II) can be optically thick for primary curvature γ-rays with $\hbar\omega > 1$ GeV, so that sufficient secondary leptons can be formed in (II).

(d) Collisions of the primary γ-rays with the soft tertiary photons (as discussed in Section 4.6.3) can create the necessary leptons.

The mechanism or combination of mechanisms involved for a certain pulsar will determine the observed luminosity in different energy bands. Mechanism (d) is considered to be important for all pulsars - especially for Vela. Mechanisms (b) and/or (c) will also be applicable to those pulsars which radiates in the X-ray bands. One can classify some well known pulsars according to these mechanisms as follows:

Crab	: (c) + (d)
Vela	: (d)
PSR 1937+214	: (d)
PSR 1509-58	: (b) + (d)

A pulsar which has mechanism (c) as a gap controlling mechanism will be called a 'Crab-type pulsar'. A pulsar which is mainly controlled by mechanism (d) is called a 'Vela-type pulsar' and two quantities characterise the latter mechanism further: The gyrofrequency ω_B at a radial distance $r = \rho R_L$ (with $\rho \approx 1$) to the gap is

$$\omega_B = eB/mc \approx 7.6\times10^{15}(\dot{P}P^{-5})^{\frac{1}{2}}\rho^{-3} \ (s^{-1}) \qquad (4.30)$$

and the average tertiary photon energy $\hbar\omega_{IR}$, calculated at the magnetic mirroring region where $v_{\parallel}$ changes direction is

$$\omega_{IR} = \omega_B^{-3}(\omega m_e c^3/e^2)^2 \approx (\dot{P}^{-3}P^{11})\rho^9 \ (s^{-1}) \qquad (4.31)$$

Pulsars with a dominating mechanism (d) can further be divided in two classes: If $\omega_B < \omega_{IR}$, the differential tertiary photon spectrum will be flat between two cutoff energies $\omega_o \ll \omega_{IR}$ and ω_{IR}. Such an outer gap is said to have V1-parameters. If $\omega_B > \omega_{IR}$, the tertiary spectrum will be mono-energetic at ω_B and the outer gap is said to have V2- parameters. Thus, V1-parameters will be applicable if

$$\dot{P}P^{-4} \lesssim 1.1\times10^{-8}, \qquad (4.32)$$

but V2-parameters will be applicable for a '>' sign. An equal sign in (4.32) gives the division between V1 and V2 and is illustrated on Figure 4.2 as a line marked 'V12'. Note that Vela and MSH have V1-parameters while Crab, PSR 1937+214 and PSR 0540-69 have V2-parameters (if the gaps of MSH, Crab and PSR 0540-69 are also dominated by mechanism (d)).

4.6.5. THE GAMMA RAY LUMINOSITY OF OUTER GAPS.

In the derivation of the γ-ray luminosities ($E_\gamma < 3$ GeV) of V1-, V2- and Crab-type pulsars, CHR assumed $\ell = w = p = 1$. Keeping these parameters free, it will be shown that these gap parameters play an important

part in determining the luminosities. This was also predicted by CHR but not quantified. Furthermore, luminosities will also be written in terms of P and $\dot{P}$ so that one can evaluate the γ-ray efficiencies of different pulsar gaps controlled by either mechanism (c) or (d).

For a Crab-type pulsar it is difficult to estimate how deep the secondary X-rays can penetrate into the gap for pair conversion by the curvature primary γ-rays. It is also unknown which mechanism ((c) or (d)) will first start to limit the gap growth and thus control the outer gap (CHR). The latter authors could at least give the minimum luminosity if mechanism (c) alone controls the outer gap:

$$L_c(\min) = 2.1\times10^{35}\rho^{5.85}\dot{P}^{0.025}P^{0.975} \tag{4.33}$$

No further attention will be given to Crab-type pulsars due to the uncertainties involved. According to CHR a more detailed calculation is possible for V1- and V2-type pulsars (i.e. mechanism (d)).

In the derivation of the number density n of tertiary photons, the γ-ray luminosity and spectrum, it was assumed that secondary electrons produce secondary γ-rays via the synchrotron process. By requiring the gap to be in a dynamic balance, this number density can be expressed as follows for V1-pulsars.

$$n_{V1} = 1.8\times10^{8}(w^2/\ell)\dot{P}^{-1}P^{3} \ (cm^{-3}) \tag{4.34a}$$

where it was taken into account that Vela was not seen by the IRAS satellite. For pulsars with V2-parameters this number density is given by

$$n_{V2} = 4.6\times10^{17}(w^2/\ell)\rho^{-6}P^{-1} \ (cm^{-3}) \tag{4.34b}$$

Then the total luminosity for a Vela type pulsar in general is

$$L_V \simeq \gamma_{\parallel}^{-2}N_p\sigma_T n\hbar\omega_1 L \tag{4.35}$$

where $\gamma_{\parallel}^2 \approx 10$ is a geometrical factor which compensates for the movement of the leptons relative to the direction of B, N_p is given by (4.15), σ_T is the Thomson cross section and $\hbar\omega_1$ is the energy of the primary γ-rays generated in the gap. The exact expression for L_V will depend on the relation between ω_B and ω_{IR} given by (4.30) and (4.31). For V1-parameters the available luminosity is (using n_{V1})

$$L_{V1} = 2.4\times10^{45} w^2 \rho^{-9} \dot{P} P^{-3} \ (\mathrm{erg.s^{-1}}) \qquad (4.36a)$$

For V2-parameters the luminosity is (using n_{V2})

$$L_{V2} = 8.4\times10^{38} w^2 \rho^{-9} P \ (\mathrm{erg.s^{-1}}) \qquad (4.36b)$$

A further requirement for consistency is that $L_V < \dot{E}$ while condition (4.32) should be satisfied for V1- and V2-parameters. This results in the following constraints on ρ

$$\text{V1:} \qquad \rho > 0.7\, w^{2/9}$$

$$\text{V2:} \qquad \rho < 1.8\, w^{2/9}$$

which are weakly dependent on w ($\approx$ 1). These constraints on ρ seem to be quite reasonable if one remembers that a gap cannot be too close or too far from the star, while the average value for $\rho \approx 1$.

Observe the correspondence between (4.33) and (4.36b). Both are applicable to Crab-like pulsars. Both $L_c(\mathrm{min})$ and L_{V2} are mainly proportional to P while the dependence of $L_c(\mathrm{min})$ on $\dot{P}$ is very small. Furthermore, $L_{V2} \approx 4000 L_c(\mathrm{min})$ (for $w = \rho = 1$) which can be understood, since (4.33) is only a lower limit for the luminosity. However, according to CHR it is difficult to combine mechanisms (c) and (d) to obtain a single expression for the luminosity.

One can see that these estimates of the luminosities depend strongly on the gap dimensions (e.g. L_{V1} has a ρ^{-9} dependence). Furthermore $L_c(\mathrm{min})$ and L_{V2} scales with P while L_{V1} scales with $\dot{P}P^{-3}$ (as remarked

by CHR) which is different from the polar cap models where the luminosity scales with $(\dot{P}P^{-3})^{\frac{1}{2}}$.

Table 4.1 gives the observed luminosities (for $E_\gamma < 3$ GeV) and the expected γ-ray luminosities for Crab, Vela, MSH and PSR 1937+214 calculated from $L_c(\min)$, L_{V1} or L_{V2}. For MSH and PSR 1937+214 upper limits for the observed luminosity were calculated for 50 MeV $< E_\gamma < 3$ GeV, assuming a Vela-type spectrum for MSH and a Crab-type spectrum for PSR 1937+214 (due to their classification according to (4.32)). All observed luminosities were calculated using a beaming factor of $\Delta\Omega/\beta = 3$ in (4.6). It can be seen that $L_c(\min)$ gives an acceptable lower limit for Crab. The estimates L_{V1} and L_{V2} are all within a factor of 10 from the observed luminosities. Mechanism (d) (with L_{V2}) predicts the observed luminosity of Crab satisfactorily.

If one requires that L_V should be equal to the observed luminosities, ρ can be estimated for each pulsar by assuming that the relative azimuthal width of a gap w, corresponds to the observed width β of a peak by means of the relation $w = 2\pi\beta$. In the latter case it was assumed that the radiation of γ-rays occurs near the light cylinder. For Crab and Vela $w \approx 0.6$, while $w \approx 2$ for MSH (the latter was estimated from Figure 3.12). This gives $\rho \approx 0.43$ for Crab, 1.1 for Vela and $\gtrsim 1.2$ for MSH. The '>' sign predicts that MSH would be invisible to COS-B. The cases where $\rho > 1$ requires a tilting of the magnetic axis relative to the spin axis such that the radial distance to the outer gap is slightly larger than R_L. This interpretation is supported by the work of Greenstein and Hartke (1983), who found the angle between $\underline{M}$ and $\underline{\Omega}$ to be 40 degrees for MSH. The same choices for w and ρ will be made in Section 4.6.6 for Crab, Vela and MSH when the VHE γ-ray luminosity will be estimated. In this way the TeV predictions will be consistent with MeV observations.

4.6.6. VHE GAMMA RAY PRODUCTION IN AN OUTER GAP.

An outer gap which is controlled by mechanism (d) can explain the generation of VHE γ-rays quite well: Some of the tertiary photons in region (II) are inverse Compton boosted by a small fraction of the secondary electrons (which also provides the observed radiation below 3 GeV) in region (II). These boosted photons acquire energies of $\simeq$ 1 TeV. According to CHR it is difficult to calculate the VHE γ-ray luminosity for mechanism (c). In this section CHR's calculation of the VHE luminosity will be repeated, but in more detail to include the dependence on w, ℓ and ρ and to discuss various other pulsars according to these estimates.

CHR showed that the distribution of energies $\gamma m_e c^2$ of secondary electrons in region (II) will be uniform between a value of $\simeq 10^7 m_e c^2$ and a value much less than that. It can then be shown from Ginzburg (1979) that the differential energy spectrum of inverse Compton boosted photons is of the form $KE^{-\frac{1}{2}}$ where K depends on the energy density of the tertiary photons and on the intensity and maximum energy of secondary electrons.

For pulsars like Vela and MSH the maximum secondary electron energy is $E_m \simeq 6$ TeV. This will also be the approximate maximum energy of the observable inverse Compton boosted VHE γ-rays. Consequently the integral flux of VHE γ-rays will be

$$F(>E) \propto E_m^{\frac{1}{2}} - E^{\frac{1}{2}} \qquad (4.37)$$

which gives a rather flat spectrum. Depending on the response function of telescopes as a function of energy, the flux may even increase with energy. Such pulsars may then be invisible at low energies ($E_\gamma \simeq$ 200 GeV) but more visible at higher energies with a sharp cutoff above 6 TeV. Grindlay et al. (1975b) reported the detection of a signal from Vela only when he selected the events with largest pulse heights (and thus largest energies), which supports this interpretation.

To estimate the expected VHE γ-ray luminosity for Vela, CHR calculated the ratio of energy loss of a secondary electron due to inverse Compton scattering to that of synchrotron radiation losses. The energy losses due to synchrotron radiation by a secondary electron with energy $\gamma m_e c^2$ which 'sees' a perpendicular magnetic field component $B/\gamma_{\parallel}$ is (Hillier, 1984):

$$(dE/dt)_S = 2\sigma_T c U_{\perp} \gamma^2 \tag{4.38a}$$

where $U_{\perp} = B^2/8\pi\gamma_{\parallel}^2$ is the energy density of the magnetic field component perpendicular to the velocity of a secondary electron. The energy loss rate due to the inverse Compton scattering of a secondary electron on a tertiary photon is

$$(dE/dt)_{IC} = (4/3)\sigma_T c U_{IR} \gamma^2 \ (erg.s^{-1}) \tag{4.38b}$$

The tertiary photon energy density is $U_{IR} = n\hbar\omega_{IR}$ for V1-parameters and $n\hbar\omega_B$ for V2 parameters.

The efficiency $\eta(S\rightarrow IC)$ of converting the gap power (4.35) to VHE γ-rays by means of the inverse Compton process is given by the ratio

$$\eta(S\rightarrow IC) = (dE/dt)_{IC}/(dE/dt)_S$$

$$= (2/3)U_{IR}/U_{\perp}$$

$$= \begin{cases} 1.7\times10^{-33}(w^2/\ell)\rho^{15}(P^{27}/\dot{P}^7)^{\frac{1}{2}} \ (V1) & (4.39a) \\ 3.3\times10^{-9} \ (w^2/\ell)\rho^{-3}(P^3/\dot{P})^{\frac{1}{2}} \ (V2) & (4.39b) \end{cases}$$

One can see that the production of VHE γ-rays by the collision of secondary electrons on tertiary photons becomes more important than synchrotron radiation (which gives the radiation below $\approx$ 3 GeV) if $U_{IR} > 1.5U_{\perp}$ (for V1-parameters) which will be applicable if

$$\dot{P}P^{-3.9}\rho^{-4.3}\ell^{0.29}w^{-0.57} \lesssim 4.4\times10^{-10} \tag{4.40}$$

Pulsars with V1-parameters satisfying both conditions (4.29) and (4.40) can thus be considered as perfect outer gap VHE γ-ray emitters. Due to the strict condition for V2-parameters (given by (4.32)), it can be shown that the condition $U_{IR} > 1.5U_{\perp}$ is never satisfied for V2-pulsars. However, it is questionable whether n_{V1} (relation (4.34a)) will still be applicable if $U_{IR} >> U_{\perp}$ since CHR derived n for the case when $U_{IR} < U_{\perp}$. If $U_{IR} >> U_{\perp}$, most of the secondary electrons' energy is transferred to the tertiary photons via the inverse Compton process and the model of CHR has to be extended to this case. With the available knowledge one may redefine an ideal VHE γ-ray pulsar conservatively as one for which $\eta(S \rightarrow IC) = 1$, so that an '=' sign in (4.40) describes such ideal VHE pulsars. The expected VHE γ-ray luminosity is obtained by multiplying (4.39) with (4.36) giving the following estimates for V1- and V2-parameters respectively (provided that $\eta(S \rightarrow IC) < 1$):

$$L_{V1}(TeV) = 4.1\times10^{12}(w^4/\ell)\rho^6(P^{21}/\dot{P}^5)^{\frac{1}{2}} \qquad (4.41a)$$

$$L_{V2}(TeV) = 2.8\times10^{30}(w^4/\ell)\rho^{-6}(P^5/\dot{P})^{\frac{1}{2}} \qquad (4.41b)$$

When comparing (4.41a) with (4.36a) one can see that the differences are drastic: A good emitter at $E_\gamma > 1$ TeV may be a poor emitter at $E_\gamma < 3$ GeV and vice versa. Furthermore, the w, ρ and ℓ dependency illustrates that wide but short gaps situated at large radial distances ($\rho > 1$) from the star may be efficient in producing VHE γ-rays. Consequently one cannot always expect the VHE γ-ray production site to be the same as the production site for γ-rays with $E_\gamma < 3$ GeV, implying the possibility of different pulse profiles in the two energy regions. Grindlay et al. (1973) observed a VHE γ-ray pulse from Vela which is not in phase with any of the MeV pulses. On the other hand, Bhat et al. (1980) observed a 0.42 phase difference between two VHE γ-ray pulses from Vela, which is consistent with the observed phase difference at MeV energies.

The differences between (4.41b) and (4.36b) are less pronounced so that one may expect VHE γ-ray pulses to be in phase with the MeV pulses. Examples thereof are the observations by Dowthwaite et al. (1984d), Tümer et al. (1985) and Bhat et al. (1986).

Table 4.1. γ-ray (E_γ < 3 GeV) luminosities calculated for the outer gap model.

pulsar	Observed luminosity [a] $L_\gamma(\lesssim 3GeV)$ (erg.s^{-1})	Expected luminosities [d] (erg. s^{-1}) L_{V1}	L_{V2}	L_c(min)
Crab	$4,5x10^{36}$	-	$9,3x10^{35}$	$3,7x10^{33}$
Vela	$6,3x10^{34}$	$4,2x10^{35}$	-	-
MSH	$< 6x10^{35}$ [b]	$1,1x10^{36}$	-	-
PSR 1937+214	$< 10^{35}$ [c]	-	$4x10^{34}$	-

(a) $\Delta\Omega/\beta = 3$

(b) $F(> 50\ MeV) < 3x10^{-6}$ (cm^{-2}.s^{-1}), $\bar{E}$ = 237 MeV

(c) $F(> 50\ MeV) < 3x10^{-6}$ (cm^{-2}.s^{-1}), $\bar{E}$ = 169 MeV

(d) $w = \rho = 1$.

Table 4.2. VHE γ-ray luminosity calculated for the outer gap model

pulsar	Observed luminosity $L_\gamma(>E_o)$ [a] (erg.s^{-1})	Expected luminosities (erg.s^{-1}) L_{V1}(TeV)	L_{V2}(TeV)
Crab	$1x10^{33}$	-	$2x10^{34}$ [g]
Vela	$2x10^{32}$	$2x10^{33}$ [d]	-
MSH	$3x10^{34}$	$2x10^{35}$ [e]	-
PSR 1937+214	$1x10^{33}$ [b]	-	$8x10^{32}$ [f]
PSR 1802-23 ?	$1x10^{35}$ [c]	$1x10^{35}$ [f]	-

(a) $\Delta\Omega/\beta = 3$, $\bar{E} = E_o$ where E_o is the threshold energy.

(b) No published flux. Flux was assumed to equal that of ref. 39.

(c) Calculated from the parameters given by ref. 111

(d) $w = 0.6$; $\rho = 1.1$

(e) $w = 2$; $\rho = 1.2$

(f) $w = \rho = 1$

(g) $w = 0.6$; $\rho = 0.43$

The observed and expected VHE γ-ray luminosities (calculated from (4.41)) for different pulsars are compared in Table 4.2. The gap dimensions w, ρ and ℓ were taken to be equal to one except for Crab, Vela and MSH where the choices of Section 4.6.5 were used to ensure that the VHE predictions are consistent with MeV observations. One can see that all estimates of the luminosity agree with the observed luminosities within a factor of 10.

A pulsar with the parameters of PSR 1802-23 seems to be the ideal VHE γ-ray pulsar. From (4.39a) it follows that $\eta(S \rightarrow IC) \approx 83\%$, i.e. nearly all the gap power is transformed to VHE γ-rays. Furthermore, $\dot{E}$ calculated from (4.1) is also relatively large so that a large amount of the available energy can be used to power the gap.

Usov (1983) predicted a maximum luminosity of 7×10^{33} erg.s^{-1} for polar cap γ-rays from PSR 1937+214 which is an order of magnitude larger than the predicted outer gap luminosity. With all the uncertainties involved, one cannot make any conclusive statement about the site of VHE γ-ray production. Turver (1985) reported a VHE γ-ray pulse which is in phase with the radio main pulse. If the radio pulses are emitted near the stellar crust, it would support Usov's prediction.

The choice of $w = 2$ and $\rho = 1.2$ for MSH yields a predicted L_{V1} (from (4.36a)) which is less than the COS-B upper limit. However, this choice predicts a VHE γ-ray luminosity which is sufficient to account for the observed VHE luminosity.

The observed triple peak at $E_\gamma > 2$ TeV for MSH may be difficult to explain but the outer gap magnetic field strength is $\approx 6 \times 10^4$ gauss which is similar to that of Vela but a factor 22 less than that of Crab. CHR remarked that the second pulse traversing the whole magnetosphere (from beam 3 in Figure 4.1) towards the observer may be absorbed in the case of Crab, since γ-rays are moving through a large magnetic field. However, such absorptions will be less efficient for Vela and MSH so that one may expect more than one VHE pulse from Vela and MSH.

The observed X-ray luminosity of MSH is $L_X \approx 5 \times 10^{34}$ erg.s^{-1}. Greenstein and Hartke (1983) suggested that the X-ray emission is of thermal origin due to electrons falling from the open magnetosphere onto the polar cap which is heated. This can be shown as follows: The maximum value of the returning electron current bombarding the polar cap is also given by N_p in (4.15). The minimum polar cap potential difference necessary to sustain radio emission is $\Delta V_{min} \approx 10^{12}$ V (Ruderman, 1981) while the maximum available potential difference from (4.14) is $\Delta V_{max} = 10^{16}$ V. Thus the minimum and maximum luminosity of returning electrons are 2×10^{33} and 10^{37} erg.s^{-1} respectively, which seems to be sufficient to heat the polar cap and produce the observed X-rays. These X-rays must also be responsible for mechanism (b) to control the outer gap. The gap equations derived by CHR are therefore not complete for MSH since the effect of mechanism (b) should be included.

To summarise, all outer gap candidates (see Table 1.2) are listed in Table 4.3. It was assumed that mechanism (d) alone controls the gap so that $\eta(S \rightarrow IC)$ from (4.39) and L_V(TeV) from (4.41) were evaluated for each pulsar, while taking condition (4.32) for V1- and V2-parameters into account. The gap dimensions were taken as $\rho = w = 1$ except for Crab, Vela and MSH for which the values derived in Section 4.6.5 were used to ensure consistency with respect to MeV observations. The expected flux at Earth was calculated from L_V(TeV) assuming a mean energy of 1 TeV and a beaming factor of $\Delta\Omega/\beta = 3$ for all pulsars. If $\eta(S \rightarrow IC) > 10$, the flux estimate was then omitted since L_V(TeV) is expected to be wrong due to the dominating inverse Compton process in region (II) of the gap. Pulsars marked with a '+' were already observed in the VHE region. The flux for Crab agrees with the transient flux observed by Gibson et al. (1982b) and Bhat et al. (1986). The rest of the fluxes agree within a factor of ten with the observed fluxes. Apart from PSR 1802-23 which needs confirmation, the two most likely but yet unobserved candidates are PSR 1800-21 and PSR 1823-13.

Table 4.3. A list of all outer gap candidates

pulsar	P(s)	$\dot{P}(s.s^{-1}) \times 10^{-15}$	d(kpc)	η(s→IC)	Expected[a] F(>1TeV)	
0136+57	0.27	10.69	2.50	3.2E+08	-	
0355+54	0.16	4.39	1.60	4.0E+06	-	+
0531+21	0.03	422.44	2.00	3.1E-05	1.2E-10	+
0540-69	0.05	479.00	55.00	5.4E-05	1.7E-14	
0540+23	0.25	15.43	2.60	2.2E+07	-	
0611+22	0.33	59.63	3.30	1.3E+07	-	+
0656+14	0.38	54.30	0.40	1.2E+08	-	
0740-28	0.17	16.83	1.50	8.7E+04	-	+
0833-45	0.09	124.69	0.50	2.8E-02	1.7E-10	+
1001-47	0.31	22.07	1.60	1.3E+08	-	
1055-52	0.20	5.83	0.92	3.4E+07	-	
1221-63	0.22	4.96	2.70	2.1E+08	-	
1317-53	0.28	9.26	3.50	7.5E+08	-	
1356-60	0.13	6.34	8.80	7.0E+04	-	
1449-64	0.18	2.75	2.20	1.3E+08	-	
1509-58	0.15	1540.00	4.20	1.8E-01	1.9E-10	+
1557-50	0.19	5.06	7.80	4.1E+07	-	
1719-37	0.24	10.82	2.50	4.5E+07	-	
1754-24	0.23	13.00	4.20	2.1E+07	-	
1800-21	0.13	125.00	5.30	3.9E+00	3.8E-10	
1802-23 ?	0.11	110.00	3.00	6.0E-01	2.7E-10	+
1821-19	0.19	5.24	6.80	2.9E+07	-	
1823-13	0.10	76.00	5.50	5.4E-01	6.8E-11	
1830-08	0.09	9.00	10.00	9.1E+01	-	
1915+13	0.19	7.20	2.40	1.4E+07	-	
1930+22	0.14	57.78	7.00	1.7E+02	-	+
1937+21	0.0015	0.00001	2.00	5.4E-04	3.8E-12	+

(a) The expected flux calculation is omitted if η(S→IC) >> 1.

\+ Pulsar was already observed at $E_\gamma > 1$ TeV.

? Pulsar is a suspect.

4.6.7. VHE TRANSIENT PHENOMENA

Gibson et al. (1982b) and Bhat et al. (1986) reported observations of transient pulsed VHE emission from the Crab pulsar. According to their observations the flux from Crab increased by a factor of ≈ 25 from the low persistent flux level. The observation of Bhat et al. is important since it yielded emission at the expected main pulse position. Smith (1986) reported that such transient phenomena may only be possible if the infrared luminosity also shows evidence of time variability. Orford (1986) also remarked that fluctuations in the infrared spectrum can create fluctuations in the VHE γ-ray spectrum. This is understandable in terms of the production mechanism discussed in Section 4.6.6.

If mechanism (d) controls the outer gap, it follows from (4.35) that the radiation below 3 GeV depends on the tertiary photon density n, but since (4.38b) also depends on n, it follows that the VHE γ-ray luminosity depends on n^2. Furthermore, a close inspection of Ginzburg's (1979) derivation of the spectrum of VHE inverse Compton boosted photons also shows this n^2-dependency - irrespective of the spectrum of the secondary electrons in region (II). Thus, if n increases with a factor of z, the observed flux below 3 GeV should also increase by that same factor, but the VHE γ-ray flux will increase with a factor of z^2. Furthermore, according to CHR, Crab's tertiary photon production is ≈ 1000 times faster than that of Vela and possibly MSH, so that transients for Crab may be more pronounced than those for Vela and MSH. In fact, the observations of MSH as reported in Chapter 3 indicated steady emission with no indication of transient emission.

Bhat et al. (1986) reported that transients with time scales of ≈ 15 minutes occur once in ≈ 100 hours of continuous observations of Crab. Consequently one can model the tertiary photon density to fit the VHE transient phenomena as follows: Let $\bar{n}$ be the average density which corresponds to the steady flux level. If the tertiary photon density is a stochastic variable with the following distribution

$$n = {}^{d}(N(\bar{n}, 1.8\bar{n})), \qquad (4.42)$$

then a 15 minute transient occurrence, where the flux level increases with a factor of $\simeq$ 25 from its steady value, would correspond to a 2.82 sigma deviation of n from $\bar{n}$, or, one such transient in 100 hours of observation.

There is one way to confirm (4.42): the binning of the count rate of infrared photons from Crab in 15 minute intervals should show fluctuations which is much larger than Poisson fluctuations. In fact, the fluctuations should follow the distribution given by (4.42), but if mechanism (c) mainly controls the gap's dimensions, the inferred dependency may not be true for Crab and one has to revise this model for VHE transients.

4.6.8. THE CROSS SECTION FOR THE INVERSE COMPTON PROCESS

Throughout this study it was assumed that the cross section for the inverse Compton process is the Thomson cross section $\sigma_T = 6.65 \times 10^{-25}$ cm^2. Consider an electron with energy $\gamma m_e c^2$ and a tertiary photon with energy $\hbar\omega_{IR} = \gamma_{IR} m_e c^2$. The Thomson cross section is only applicable if $\gamma\gamma_{IR} < \frac{1}{2}$, or, using (4.31) with $p \simeq 1$, gives

$$\dot{P} P^{-3.7} > 3.7 \times 10^{-10} E_{12}^{2/3} \qquad (4.43)$$

where E_{12} is the energy of the inverse Compton boosted photon in units of 10^{12} eV.

If condition (4.43) is violated, one should replace the Thomson cross section with the smaller Klein Nishima cross section (see e.g. Ginzburg, 1979). A further investigation of the VHE γ-ray luminosity equation for pulsars with V1-parameters shows that $L_{V1}(\text{TeV}) \propto \sigma^2 n^2$ where σ is the cross section for inverse Compton scattering. However, according to CHR's work $n \propto \sigma^{-2}$ so that $L_{V1}(\text{TeV}) \propto \sigma^{-2}$, i.e. the luminosity increases with decreasing cross section. This is not necessarily true since the violation of condition (4.43) is similar to condition (4.40) which implies that $U_{IR} > U_\perp$ and was derived by CHR for the case where $U_\perp > U_{IR}$. Thus,

a more generalised derivation of CHR's gap equations are necessary to draw any conclusions about pulsars violating (4.43).

The Vela pulsar will violate condition (4.43) for $E_{12} > 4$ while this violation will occur at $E_{12} > 10$ for MSH. In these cases the luminosity may even increase due to the smaller cross section but this is not certain as mentioned before. Pulsars with V2-parameters where $E_{12} < 10$ (e.g. Crab and PSR 1937+214) will never violate (4.43) since condition (4.32) for V2-parameters prevents that.

4.7. CONCLUSIONS.

It seems as if most polar cap models gives a γ-ray luminosity which scales with $B_s/P^2 \propto (I\Omega\dot{\Omega})^{\frac{1}{2}}$. Slight departures from this scaling law is due to the inclusion of pair production attenuation of γ-rays above the polar cap. Such detailed models predict a high energy (between 3 and 30 GeV) cutoff for observable γ-rays. Thus, polar cap models cannot provide VHE γ-rays from pulsars like Crab, Vela and MSH. From the modified polar cap model of Usov it follows that pulsars like Crab and Vela can radiate polar cap γ-rays with maximum energies of a few hundred MeV, while MSH cannot radiate any polar cap γ-rays at all. However, only millisecond pulsars with very small values of P and $\dot{P}$ can provide a maximum observable polar cap γ-ray energy of $\approx$ 1 TeV. The only pulsar satisfying this condition so far is PSR 1937+214 which was indeed observed by Turver (1985) at $E_\gamma > 1$ TeV. The Durham group identified a VHE pulse in phase with the radio main pulse and if the latter originates at the stellar surface, it means that the observed VHE pulse also originates at the stellar surface, thus confirming Usov's predictions.

The outer gap model of CHR seems to be very promising to explain many radiation properties of pulsars for which $I\Omega\dot{\Omega} > 10^{34}$ erg.s^{-1}. For most pulsars it seems as if mechanism (d) is the most important gap controlling mechanism. The main process involved for this mechanism is the following: Primary γ-rays are created by means of the inverse Compton scattering

of infrared (tertiary) photons in a so-called outer gap by the primary electrons originating from the polar caps. It is also these primary γ-rays which create the necessary infrared photons for the gap by means of two further generations of electron photon cascades. For this mechanism all pulsars can be classified in two classes with respect to the energy of the tertiary photons, i.e. those with V1-parameters (e.g. Vela and MSH) and those with V2-parameters (e.g. Crab and PSR 1937+214). Other mechanisms can also control a gap: Firstly the case where thermal X-rays from the polar cap sustain the gap (mechanism (b)). MSH is a good example of a source where this mechanism may be important. Secondly, if the X-rays produced in the outer gap sustain the gap itself (mechanism (c)). However, these processes received little attention by CHR. It is thus important that CHR's outer gap model should be extended to the case where any combination of mechanisms controls the gap.

It is evident from this study that outer gap pulsars produce VHE γ-rays with an efficiency which increases with increasing P and decreasing $\dot{P}$ which is contrary to expectation. The predicted luminosities are however in good agreement with the observations of the five known TeV pulsars (Table 4.2).

In some cases the polar cap model may be used in combination with the outer gap to explain the observations. According to Smith (1986) the main and second pulses of Crab and Vela are produced by outer gaps while the interregion emission is produced by polar cap emission. In this case the model of Harding (1981) and Usov (1983) can be used to describe this interregion emission. See Figure 2.13a as an illustration of these possible distinct emission regions. The outer gap model of CHR also predicts a VHE luminosity for PSR 1937+214 which agrees roughly with the observed luminosity. It seems then as if the polar cap and outer gap models compete for the VHE radiation from PSR 1937+214. One will be able to answer this question if the site of radio emission can be determined, since the observed VHE γ-rays are produced at the same site as the radio emission.

It was shown that pulsars satisfying the equation

$$\dot{P}P^{-3.9}\rho^{-4.3} \approx 4.4\times10^{-10} \qquad (4.44)$$

are the ideal VHE γ-ray pulsars under the outer gap model of CHR for mechanism (d). From this requirement it followed that a pulsar with the tentatively identified parameters of PSR 1802-23 is an ideal VHE γ-ray pulsar. Other such high priority pulsars are PSR 1800-21 and PSR 1823-13. It is important to know that such pulsars are TeV loud but MeV quiet, so that they need not be COS-B sources.

VHE transients may be explained by fluctuations in the infrared emission (Smith, 1986 and Orford, 1986). From this study it followed that the luminosity at $E_\gamma < 3$ GeV depends on the number density n of infrared photons, while the VHE γ-ray luminosity depends on n^2, so that infrared fluctuations will cause even more pronounced VHE fluctuations. One can confirm Crab's VHE transient phenomena if one standard deviation of the observed infrared flux is nearly twice the average flux level, rather than the classic Poisson value which is the square root of the average flux level. According to this study it seems then as if there are models available to explain VHE γ-ray emission from pulsars. However, these models still need some refinements with respect to the following aspects:

1. The γ-ray luminosity for any gap controlling mechanism separately,

2. the γ-ray luminosity for a combination of mechanisms and

3. pulsars satisfying $\eta(S\rightarrow IC) >> 1$.

CHAPTER 5

CONCLUSIONS

When evaluating most VHEGRA results, one can see that this astronomy is facing a dilemma: The analysis in Section 1.5 indicated that a periodic γ-ray signal's DC excess (in standard deviations) above the cosmic ray background depends on the duty cycle of the peak on the light curve, while the observed signal strength of e.g. the Crab seems to depend on the sample size. This anomalous behaviour can have three explanations, the second and third ones being more probable than the first: (a) Nearly all reports are statistical fluctuations from the cosmic ray background, (b) the source emits VHE γ-rays at a mean intensity level which is below the sensitivity level of most telescopes, but the fluctuations are much larger than the expected Poisson fluctuations. (c) most VHEGRA sources are of true transient nature with no steady radiation.

However, one may be on the brink of solving the VHEGRA dilemma completely: Observations of 4U 0115+63 (Chadwick et al., 1985b), Vela X-1 (North et al., 1987) and MSH (Chapter 3) yielded steady γ-ray signals with virtually no evidence of time variability.

The report of Lamb et al. (1986) on 4U 0115+63 cannot be taken as evidence for time variability since their data were analysed with the 'transient' technique instead of Chadwick et al.'s 'coherent' technique. It was discussed in Chapter 3 that one cannot conclude from a transient analysis that a source is transient and one has to treat the data in the same way as it was done in Section 4.3.6 to determine whether the emission was steady.

The event which will however establish VHEGRA as a 'respectable' astronomy is the discovery of a very strong source. Is this still possible given the existing telescopes and sky coverage? Now, if the distance to one of these steady sources was 0.5 kpc, the observed count rate would

at least have been twice the background rate. For a typical sample size of 74 000, a signal strength of 50% and using relation (2.61) for the Rayleigh power, one would have identified such a pulsar with a p-level of $\approx 10^{-2000}$. Is it then a 'Cosmic Conspiracy' which places luminous sources far from Earth and less luminous sources (e.g. Vela pulsar) closer to Earth so that one observes only $\approx 10^{-6}$ effects? This is certainly untrue and if other sources like 4U 0115+63, Vela X-1 or MSH can be discovered which lie close to Earth (e.g. 0.5 or 1 kpc) the dilemma may be solved.

It may also be worthwhile if VHE γ-ray astronomers search for sources which cause the ON-source count rate to be double the OFF-source count rate. The Northern Sky was covered by VHE sky surveys (Weekes, Helmken and L'Heureux, 1979) while few observations of the Southern Sky were done (see Section 1.4). Furthermore, most candidate pulsars and COS-B sources lie in the Southern Sky, simply because most of the galactic disc is observable from the Southern hemisphere. Thus, it is statistically and on the basis of COS-B observations, more probable to discover such ideal VHE γ-ray sources in the Southern Sky. Such a source can be easily identified by means of a single drift scan and the most likely candidates to observe are the unidentified COS-B sources, short period pulsars and undiscovered pulsars in supernova remnants. The latter objects are interesting to study:

The radio pulse of a pulsar may be a narrow pencil beam which can easily be missed during radio surveys. However, the γ-ray beam may be fan shaped which will always be visible due to geometrical considerations (CHR). Consequently some supernova remnants may contain young unknown pulsars which may be TeV loud. If the position of such a TeV loud ($F_\gamma(>1\ \text{TeV}) > 10^{-9}\ \text{cm}^{-2}.\text{s}^{-1}$) pulsar does not coincide with a COS-B point source, it should be MeV quiet in the sense that the flux $F_\gamma(> 50\ \text{MeV}) < 3\times10^{-6}\ \text{cm}^{-2}.\text{s}^{-1}$ from this pulsar. In fact, from the outer gap model of CHR one can see that this is possible: Using relations (4.36a) and (4.41a), one will have a TeV loud but MeV quiet pulsar if

$$\dot{P}P^{-3.9} \approx 4.6\times10^{-10}\ell^{-0.29}\rho^{4.3} \qquad (5.1)$$

Consequently those pulsars in the vicinity of the line 'VHE' in Figure 4.2 will be prime candidates. Confirmed radio pulsars which lie close to this line are PSR 1800-21 and PSR 1823-13.

This study shows that it is worthwhile to do a single drift scan through each unidentified COS B source, all supernova remnants and the pulsars lying to the left of the 'DLOG' line on Figure 4.2. If the ON-source count rate does not increase significantly for a single scan, one should drop that source and continue with the next one. If the count rate ON-source doubles for a COS-B source or a supernova remnant, one can search for a periodicity in the data. For a sinusoidal light curve, and an OFF source count rate of ≈ 40 min^{-1}, relation (2.61) would imply a Rayleigh p-level of $\approx 10^{-22}$ for the single 10 min data set. If one searches for periodicity in the range from 1 ms up to $\approx$ 1 s (i.e. 5×10^5 IFS, see relation (2.35)) a new pulsar can be identified at a p-level of $\approx 5\times10^{-17}$. The first identification of such a pulsar is the 12.59 ms pulsar in Cyg X-3 by Chadwick et al. (1985c), but this pulsar seems to be time variable in its VHE output so that this identification is not yet firm. Thus, given the apparent poor sensitivity levels of VHEGRA, it may still be able to yield new sources and stimulate other astronomies.

Meanwhile VHEGRA must be contented with the present sample of VHE γ-ray sources which yield 6σ effects at most. In such cases the statistical treatment of data should be correctly done and the prime requirement for data analysis is that the data should form a random sample. The Gini test was given as an additional check for Poisson homogeneity in DC data. In the case of periodic data one should derive the distribution of the test statistic from the experimental data to confirm randomness (see e.g. Figures 3.10 and 3.13). Time variability can be identified by means of 'change point procedures': Lombard and Schultz (1986) was the first to develop a technique to detect a change in a light curve with time or space.

The identification of a periodic signal is done through the use of a test for uniformity. In Section 2.3 it was shown that most tests are powerful for certain forms of light curves. If one persists in using a test like Pearson's χ^2 with say twenty bins, sources will usually be identified with

duty cycles of ≈ 1/20. However, statistical fluctuations with such duty cycles may also be identified. If one has a priori knowledge of the light curve, one can use some form of Z^2_m to test for such a signal. Future observations of MSH will require the use of the $2n\bar{R}^2_3$ statistic, since radiation was seen only at the third harmonic. However, none of the Z^2_m-, Protheroe- or Watson tests will be reliable to identify a signal if nothing is known a priori about the light curve.

If one had used the Z^2_{10}-test to identify MSH, a p-level of $\approx 8\times10^{-4}$ would have been obtained. The effect of a search within one IFS (see Section 2.3.5) would have introduced a factor of underestimation of ≈ 20. Consequently MSH would have been identified at a confidence level of 98.4% which would have caused the identification to be questionable. The theory of density estimation (see Section 2.4) shows that the error of any density estimate consists of the well known variance and less known bias components. These components are controlled by the choice of a smoothing parameter. The very important Z^2_m-test for uniformity results if one takes the mean integrated squared distance between the Fourier Series density estimator of a light curve and the uniform density. The use of the Hart-rule (relation (2.56)) to estimate objectively the optimal number of harmonics $\hat{m}$ for a data set, resulted in the H_m-test for uniformity (see Section 2.5) - a test which is powerful for a wide range of light curves and should be used if nothing is known a priori about the light curve (which is the case for any new candidate source studied). The application of this test to the MSH data resulted in a p-level of ≈ 10^{-4} while the p-level's factor of underestimation due to the search within one IFS was ≈ 10 instead of 20 (as it was with Z^2_{10}). Consequently MSH could be identified at a confidence level of 99.9%.

Another use of the Hart-rule is to be of assistance in the estimation of the signal strength. If the background region in a light curve is too small to be estimated, it would be best to use the theory of characteristic functions (see Sections 2.3.1 and 2.6) to model the light curve. To estimate a light curve, it is proposed that kernel density estimators should be used (see e.g. Figure 2.12). Such a KDE is a much closer presentation of the true light curve than the histogram. Apart from obtaining a smooth estimate of the light curve, relation (2.51) gives the optimal

choice of the important smoothing parameter $\hat{h}$. The latter is equivalent to the bin width of the histogram, but the γ-ray astronomer is now relieved from the responsibility of selecting h for his data. Astronomers would be interested to know the distribution of h for a given light curve and sample size. This problem has yet to be tackled by Statisticians but one may expect the variance of $\hat{h}$ to increase with decreasing sample size (n) so that an oversmoothed light curve may be obtained for $n < 50$ (see Figure 2.15). For small sample sizes (e.g. in UHEGRA) it is suggested that relation (2.51) should be avoided and the astronomer should select h more subjectively, i.e. such that h is less than the expected duty cycle of radiation. The use of the histogram for $n < 50$ can also be considered if a 'pleasing' graph cannot be obtained with the KDE.

The reanalysis of the data on the pulsar suspect PSR 1802-23 yielded a final confidence level of 98.6% which is less than the confidence level of 99.8% stated by Raubenheimer et al. (1986): The main reason being the overlooking of the factor of underestimation when searching within one IFS. Follow up observations are however necessary since Chapter 4 indicates that this is a prime candidate for TeV γ-radiation.

The result on MSH is important in the sense that the radiation is coherent while the fluctuations in the signal strength from night to night are consistent with the fluctuations expected from a time independent signal strength. Consequently one can consider the observed radiation from MSH to be steady. In Chapter 4 it was shown that the outer gap model of CHR can explain the observed VHE luminosity if the magnetic axis is tilted with respect to the rotational axis (this tilting was originally proposed by Greenstein and Hartke (1983)) such that the radial distance to the outer gap is ≈ 1.2 times the light cylinder radius while the azimuthal width of the gap is approximately twice the light cylinder radius (which is also consistent with the broad peaks on the VHE light curve). These interpretations of MSH yield a flux below 3 GeV which is somewhat below the sensitivity level of COS-B which is consistent with the fact that no strong signal was observed from MSH above 50 MeV. The only problem with MSH is the observed triple peak which may be difficult to explain.

To conclude, it is a certainty that by the proper handling of the data and by using modern statistical techniques, the reliability of VHEGRA results may be enhanced to a large extent. Furthermore, it was shown that reported VHEGRA results on isolated pulsars can be explained by means of existing models.

```
      SUBROUTINE SKERN(N,PHASE,S,X,Y,H1)
C
C THIS SUBROUTINE ESTIMATES THE LIGHT CURVE AND THE CORRESPONDING
C   'CONFIDENCE BAND' FOR A GIVEN SET OF PHASES.
C
      IMPLICIT REAL*8 (A-H,O-Z)
      DIMENSION PHASE(1),THE(1000),X(1000),Y(3,1000)
      DIMENSION RAL(10001),RALE(10001),APK(10001),BPK(10001)
      TPI=2.0D0*3.14159265359D0
C
C NL CONTAINS THE NUMBER OF PHASES IN WHICH THE LIGHT CURVE SHOULD BE
C   CALCULATED. THE USER IS FREE TO CHANGE THIS NUMBER - UNLESS IT DOES
C   NOT CONFLICT WITH THE DIMENSIONS OF X AND Y.
C
      NL=1000
C
C NP = TOTAL NUMBER OF HARMONICS THAT WILL BE USED
C      THE LAST FEW OF THEM ARE USUALLY UNIMPORTANT FOR BROAD LIGHT
C      CURVES BUT MAY BECOME IMPORTANT FOR NARROW CRABLIKE LIGHT CURVES.
C      IT IS BETTER TO LEAVE NP UNCHANGED
C
      NP=1000
C
C INPUT: N, PHASE, S
C *******
C N = SAMPLE SIZE (NUMBER OF FOLDED PHASES FROM ARRIVAL TIMES).
C
C PHASE = VECTOR CONTAINING THE N PHASES WITH 0 < PHASES < 1.
C
C S = NUMBER OF STANDARD DEVIATIONS FOR THE 'CONFIDENCE BAND'
C    S = 2  IS A GOOD CHOICE AND DEFINES A 95% 'CONFIDENCE BAND'
C
C OUTPUT: X,Y,H1
C ********
C
C X(I)=I/NL FOR I=1 TO NL: CONTAINS THE NL EQUISPACED PHASE VALUES.
C   THUS, X(1)=1/NL AND X(NL)=1. THE SCALE OF THE PHASES IS
C   THEREFORE BETWEEN 0 AND 1
C
C Y(J,I) FOR I=1 TO NL, CONTAINS THE FOLLOWING INFORMATION:
C   J=1 => DENSITY ESTIMATE NORMALISED TO THE SAMPLE SIZE N AND NOT 1
C   J=2 => DENSITY ESTIMATE PLUS ERROR AT S STANDARD DEVIATIONS
C   J=3 => DENSITY ESTIMATE MINUS ERROR AT S STANDARD DEVIATIONS
C   THE WORD 'STANDARD DEVIATION' REFERS TO THE GAUSSIAN PROPERTY OF
C   OF THE KERNEL DENSITY ESTIMATORS
C
C H1 = SMOOTHING PARAMETER FOR THE SWANEPOEL KERNEL DENSITY ESTIMATOR.
C    THE SCALE IS BETWEEN 0 AND 0.5.
C    THE TIME RESOLUTION OF THE KDE IS APPR. 4H1.
C    IF ONE OBTAINS 4H1 MUCH LARGER THAN 1, THE
C    RESULTING LIGHT CURVE WILL ONLY BE A STRAIGHT LINE, WHICH MEANS
C    THAT NO SIGNIFICANT GAMMA RAY SIGNAL IS PRESENT IN THE DATA.
```

```
      Z=DFLOAT(N)
C
C TRANSFORMATION OF PHASES FROM (0,1) INTERVAL TO THE (0,2PI) INTERVAL:
C
      DO 1 I=1,N
      PHASE(I)=PHASE(I)*TPI
    1 CONTINUE
C
C APK(IP) AND BPK(IP) (FOR IP=1 TO NP) CONTAINS RESPECTIVELY
C   THE COSINE AND SINE (EMPIRICALLY DETERMINED)
C   TRIGONOMETRIC MOMENTS FOR ALL NP HARMONICS RESPECTIVELY.
C RAL(IP) IS PROPORTIONAL TO THE 'RAYLEIGH POWER' OR RESULTANT LENGTH
C   SQUARED FOR THE IP'TH HARMONIC.
C RALE(IP) IS AN UNBIASED ESTIMATOR OF THE RESULTANT LENGTH SQUARED
C   OF THE IP'TH CHARACTERISTIC FUNCTION.
C
      DO 3 IP=1,NP
      APK(IP)=0.0D0
      BPK(IP)=0.0D0
      DO 2 J=1,N
      THET=ANGLE(IP,PHASE(J))
      APK(IP)=APK(IP)+DCOS(THET)/Z
    2 BPK(IP)=BPK(IP)+DSIN(THET)/Z
      RAL(IP)=APK(IP)**2+BPK(IP)**2
      RALE(IP)=(Z*RAL(IP)-1.0D0)/(Z-1.0D0)
    3 CONTINUE
C
C ESTIMATION OF THE OPTIMAL SMOOTHING PARAMETER 'HNK':
C   REMEMBER THAT THIS PARAMETER IS TRANFORMED TO RADIANS FOR THE SAKE
C   OF COMPUTATION.
C   SMIN WILL CONTAIN THE MINIMUM OF THE H-DEPENDENT TERMS OF THE 'MISE'
C   FOR ALL THE PREVIOUS SEARCHES OF H.
C
      SMIN=1.0D+15
C
C THE NEXT LOOP SEARCHES FOR THE OPTIMAL H BETWEEN 0.1% AND 50%:
C   IT IS UNLIKELY THAT H WILL FALL OUTSIDE THIS RANGE.
C
      DO 5 IH=1,500
      HN=TP1*DFLOAT(IH)/10000.0D0
      SOMC=0.0D0
      DO 4 IP=1,NP
      ARG=DFLOAT(IP)*HN
      IF(ARG.GT.100.0D0)GOTO 55
      GAM=FT(ARG)
      SOMC=SOMC+GAM**2*RAL(IP)-2.0D0*GAM*RALE(IP)
    4 CONTINUE
   55 IF(SMIN.GT.SOMC)THEN
         HNK=HN
         SMIN=SOMC
      ENDIF
    5 CONTINUE
C
C 'SMIN' CONTAINS NOW THE MINIMUM OF THE H-DEPENDENT TERMS OF THE MISE.
C 'HNK' IS THE ESTIMATE OF THE OPTIMAL H (IN RADIANS).
```

```
C THE FOLLOWING LOOP SET THE VALUES OF X(I) AND THE STARTING VALUE
C   FOR Y(1,I).
C
      DO 6 I=1,NL
      X(I)=DFLOAT(I)/DFLOAT(NL)
      Y(1,I)=1.0D0
    6 THE(I)=X(I)*TPI
C
C THE FOLLOWING LOOP CALCULATES THE DENSITY FUNCTION (LIGHT CURVE)
C    Y(1,I) IN NL EQUIDISTANT POINTS
C
      DO 7 IP=1,NP
      ARG=HNK*DFLOAT(IP)
      IF(ARG.GT.100.0D0)GOTO 8
      GAM=FT(ARG)
      DO 7 I=1,NL
      THIP=ANGLE(IP,THE(I))
      Y(1,I)=Y(1,I)+2.0D0*GAM*(APK(IP)*DCOS(THIP)+BPK(IP)*DSIN(THIP))
    7 CONTINUE
C
C H1 IS THE VALUE OF THE OPTIMAL SMOOTHING PARAMETER BETWEEN 0 AND 1
C
    8 H1=HNK/TPI
C
C THE FOLLOWING LOOP MULTIPLIES THE DENSITY FUNCTION (NORMALISED ON
C   THE INTERVAL 0 TO 1) WITH THE SAMPLE SIZE SO THAT THE AREA UNDER THE
C   LIGHT CURVE IS N IF INTEGRATION IS DONE BETWEEN 0 AND 1.
C
C THE ERROR AT EACH PHASE X(I) IS ALSO ESTIMATED:
C
      DO 9 I=1,NL
      Y(1,I)=Y(1,I)*Z
      IF(Y(1,I).LT.1.0D0)Y(1,I)=1.0D0
      ERROR=S*DSQRT(0.375D0*Y(1,I)/H1)
      Y(2,I)=Y(1,I)+ERROR
      Y(3,I)=Y(1,I)-ERROR
    9 CONTINUE
      RETURN
      END
C
C THIS SUBROUTINE MULTIPLIES THE ANGLE 'THET' WITH THE INTEGER IP
C   FOR FURTHER USE IN TRIGONOMETRIC FUNCTIONS. THE PURPOSE OF THIS
C   IS TO AVOID ANY PRECISION ERRORS.
C
      FUNCTION ANGLE(IP,THET)
      IMPLICIT REAL*8 (A-H,O-Z)
      TPI=2.0D0*3.14159265359D0
      AK=DFLOAT(IP)*THET/TPI
      NAK=AK
      ANGLE=(AK-DFLOAT(NAK))*TPI
C
C ANGLE CONTAINS THE VALUE OF IP*THET MINUS AN INTEGER TIMES 2PI
C
      RETURN
      END
```

```
C
C FT CONTAINS THE FOURIER TRANSFORM OF THE KERNEL FOR THE
C    PARAMETERS IP AND H
      FUNCTION FT(ARG)
      IMPLICIT REAL*8 (A-H,O-Z)
      FT=0.0D0
      IF(ARG.GT.100.0D0)RETURN
      FT=4.0D0/(4.0D0+ARG**4)
      RETURN
      END
```

```
      SUBROUTINE HTEST(N,PHASE,M,PROB)
C
C H-TEST FOR UNIFORMITY
C   THIS PROGRAM ACCEPTS 'N' PHASES BETWEEN 0 AND 1 IN THE VECTOR
C   'PHASE'.
C THE OPTIMAL NUMBER OF HARMONICS 'M' IS DETERMINED BY THE HART-RULE.
C THE P-LEVEL IS GIVEN BY 'PROB'.
C
      IMPLICIT REAL*8 (A-H,O-Z)
      REAL*4 A,P
      DIMENSION PHASE(1),C(20),S(20),TH(20),R(20)
      DATA TH/.522,.495,.453,.425,.402,.385,.375,.353,.352,.364,
     1        .343,.329,.327,.322,.298,.285,.292,.308,.308,.231/
      DATA R/1.065,1.981,2.117,2.166,2.177,2.172,2.190,2.125,2.144,2.272
     1,2.171,2.114,2.149,2.131,1.984,1.957,2.026,2.239,2.150,1.744/
      TPI=2.0D0*3.14159265359D0
      Z=DFLOAT(N)
      DO 1 I=1,20
      C(I)=0.0D0
    1 S(I)=0.0D0
      DO 2 I=1,N
      DO 2 J=1,20
      ARG=DFLOAT(J)*PHASE(I)*TPI
      C(J)=C(J)+DCOS(ARG)
      S(J)=S(J)+DSIN(ARG)
    2 CONTINUE
      HRULE=0.0D0
      HMIN=-1000.
      M=1
      DO 3 J=1,20
      RAL=2.0D0*(C(J)**2+S(J)**2)/Z
      HRULE=HRULE+RAL-4.
      IF(HMIN.LT.HRULE)THEN
         M=J
         HMIN=HRULE
      ENDIF
    3 CONTINUE
      HT=HMIN+4.D0
      A=TH(M)*HT
      P=R(M)
      CALL MDGAM(A,P,PR,IER)
      PROB=1.D0-PR
      IF(M.EQ.1)PROB=DEXP(-0.5D0*HT)
      RETURN
      END
```

ACKNOWLEDGEMENTS

The author wishes to express his gratitude towards the following:

Prof. B.C. Raubenheimer as promotor of this thesis for his guidance, continued interest and support.

Prof. J.W.H. Swanepoel as co-promotor for his invaluable advice and support.

The CSIR for the Special Merit Award and financial support.

Dr. R. Buccheri, the COS-B and the Caravane Collaboration for making available the complete COS-B data base to the PU/CSIR Cosmic Ray Research Unit.

The Personnel of the PU/CSIR Cosmic Ray Research Unit for their support and for useful discussions with many of the members.

Mr. Nols Muller for the drawing of some figures and Mrs. Rina Kahl for helping with the typing.

My wife Estie, for her continuous support, motivation, understanding and help with the typing.

REFERENCES

1. Backer, D.C., Kulkarni, S.R., Heiles, C., Davis, M.M. and Goss, W.M. 1982. A millisecond pulsar. Nature, 300:615-618.

2. Baltrusaitis, R.M., Cassiday, G.L., Cooper, R., Elbert, J.W., Gerhardy, P.R., Loh, E.C., Mizumoto, Y, Sokolsky, P., Sommers, P. and Steck, D. 1985. Evidence for 500 TeV Gamma-ray emission from Hercules X-1. Astrophys J, 293:L69-L72.

3. Beran, R.J. 1969. Asymptotic theory of a class of tests for uniformity of a circular distribution. Annals of Mathematical Statistics, 40:1196-1206.

4. Bhat, P.N., Gupta, S.K., Ramana Murthy, P.V., Sreekantan, B.V., Tonwar, S.C. and Vishwanath, P.R. 1980. Pulsed High Energy Gamma Rays from Vela Pulsar. Astron Astr, 81:L3-L5.

5. Bhat, P.N., Ramana Murthy, P.V., Sreekantan, B.V. and Vishwanath, P.R. 1986. A very high energy Gamma Ray burst from the Crab Pulsar. Nature, 319:127-128.

6. Bickel, P.J. and Rosenblatt, M. 1973. On some global measures of the deviations of density function estimates. Ann Stat, 1(6):1071-1095.

7. Boriakoff, V., Buccheri, R. and Fauci, F. 1983. Discovery of a 6.1 ms binary pulsar PSR 1953+29. Nature, 304:417-419.

8. Buccheri, R. 1981. X-ray and gamma-ray observations of pulsars. (In Sieber, W. and Wielebinski, R., eds Pulsars. Dordrecht : D. Reidel Publishing Company.) 241-250.

9. Buccheri, R., Bennett, K., Bignami, G.F., Bloemen, J.B.G.M., Boriakoff, V., Caraveo, P.A., Hermsen, W., Kanbach, G., Manchester, R.N., Masnou, J.L., Mayer-Hasselwander, H.A., Ozel, M.E., Paul, J.A., Sacco, B., Scarsi, L. and Strong A.W. 1983. Search for pulsed γ-ray emission from radio pulsars in the COS-B data. Astron Astr, 128:245-251.

10. Buccheri, R. and Sacco, B. 1984. Time analysis in Astronomy: Tools for Periodicity Searches. (In Proceedings of the International Workshop on data analysis in Astronomy. Erice (Sicily)). Plenum Press. Preprint.

11. Buccheri, R. 1985. Periodicity search in High energy Astrophysics. Steps for a reliable data analysis. (In Proceedings of the Workshop on Techniques in Ultra High Energy γ-ray Astronomy. La Jolla, (USA)) 98-103.

12. Buccheri, R., D'Amico, N., Hermsen, W. and Sacco, B. 1985. Statistical significance of the 59 s periodicity of Geminga and 1E0630+178. Nature, 316:131-132.

13. Buccheri, R. 1986. Personal communication.

14. Chadwick, P.M., Dowthwaite, J.C., Harrison, A.B., Kirkman, I.W., McComb, T.J.L., Orford, K.J., and Turver, K.E. 1985a. Association of the 6 ms pulsar PSR 1953 with the COS-B Gamma Ray source 2CG 065. Nature, 317:236-238.

15. Chadwick, P.M., Dowthwaite, J.C., Harrison, A.B., Kirkman, I.W., McComb, T.J.L., Orford K.J. and Turver, K.E. 1985b. 4U 0115+63: an energetic Gamma Ray Binary Pulsar. Astron Astr, 151:L1-L3.

16. Chadwick, P.M., Dipper, N.A., Dowthwaite, J.C., Gibson, A.I., Harrison, A.B., Kirkman, I.W., Lotts, A.P., Mcrae, H.J., McComb, T.J.L., Orford, K.J., Turver, K.E. and Walmsley, M. 1985c. A 12.6 ms Pulsar in Cygnus X-3. Nature, 318:642-644.

17. Chandler, J.F. 1985. Personal communication.

18. Chanmugan, G. and Gabriel, M. 1971. Magnetic field decay of neutron stars. Astron Astr, 11:268-269.

19. Chardin, G. 1986. Cygnus X-3 at high energies: A critical review. (In Proceedings of the sixth Astrophysics Meeting, Les Arcs (France)) Preprint.

20. Charman, W.N., Jelley, J.V., Orman, P.R., Drever, R.W.P. and McBreen, B. 1968. Search for High Energy Gamma Rays from CP 1133. Nature, 220:565-566.

21. Cheng, A., Ruderman, M.A. and Sutherland, P. 1976. Current flow in pulsar magnetospheres. Astrophys J, 203:209-212.

22. Cheng, K.S., Ho, C. and Ruderman, M.A. 1986. Energetic radiation from rapidly spinning pulsars. 1.Outer magnetospheric gaps. Astrophys J, 300:500-521.

23. D'Amico, N. 1986. Personal communication.

24. Danaher, S., Fegan, D.J., Porter, N.A. and Weekes, T.C. 1981. Observations of Cygnus X-3, M87, 3C237 and SS433 at energies greater than 10^{12} eV. 17th P Int Cosm Ray, 1:34-37.

25. Davis, K.B. 1975. Mean square error properties of density estimates. Ann Statist, 3(4):1025-1030.

26. Davis, K.B. 1977. Mean integrated square error properties of density estimates. Ann Statist, 5(3):530-535.

27. Davis, K.B. 1981. Estimation of the Scaling Parameter for a Kernel-type Density Estimate. J Am Stat A, 76(375):632-636.

28. De Jager, H.I. 1985. The optimization of a Cerenkov detector for the registration of 1 TeV gamma rays. Potchefstroom. 98p. (Thesis (MSc)- PU for CHE)

29. De Jager, O.C., Swanepoel, J.W.H., Raubenheimer, B.C. and Van der Walt, D.J. 1985. A new approach to evaluate gamma-ray measurements. 19th P Int Cosm Ray, 3:481-484. (Paper 1).

30. De Jager, H.I., De Jager, O.C., North, A.R., Raubenheimer, B.C., Van der Walt, D.J. and Van Urk, G. 1986a. The design and evaluation of a 1 TeV gamma ray telescope. South African Journal of Physics, 9(3):107-118

31. De Jager, O.C., Swanepoel, J.W.H. and Raubenheimer, B.C. 1986b. Kernel density estimators applied to gamma ray light curves. Astron Astr, 170:187-196. (Paper 2)

32. De Jager, O.C., Swanepoel, J.W.H. and Raubenheimer, B.C. 1987. Kernel density estimators applies to gamma-ray light curves. (In Proceedings of the NATO Advanced Research Workshop, Durham (UK)). To be published by D.Reidel. (Paper 3).

33. De Jager, H.I. and De Jager, O.C. 1987. Ohmic heating: A possible spindown mechanism for long period isolated pulsars. Submitted to Astron Astr.

34. Downs, G.S. 1981. JPL pulsar timing observations. 1.The Vela pulsar. Astrophys J, 249:687-697.

35. Dowthwaite, J.C., Gibson, A.I., Harrison, A.B., Kirkman, I.W., Lotts, A.P., Mcrae, J.H., Orford, K.J., Turver, K.E. and Walmsley, M. 1983. Ultra High energy Gamma Rays from Cygnus X-3. Astron Astr, 126:1-6.

36. Dowthwaite, J.C., Harrison, A.B., Kirkman, I.W., Mcrae, H.J., Orford, K.J., Turver, K.E. and Walmsley, M. 1984a. M31: an extragalactic source of 100 GeV Gamma Rays. Aston Astr, 136:L14-L15.

37. Dowthwaite, J.C., Harrison, A.B., Kirkman, I.W., Mcrae, J.H., Orford, K.J., Turver, K.E. and Walmsley, M. 1984b. The galactic plane: A source of 1000 GeV gamma rays. Astron Astr, 142:55-58.

38. Dowthwaite, J.C., Harrison, A.B., Kirkman, I.W., Mcrae, H.J., Orford, K.J., Turver, K.E. and Walmsley, M. 1984c. Hercules X-1 - a 1000 GeV Gamma Ray Pulsar. Nature, 309:691-693.

39. Dowthwaite, J.C., Harrison, A.B., Kirkman, I.W., Mcrae, H.J., McComb, T.J.L., Orford, K.J., Turver, K.E. and Walmsley, M. 1984d. Evidence for Pulsed 1000 GeV Gamma Rays from the Crab Pulsar. Astrophys J, 286:L35-L38.

40. Eadie, W.T., Drijard, D., James, F.E., Roos, M. and Sadoulet, B. 1971. Statistical methods in Experimental Physics. Amsterdam : North Holland.

41. Ebneter, K. and Balick, B. 1983. Centaurus A. Publications of the Astronomical Society of the Pacific, 95:675-690.

42. Erickson, R.A., Fickle, R.K. and Lamb, R.C. 1976. Search for pulsed gamma rays of $\approx 10^{13}$eV from NP 0532. Astrophys J, 210:539-543.

43. Fan, C.Y., Wu, J and Hang, H. 1982. Scaling from Jupiter to pulsars and mass spectrum of pulsars. Astrophys J, 260:353-361.

44. Fazio, G.G., Helmken, H.F., Rieke, G.H. and Weekes, T.C. 1968. Upper Limits to Gamma Ray Fluxes from three Pulsating Radio Sources. Nature, 220:892-893.

45. Fegan, D.J., Cawley, M.F., Gibbs, K., Gorham, P.W., Lamb, R.C., Porter, N.A., Reynolds, P.T., Stenger, V.J. and Weekes, T.C. 1987. Search for a 12.59 ms pulsar in Cygnus X-3 at E > 400 GeV. (In Proceedings of the NATO Advanced Research Workshop, Durham (UK)). To be published by D.Reidel.

46. Gail. M.H. and Gastwirth, J.L. 1978. A Scale-free Goodness-of-fit Test for the Exponential Distribution based on the Gini Statistic. J Roy Sta B, 40(3):350-357.

47. Gans, D.J. 1984. The Search for Significance: Different Tests on the same Data. J Stat Comp, 19:1-21.

48. Gerardi, G., Buccheri, R., Sacco, B. 1982. Comparison of Fourier with alternative techniques for periodicity searches in the case of unidimensional point serie. Application to the arrival time of Gamma Ray photons as detected by the COS-B satellite. (In Proceedings of "COMPSTAT 82", Toulouse (France)) Preprint.

49. Gibson, A.I., Harrison, A.B., Kirkman, I.W., Lotts, A.P., Mcrae, H.J., McComb, T.J.L., Orford, K.J., Turver, K.E., Walmsley, M. 1982a. The University of Durham Gamma Ray facility at Dugway. (In Ramana Murthy, P.V. and Weekes, T.C. eds Proceedings of International Workshop on Very High Energy Gamma Ray Astronomy. Ootacamund (India)) Smithsonian Institution, U.S.A. 97-114.

50. Gibson, A.I., Harrison, A.B., Kirkman, I.W., Lotts, A.P., Mcrae, H.J., Orford, K.J., Turver, K.E. and Walmsley, M. 1982b. Transient emission of ultra-high energy pulsed Gamma Rays from Crab pulsar PSR 0531. Nature, 296:833-835.

51. Ginzburg, V.L. 1979. Theoretical physics and astrophysics. Oxford : Pergamon Press.

52. Goldreich, P. and Julian, W.H. 1969. Pulsar electrodynamics. Astrophys J, 157:869-880.

53. Gorham, P.W., Cawley, M.F., Fegan, D.J., Gibbs, K.G., Kenny, S., Lamb, R.C., Liebing, D.F., Porter, N.A., Stenger, V.J. and Weekes, T.C. 1986a. Hercules X-1: Pulsed γ-rays detected above 250 GeV. Accepted by Astrophys J.

54. Gorham, P.W., Cawley, M.F., Fegan, D.J., Gibbs, K.G., Lamb, R.C., Liebing, D.F., Porter, N.A., Stenger, V.J. and Weekes, T.C. 1986b. Pulsed TeV gamma-rays detected from Hercules X-1 during X-ray source eclipse. Accepted by Astrophys J L.

55. Graser, U. and Schönfelder, V. 1983. Search for pulsed gamma-ray emission at MeV energies from 24 radio pulsars. Astrophys J, 273:681-687.

56. Greenstein G. and Hartke, G.J. 1983. Pulselike character of blackbody radiation from neutron stars. Astrophys J, 271:283-293.

57. Greenwood, J.A. and Durand, D. 1955. The distribution of Length and Components of the sum of n Random Unit Vectors. Annals of Mathematical Statistics, 26:233-246.

58. Grindlay, J.E., Hanbury Brown, R. and Allen, L.R. 1973. First results of a Southern Hemisphere Search for gamma ray sources at $E \geq 3 \times 10^{11}$ eV. 13th P Int Cosm Ray, 1:439-445.

59. Grindlay, J.E. 1975. Compton-synchrotron model for the nucleus of Centaurus A. (NGC 5128). Astrophys J, 199:49-53.

60. Grindlay, J.E., Helmken, H.F., Hanbury Brown, R., Davis, J. and Allen, L.R. 1975a. Evidence for the detection of gamma rays from Centaurus A at $E_\gamma \geq 3 \times 10^{11}$ eV. Astrophys J, 197:L9-L12.

61. Grindlay, J.E., Helmken, H.F., Hanbury Brown, R., Davis, J. and Allen, L.R. 1975b. Results of a Southern Hemisphere search for gamma-ray sources at $E_\gamma \geq 3 \times 10^{11}$ eV. 14th P Int Cosm Ray, 1:89-94.

62. Grindlay, J.E., Helmken, H F. and Weekes, T.C. 1976. Evidence for a variable flux of $>10^{11}$eV Gamma Rays from NP 0532. Astrophys J, 209:592-601.

63. Gupta, S.K., Ramana Murthy P.V., Sreekantan, B.V. and Tonwar, S.C. 1978. High-energy pulsed gamma rays from pulsars. Astrophys J, 221:268-273.

64. Gupta, S.K., Ramana Murthy, P.V. and Sreekantan, B.V. 1982. Pulsed high energy gamma ray emission from Crab pulsar. (In Ramana Murthy, P.V. and Weekes, T.C. eds Proceedings of International Workshop on Very High Energy Gamma Ray Astronomy. Ootacamund (India)) Smithsonian Institution, U.S.A. 273-274.

65. Harding, A.K. 1981. Pulsar γ-rays: Spectra, Luminosities and Efficiencies. Astrophys J, 245:267-273.

66. Hart, J.D. 1985. On the choice of a truncation point in Fourier Series Density Estimation. J Stat Comp, 21:95-116.

67. Hearn, D. 1969. Consistent analysis of gamma-ray astronomy experiments. Nuclear instruments and Methods, 70:200-204.

68. Hecht, E. and Zajac, A. 1980. Optics. Massachusetts : Addison-Wesley Publishing Company.

69. Helfand, D.J. 1982. X-rays from radio pulsars: The portable supernova remnants. (In Proceedings of IAU symp. no.101 "Supernova remnants and their X-ray emission". Venice, (Italy)) Preprint.

70. Helfand, D.J. and Becker, R.H. 1984. Observation of stellar remnants from recent supernovae. Nature, 307:215-221.

71. Heyvaerts, J. and Signore, M. 1981. Expected characteristics of pulsar gamma-ray radiation and the problem of its location. Astron Astr, 96:36-51.

72. Hillier, R. 1984. Gamma Ray Astronomy. Oxford : Clarendon Press.

73. Hoeffding, W. 1948. A class of statistics with aymptotically normal distribution. Annals Mathematical Statstistics, 19:293-325.

74. Hoel, P.G. 1971. Introduction to Mathematical Statistics. New York : John Wiley & Sons Inc.

75. Huang, J-H., Huang, K-L. and Peng, Q-H. 1983. Pulsar statistics and two types of pulsars. Astron Astr, 117:205-208.

76. Jelley, J.V. 1982. Flashes in a dustbin and other reflections. (In Ramana Murthy, P.V. and Weekes, T.C. eds. Proceedings of International Workshop on Very High Energy Gamma Ray Astronomy. Ootacamund (India)) Smithsonian Institution, U.S.A. 3-20.

77. Jelley, J.V. 1986. Personal communication.

78. Jennings, D.M., White, G., Porter, N.A., O'Mongain, E., Fegan, D.J. and White, J. 1974. Results of a Search for 10^{12}eV Gamma Rays from Pulsars. Nuov Cim B, 20(1):71-82

79. Kanbach, G., Bennett, K., Bignami, G.F, Buccheri, R., Caraveo, P., D'Amico, N., Hermsen, W., Lichti, G.G., Masnou, J.L., Mayer-Hasselwander, H.A., Paul, J.A., Sacco, B., Swanenburg, B.N. and Wills, R.D. 1980. Detailed characteristics of the high-energy gamma radiation from PSR 0833-45 measured by COS-B. Astron Astr, 90:163-169.

80. Kulkarni, S.R. 1986. Optical identification of binary pulsars: Implications for magnetic field decay in neutron stars. Astrophys J, 306:L85-L89.

81. Kundt, W. 1981. Do neutron star magnetic fields decay? Astron Astr, 98:207-210.

82. Lake, R. 1981. Time and Frequency Transfer using SABCTV. Journal of the Institution of Electronics and Telecommunication Engineers, 27(10):456-459.

83. Lamb, R.C., Cawley, M.F., Fegan, D.J., Gibbs, K.G., Gregory, A.G., Gorham, P.W., Lewis, D.A., Porter, N.A., Stenger, V.J. and Weekes, T.C. 1987. Pulsed TeV gamma-rays from 4U 0115+63. (In Proceedings of the NATO Advanced Research Workshop, Durham (UK)). To be published by D.Reidel.

84. Leahy, D.A., Elsner, R.F., Weisskopf, M.C. 1983. On searches for periodic pulsed emission: The Rayleigh Test compared to Epoch Folding. Atrophys J, 272:256-258.

85. Lehman, E.L. 1959. Testing Statistical Hypotheses. New York : John Wiley and Sons, Inc.

86. Li, T-P. and Ma, Y-Q. 1983. Analysis methods for results in Gamma Ray Astronomy. Astrophys J, 272:317-324.

87. Lombard, F. and Schultz, D.M. 1986. Application of a CUSUM technique to gamma ray astronomy. Preprint.

88. Lombard, F. 1987. Personal communication.

89. Lyne, A.G., Manchester, R.N. and Taylor, J.H. 1985. The galactic population of pulsars. Monthly Notices of the Royal Astronomical Society, 213:613-639.

90. Manchester, R.N. and Taylor, J.H. 1977. Pulsars. San Fracisco : Freeman.

91. Manchester, R.N., Durdin, J.M. and Newton, L.M. 1985. A second measurement of a pulsar braking index. Nature, 313:374-376.

92. Manchester, R.N., D'Amico, N. and Tuohy, I.R. 1985. A search for short-period pulsars. Monthly notices of the Royal Astronomical Society, 212:975-986.

93. Manchester, R.N., Tuohy, I.R. and D'Amico N. 1982. Discovery of Radio Pulsations from the X-ray Pulsar in the Supernova Remnant G320.4-1.2. Astrophys J, 262:L31-L33.

94. Mardia, K.V. 1972. Statistics of directional data. New York : Academic Press.

95. Mayer-Hasselwander, H.A. 1985. Explanatory supplement to the COS-B final database. München : Max Planck Institute.

96. Middleditch, J. and Nelson, J. 1976. Studies of optical pulsations from HZ Herculis/Hercules X-1: A determination of the mass of the neutron star. Astrophys J, 208:567-586.

97. Morini, M. 1983. Inverse Compton gamma rays from pulsars - 1. The Vela pulsar. Monthly notices of the Royal Astronomical Society, 202:495-510.

98. Muslimov, A.G. and Tsygan, A.I. 1985. Neutron star superconductivity and superfluidity, and the decay of pulsar magnetic fields. Sov Astr L, 11(2):80-83.

99. Nesphor, Y.I., Zyskin, Y.L., Mukanov, J.B., Stephanian, A.A. and Fomin, V.P. 1981. Very high energy γ-rays from Cygnus X-3. Philosophical Transactions of the Royal Society of London, 301:633-634.

100. North, A.R., Raubenheimer, B.C., De Jager, O.C., Van Tonder, A.J. and Van Urk, G. 1987. Pulsed TeV gamma-rays from Vela X-1. Accepted by Nature

101. O'Mongain, E. 1973. Application of Statistics to results in Gamma Ray Astronomy. Nature, 241:376-379.

102. Orford, K.J. 1986. Personal communication.

103. Ostriker, J.P. and Gunn, J.E. 1969. On the nature of Pulsars. 1.Theory. Astrophys J, 157:1395-1417.

104. Parzen, E. 1962. On estimation of a probability density function and mode. Annals of Mathematical Statistics, 33:1065-1076.

105. Porter, N.A. and Weekes, T.C. 1978. Gamma ray astronomy from 10^{11} to 10^{14} eV using the Atmospheric Cerenkov Technique. Smithsonian Astrophysical Observatory. Special report 381.

106. Protheroe, R.J. 1985. A new statistic for the analysis of circular data in gamma-ray astronomy. 19th P Int Cosm Ray, 3:485-488.

107. Protheroe, R.J.: 1985. (In Proceedings of the Workshop on Techniques in Ultra High Energy γ-ray astronomy. Adelaide (Australia)) Preprint.

108. Protheroe, R.J. 1987. Statistical analysis in high energy gamma ray astronomy. (In Proceedings of the NATO advanced research workshop on high energy gamma ray astronomy. Durham (UK)) To be published by D.Reidel.

109. Quesenberry, C.P. and Miller, F.L. 1977. Power studies for some Tests for Uniformity. J Stat Comp, 5:169-191.

110. Raubenheimer, B.C., Van Urk, G. and De Villiers, E.J. 1983. An experiment to detect UHE γ-ray sources. 18th P Int Cosm Ray 8:24-28.

111. Raubenheimer, B.C., North, A.R., De Jager, O.C., Van Urk, G. and Van Tonder, A.J., 1986. Pulsed Very High Energy Gamma Rays from the COS-B source 2CG 006-00. Astrophys J, 307:L43-L47.

112. Rosenblatt, M. 1956. Remarks on some nonparametric estimates of a density function. Annals of Mathematical Statistics, 27:832-837.

113. Ruderman, M.A. and Sutherland, P.G. 1975. Theory of pulsars: Polar gaps, sparks and coherent microwave radiation. Atrophys J, 196:51-72.

114. Ruderman, M.A. 1981. Evolution and radiation in pulsar polar cap models. (In Sieber, W. and Wielebinski, R., eds. Pulsars. Dordrecht : D. Reidel Publishing Company.) 87-97.

115. Schönfelder, V. 1985. Wie aussichtsreich ist die Suche nach Gamma-Pulsaren? Naturwissenschaften, 72:133-138.

116. Seward, F.D. and Harnden, F.R. 1982. A new, fast X-ray Pulsar in the Supernova Remnant MSH 15-52. Astrophys J, 256:L45-L47:

117. Seward, F.D., Harnden, F.R., Murdin, P. and Clark, D.H. 1983. MSH 15-52: A Supernova Remnant containing two compact X-ray sources. Astrophys J, 267:698-710.

118. Shaban, S.A. 1980. Change point problem and two-phase regression: an annotated bibliography. International Statististical Review, 48:83-93.

119. Smith, F.G. 1977. Pulsars. Cambridge : Cambridge University Press.

120. Smith, F.G. 1986. Personal communication.

121. Swanenburg, B.N., Bennett, K., Bignami, G.F., Buccheri, R., Caraveo, P., Hermsen, W., Kanbach, G., Lichti, G.G., Masnou, J.L., Mayer-Hasselwander, H.A., Paul, J.A., Sacco, B., Scarsi, L. and Wills, R.D. 1981. Second COS-B catalog of high-energy gamma-ray sources. Astrophys J, 243:L69-L73.

122. Swanepoel, J.W.H. 1987. Optimal kernels when estimating non-smooth densities. Accepted by Communications in Statistics - Theory and Methods

123. Tümer, O.T., Wheaton, W.A., Godfrey, C.P. and Lamb, R.C. 1985. Very high energy gamma rays from the Crab pulsar. 19th P Int Cosm Ray, 1:139-142.

124. Turver, K.E. 1985. Ground-based very high energy gamma ray astronomy - observational highlights. 19th P Int Cosm Ray, 9:399-406.

125. Trümper, J., Pietsch, W., Reppen, C., Voges, W., Staubert, R. and Kendziorra, E. 1978. Evidence for strong cyclotron line emission in the hard X-ray spectrum for Hercules X-1. Astrophys J, 219:L105-L110.

126. Usov, V.V. 1983. Expected high-frequency radiation from the 1.5 ms pulsar. Nature, 305:409-410.

127. Vardeman, S. and Ray, D. 1985. Average run lengths for CUSUM schemes when observations are esponentially distributed. Technometrics, 27(2):145-150.

128. Vasseur, J., Paul, J., Parlier, B., Leray, J.P., Forichon, M., Agrinier, B., Boella, G., Maraschi, L., Treves, A., Buccheri, R., Cuccia, L. and Scarsi, L. 1971. Search for pulsed gamma ray emission above 50 Mev from NP 0532. Nature, 233:46-48.

129. Von Ballmoos, P., Diehl, R. and Schönfelder, V. 1985. Cen A observations at MeV-energies. 19th P Int Cosm Ray 1:273-276.

130. Watson, G.S. and Leadbetter, M.R. 1963. On the estimation of the probability density I. Annals of Mathematical Statistics, 34:480-491.

131. Weekes, T.C., Helmken, H.F. and L'Heureux, J. 1979. The Mt. Hopkins sky survey for gamma rays of energy 100-1000 GeV. II. Point Sources. 16th P Int Cosm Ray, 1:126-131.

132. Weekes, T.C., Lamb, R.C. and Hillas, A.M. 1987. Hercules - A new instrument for TeV astronomy. (In Proceedings of the NATO Advanced Research Workshop, Durham (UK)). To be published by D.Reidel.

133. Weekes, T.C. 1986. Cygnus X-3: Source of very high energy gamma-rays and very high energy gamma-ray observations of Hercules X-1 and 4U0115+63. Preprint.

134. Weisskopf, M.C., Elsner, R.F., Darbro, W., Leahy, D., Naranan, S., Sutherland, P.G., Grindlay, J.E., Harnden, F.R. and Seward, F.D. 1983. The period history of the X-ray pulsar in MSH 15-52. Astrophys J, 267:711-712.

135. Wills, R.D., Bennet, K., Bignami, G.F., Buccheri, R., Caraveo, P. D'Amico, N., Hermsen, W., Kanbach, G., Lichti, G.G., Masnou, J.L., Mayer-Hasselwander, H.A., Paul, J.A., Sacco, B. and Swanenburg, B.N. 1980. High-Energy Gamma-Ray sources observed by COS-B. (In Proceedings of the COSPAR Symposium on Non-Solar Gamma Rays, Advances in Space Exploration), 7:43.

136. Xia, X.Y., Qiao, G.J., Wu, X.J. and Hou, Y.Q. 1985. Inverse Compton scattering in strong magnetic fields and its possible application to pulsar emission. Astron Astr, 152:93-100.